Doctoral thesis for a doctoral degree
at the Graduate School of Life Sciences
Julius-Maximilians-Universität Würzburg

Section Biomedicine

**The role of enteric glial cells
under inflammatory conditions of the intestine**

**Die Rolle von enterischen Gliazellen
unter entzündlichen Bedingungen im Darm**

submitted by

Corinna Rosenbaum

born in Bonn

Würzburg 2016

Submitted on ....

Members of the commitee

Chairperson: Prof. Dr. Thomas Dandekar
Primary supervisor: Prof. Dr. Heike Walles
Supervisor (second): PD Dr. Beate Niesler
Supervisor (third): Prof. Dr. Erhard Wischmeyer

Date of public defense ....

Date of receipt of certificates ....

Contents

Contents

Abstract

The enteric nervous system (ENS) innervates the gastrointestinal (GI) tract and controls central aspects of GI physiology including contractility of the intestinal musculature, glandular secretion and intestinal blood flow. The ENS is composed of neurons that conduct electrical signals and of enteric glial cells (EGCs). EGCs resemble central nervous system (CNS) astrocytes in their morphology and in the expression of shared markers such as the intermediate filament protein glial fibrillary acidic protein (GFAP). They are strategically located at the interface of ENS neurons and their effector cells to modulate intestinal motility, epithelial barrier stability and inflammatory processes. The specific contributions of EGCs to the maintenance of intestinal homeostasis are subject of current research.

From a clinical point of view EGC involvement in pathophysiological processes such as intestinal inflammation is highly relevant. Like CNS astrocytes ECGs can acquire a reactive, tissue-protective phenotype in response to intestinal injury. In patients with chronic inflammatory bowel diseases (IBD) such as Crohn's disease and ulcerative colitis, alterations in the EGC network are well known, particularly a differential expression of GFAP, which is a hallmark of reactive gliosis in the CNS.

With increasing recognition of the role of EGCs in intestinal health and disease comes the need to study the glial population in its complexity. The overall aim of this thesis was to comprehensively study EGCs with focus on the reactive GFAP-expressing subpopulation under inflammatory conditions *in vivo* and *in vitro*. In a first step, a novel *in vivo* rat model of acute systemic inflammation mimicking sepsis was employed to investigate rapidly occuring responses of EGCs to inflammation. This study revealed that within a short time frame of a few hours, EGCs responded to the inflammation with an upregulation of Gfap gene expression. This inflammation-induced upregulation was confined to the myenteric plexus and varied in intensity along the intestinal rostro-caudal axis. This highly responsive myenteric GFAP-expressing EGC population was further characterized *in vivo* and *in vitro* using a transgenic mouse model (hGFAP-eGFP mice). Primary purified murine GFAP-EGC cultures *in vitro* were established and it was assessed how the transcriptomic and proteomic profiles of these cells change upon inflammatory stimulation. Here, myenteric GFAP-EGCs were found to undergo a shift in gene expression profile that predominantly affects expression of genes associated with inflammatory responses. Further, a secretion of inflammatory mediators was validated on protein level. The GFAP$^+$ subpopulation is hence an active participant in inflammatory pathophysiology. In an acute murine IBD model *in vivo*, GFAP-EGCs were found to express components of the major histocompatibility complex (MHC) class II in inflamed tissue, which also indicates a crosstalk of EGCs with the innate and the adaptive lamina propria immune system in acute inflammation. Taken together, this work advances our knowledge on EGC (patho-)physiology by identifying and characterizing an EGC subpopulation rapidly responsive to inflammation. This study further

Abstract

provides the transcriptomic profile of this population *in vivo* and *in vitro*, which can be used to identify targets for therapeutic intervention. Due to the modulating influence of EGCs on the intestinal microenvironment, the study further underlines the importance of integrating EGCs into *in vitro* test systems that aim to model intestinal tissues *in vitro* and presents an outlook on a potential strategy.

Zusammenfassung

Das enterische Nervensystem (ENS) innerviert den gastrointestinalen Trakt und kontrolliert zentrale Aspekte der gastrointetinalen Physiologie, wie die Kontraktilität der intestinalen Muskulatur, Sekretion und den intestinalen Blutfluss. Das ENS setzt sich aus elektrisch leitenden Neuronen und enterischen Gliazellen (EGZ) zusammen. EGZ ähneln Astrozyten des zentralen Nervensystems (ZNS) hinsichtlich ihrer Morphologie und der Expression gemeinsamer Marker wie dem Intermediärfilament Saures Gliafaserprotein (GFAP von engl. glial fibrillary acidic protein). EGZ sind strategisch an der Kontaktstelle zwischen ENS-Neuronen und deren Effektorzellen positioniert, um die intestinale Motilität, die epitheliale Barrierestabilität sowie inflammatorischen Prozesse zu modulieren. Die spezifische Beteiligung der EGZ an der Aufrechterhaltung der Darmhomöostase wird gegenwärtig erforscht.

Aus klinischer Sicht ist die Beteiligung von EGZ an pathophysiologischen Prozessen wie der intestinalen Entzündung besonders relevant. Wie ZNS-Astrozyten können EGZ bei intestinalen Schädigungen einen reaktiven, gewebe-protektiven Phänotyp annehmen. Bei Patienten mit chronisch-entzündlichen Darmerkrankungen (IBD, von engl. inflammatory bowel disease) wie Morbus Crohn und Colitis ulcerosa sind Veränderungen im EGZ-Netzwerk bekannt, besonders eine veränderte Expression von GFAP, welches ein prominentes Kennzeichen der reaktiven Gliose im ZNS ist.

Nachdem sich die Bedeutung der EGZ im gesunden und kranken Darm zunehmend herausgestellt hat, muss ein stärkerer Fokus auf die Erforschung der glialen Population gelegt werden. Die Zielsetzung dieser Arbeit war die umfassende Untersuchung der EGZ mit Fokus auf die reaktive GFAP-exprimierende Population unter entzündlichen Bedingungen *in vivo* und *in vitro*. In einem ersten Schritt wurde ein neuartiges *in vivo*-Rattenmodell einer akuten systemischen Entzündung verwendet, um die schnell stattfindenden Veränderungen der EGZ unter entzündlichen Bedingungen zu untersuchen. Diese Studie ergab, dass innerhalb von wenigen Stunden EGZ mit einer Hochregulation der Gfap-Genexpression auf die Entzündung reagieren. Diese entzündungsinduzierte Hochregulation war lokal auf den myenterischen Plexus begrenzt und entlang der rostro-kaudalen Achse des Darms unterschiedlich stark ausgeprägt. Die responsive, GFAP-exprimierende myenterische EGZ-Population wurde daraufhin *in vivo* und *in vitro* charakterisiert unter Zuhilfenahme eines transgenen Mausmodells (hGFAP-eGFP-exprimierende Mäuse). Primäre, aufgereinigte GFAP-EGZ-Zellkulturen wurden etabliert und dahingehend untersucht, wie sich das transkriptomische und proteomische Profil der Population unter entzündlichen Bedingungen verändert. Hierbei wurde reproduzierbar eine Verschiebung des transkriptomischen Profils myenterischer GFAP-exprimierender EGZ gefunden. Die davon betroffenen Gene sind vorwiegend mit Immunantworten assoziiert. Weiterhin wurde die Sekretion solcher Immunmediatoren auf Proteinebene validiert. Die GFAP$^+$ Subpopulation ist somit ein aktiver Modulator entzündlicher pathophysiologischer Prozesse. In einem akuten IBD-Mausmodell konnte weiterhin

Zusammenfassung

gezeigt werden, dass GFAP-EGZ verstärkt Komponenten des Haupthistokompatibilitätskomplex (MHC) Klasse II im entzündeten Gewebe exprimieren. Dies weist auf eine direkt Interaktion der EGZ mit dem Immunsystem in der Lamina propria hin.

Insgesamt konnte mit dieser Arbeit das Wissen über die (Patho-)Physiologie von EGZ erweitert werden, indem eine schnell responsive EGZ-Subpopulation identifizert und charakterisiert wurde. Weiterhin wurde im Rahmen dieser Arbeit das gesamte Transkriptomprofil der GFAP-Subpopulation *in vivo* und *in vitro* veröffentlicht, welches für weitere Studien zur Identifikation möglicher therapeutischer Anwendungen genutzt werden kann. Aufgrund des modulierenden Einflusses der EGZ auf die Darmphysiologie betont diese Studie die Notwendigkeit EGZs in *in vitro*-Gewebemodelle des Darms zu integrieren und präsentiert einen Ausblick auf eine mögliche Strategie.

List of Abbreviations and Units

Abbreviations

αSMA	α-smooth muscle actin
2D	two-dimensional
3D	three-dimensional
AF	Alexa Fluor
ANS	autonomic nervous system
APC	Antigen-presenting cells
AT	annealing temperature
ATP	adenosine triphosphate
B-FABP	brain-specific fatty acid binding protein
BABB	benzyl alcohol & benzyl benzoate
BBB	blood-brain-barrier
BSA	bovine serum albumin
CD	Crohn's disease
CD	cluster of differentiation
cDNA	copyRNA
CIITA	class II, major histocompatibility complex, transactivator
CNS	central nervous system
Cy^{TM}3	Indocarbocyanine
DAI	disease activity index
DAPI	4',6-diamidino-2-phenylindole
DC	dendritic cell
DMEM	Dulbecco's Modified Eagle Medium
DNase	Desoxyribonuclease
DSS	dextran sulphate sodium
DTT	dithiothreitol
E	efficiency
E. coli	Escherichia coli
ECM	extracellular matrix
EDTA	Ethylenediaminetetraacetic acid
EGC	enteric glial cell
eGFP	enhanced green fluorescent protein
ELISA	enzyme linked immunosorbent assay
ENCC	enteric neural crest cell
ENS	enteric nervous system
eNTPDase	ecto-nucleoside triphosphate diphosphohydrolase
FACS	fluorescence-activated cell sorting
FCS	fetal calf serum

List of Abbreviations and Units

GABA . . . . γ-aminobutyric acid
GALT . . . . gut-associated lymphoid tissue
GEO . . . . Gene Expression Omnibus
GFAP . . . . glial fibrillary acidic protein
GI . . . . gastrointestinal
GO . . . . Gene Ontology
GOI . . . . gene of interest
GSE . . . . GEO series
H&E . . . . hematoxylin and eosin
hGFAP . . . . human glial fibrillary acidic protein
HPRT . . . . hypoxanthine phosphoribosyltransferase
HSCR . . . . Hirschsprung's disease
i.e. . . . . *id est*, it is
IBD . . . . inflammatory bowel diseases
IEB . . . . intestinal epithelial barrier
IEC . . . . intestinal epithelial cell
IFN . . . . interferon
IgA . . . . immunoglobulin A
IHC . . . . Immunohistochemistry
IL . . . . interleukin
ILF . . . . isolated lymphoid follicle
iNOS . . . . inducible nictric oxide synthase
IP-10 . . . . Interferon-γ induced protein 10
LCM . . . . laser capture microdissection
LMMP . . . . Small intestinal longitudinal muscle-myenteric plexus
LP . . . . lamina propria
LPS . . . . lipopolysaccharide
LSFM . . . . light sheet fluorescence microscopy
M cell . . . . microfold cells
MCP-1 . . . . Monocyte chemoattractant protein 1
MHC . . . . major histocompatibility complex
Mip-1α . . . . macrophage inflammatory protein 1α
mRNA . . . . messenger RNA
NEAA . . . . Non-Essential Amino Acids
NO . . . . nitric oxide
OCT . . . . optimal cutting temperature
P . . . . passage
p75NTR . . . . p75 neurotrophin receptor
PAMP . . . . pathogen-associated molecular pattern
PBS^{+} . . . . Phosphate buffered saline with magnesium and calcium ions
PBS^{-} . . . . Phosphate buffered saline without magnesium and calcium ions
PFA . . . . paraformaldehyde

PGP 9.5	Protein gene product 9.5
PLP	proteolipid protein
POI	postoperative ileus
PP	Peyer's patch
qPCR	quantitative polymerase chain reaction
Ref	reference gene
RIN	RNA integrity number
RNA	ribonucleic acid
ROS	reactive oxygen species
RQI	RNA quality indicator value
RT	room temperature
SD	standard deviation
SDEGs	significantly differentially expressed genes
SIRS	systemic inflammatory response syndrome
SIS	Small intestinal submucosa without mucosal layer
SIS-muc	Small intestinal submucosa with preserved mucosal layer
SMP	submucosal plexus
Sod2	Superoxide dismutase 2
Sox	SRY-related HMG-box
T_H	helper T cells
TLR	Toll-like receptor
TNBS	trinitrobenzene sulfonic acid
TNF	tumor necrosis factor
TS	transcript size
UC	ulcerative colitis
UCHL1	Ubiquitin carboxy-terminal hydrolase L1
UV	ultaviolet

Countries

(AT)	(Austria)
(F)	(France)
(G)	(Germany)
(I)	(Italy)
(NL)	(Netherlands)
(UK)	(United Kingdom)
(US)	(United States)

Units

°C	degree Celcius

List of Abbreviations and Units

μm	micrometer
bp	base pairs
cm	centimeter
g	unit of gravitational force
h	hour(s)
m^2	square meter
mA	milliampere
min	minutes
mm	millimeter
W	Watt
w/v	weight/volume

List of Figures

List of Figures

List of Tables

List of Tables

1 Introduction

1.1 Anatomy and function of the gastrointestinal tract

The central function of the gastrointestinal (GI) tract is the processing of ingested food into absorbable components, their subsequent uptake into the blood and lymph and the excretion of non-absorbed components [1]. This process is regulated by a complex interplay of intestinal innervation and hormone secretion.

The intestine is the GI segment that extends from the pylorus to the anal canal and consists of the small and the large intestine. The small intestine (*intestinum tenue*) is composed of the duodenum, the jejunum and the ileum. The large intestine (*intestinum crassum*) commences with the cecum, followed by the colon and finally the rectum and anal canal [2]. The organization of the intestinal wall is conserved throughout the GI tract and is composed of four coats: serous, muscular, submucous and mucous [2]. The outer serous coat (*tunica serosa*) lines the GI wall. The muscular coat (*tunica muscularis*) consists of two layers of smooth muscle tissue, the external longitudinal layer (*stratum longitudinale*) and the internal circular layer (*stratum circulare*). The major proportion of cell bodies of the gastrointestinal nervous system is allocated between the longitudinal and circular muscular fibers , forming the myenteric plexus (*Auerbach's plexus*) (see figure 1.1). The submucous coat (*tela submucosa*) is a loose connective tissue
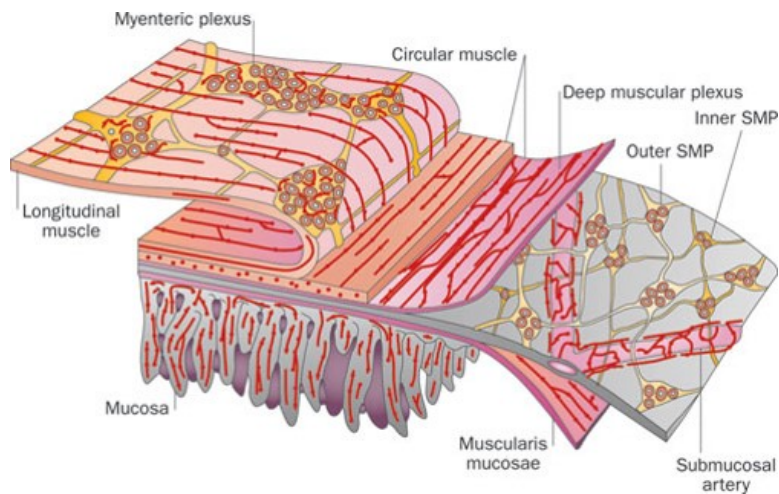
Figure 1.1: Anatomical structure of the gut and organization of the human ENS. Ganglionated neurons lie in the myenteric plexus situated between the longitudinal and the circular muscle layer or in the submucosal plexus (SMP) between the circular muscle and the mucosa. Nerve fiber bundles connect the ganglia to form the plexus structures and interconnect the plexuses. Enteric neurons innervate the longitudinal and circular muscle, the muscularis mucosae, intrinsic blood vessels and the mucosa. From [3]

.

that connects the muscular layer with the mucosa and contains enteric nerve cells organized in the submucosal plexus (*Meissner's plexus*). The myenteric and submucosal ganglia networks are well interconnected. The mucous coat (*tunica mucosa*) consists of a thin layer of muscular (*muscularis mucosae*) and connective tissue (*lamina propria mucosae*), harboring the mucous plexus, covered by the innermost epithelial layer (*epithelium mucosae*). The mucosal epithelium represents the body's largest contact area body with approx. 400 m^2 and mainly consists of absorptive cells called enterocytes and secretory cells such as goblet cells and enteroendocrine cells, which are modulated by intrinsic and extrinsic nerve fibers of the peripheral nervous system [4].

1.2 The enteric nervous system circuitry

The intrinsic nervous system of the GI tract, the enteric nervous system (ENS), is the largest fraction of the peripheral nervous system. It contains 200-600 million neurons in humans, which is comparable to the number of neurons in the spinal cord. In its neurotransmitter repertoire the ENS is similarly equipped as the central nervous system (CNS) [3, 5]. The neurons include afferent sensory neurons that perceive the physiological status of the GI tract and relay these information via interneurons to efferent motor neurons. Motor neurons then act on different effector cells including smooth muscle cells, pacemaker cells, blood vessels, mucosal glands, lymphoid tissue and epithelia (see figure 1.2) [6]. The basic function of the ENS is hence to orchestrate contraction of the musculature with glandular secretion and intestinal blood flow into an organized digestive behavior. The prototypic example of intestinal muscular activity organized by the ENS is the the peristaltic reflex, a motility pattern that propels food distally. The peristaltic motility pattern is initiated when a food bolus in the lumen stimulates afferent (mechano-)sensory neurons. These synapse with interneurons that activate different efferent motor neurons: Excitatory motor innervation is activated in the longitudinal muscle coat ahead of the food contents, while at the same time inhibitory motor innervation is activated in the ciruclar muscle coat of the same segment. This leads to a contraction of the longitudinal muscle and a simultaneous relaxation of the circular muscle, which induces a widening of the tube's diameter. The segment ahead of the food bolus is the receiving segment, its widened lumen is prepared to receive the food. The segment behind the food bolus the the propulsive segment. Here, the longitudinal muscle coat relaxes and the circular muscle contracts simultaneously, which propels the food forward [7, 8]. This intrinsic circuitry allows the ENS to control gastrointestinal functions autonomously without input from the CNS. Despite its autonomic nature, the ENS is well integrated into the extrinsic autonomic nervous system (ANS) and receives input from the sympathetic and the parasympathetic nervous system (see figure 1.2). Parasympathetic innervation transmits signals from the CNS to the ENS innervation of the GI musculature and allows control of digestive processes [7, 10]. Sympathetic innervation synapses with ENS neurons and additionally innervate
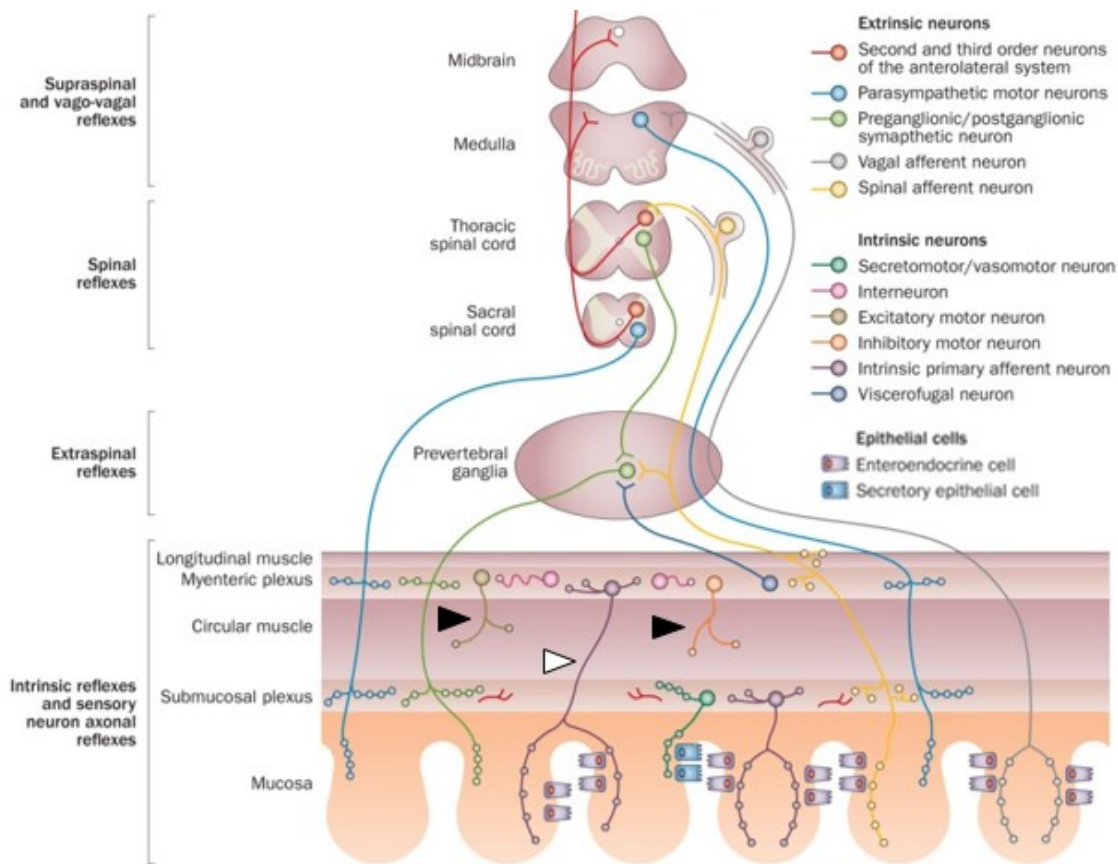
Figure 1.2: Schematic display of the extrinsic and intrinsic neural circuits of the ENS.
Intrinsic afferent neurons of the ENS (white arrowheads) relay information on the physiological status
of the GI tract to motor neurons (black arrowheads) via interneurons. This intrinsic neural circuitry is
integrated into the extrinsic parasympathetic and sympathetic nervous system. Efferent parasympathetic
neurons with cell bodies in the medulla (brainstem) and sacral spinal cord innervate the tissue (light
blue). Efferent sympathetic postganglionic neurons innervate the GI tissue after receiving input from
preganglionic sympathetic neurons (green). Afferent neurons relay information to the CNS via vagal
(grey) and the spinal (yellow) pathways. Adapted from [9]
.

blood vessels and the mucosa, mediating suppression of digestive functions [7].

In addition to these efferent (i.e. away from the CNS) motoneurons the parasympathetic and
sympathetic pathways also contain afferent (i.e. towards the CNS) sensory neurons. Those relay
information to the CNS on the nature of luminal contents, which includes not only ingested food
but also the enteric microbiota. Interestingly, the gut microbiota can affect CNS-functions by
these signaling pathways, regulating brain chemistry and affecting the neuro-endocrine system
associated with anxiety and depressive-like behavior [11].

The efferent and afferent extrinsic fibers and their integration into CNS and ENS build up a
reflex circuit (vagovagal reflex), that allows a reciprocal regulation along the so-called gut-brain-

axis. However, the GI musculature is not the only target in this neural reflex mechanism, also the mucosa and its implemented enteric immune system are part of this regulation.

Enteric neurons can be biochemically classified into subtypes based on their neurotransmitters or neurotransmitter-synthesizing enzymes, among those are acetylcholine, noradrenaline, nitric oxide (NO) and serotonin. Developmentally, the ENS originates from migratory enteric neural crest cells (ENCCs) that colonize the gut, mainly in a rostral to caudal direction [12]. While ENCCs migrate along the length of the gut, they proliferate extensively and a proportion begins to differentiate by expressing early neuronal markers such as ubiquitin carboxy-terminal hydrolase L1 (UCHL1) and RNA binding proteins HuC/D [5, 13]. At specific time points (so called "birth dates"), neurons exit the cell cycle and terminally differentiate into neuronal subtypes.
If ENCCs fail to fully colonize the gut, congenital gut motility disorders arise, the most common is Hirschsprung's disease (HSCR) with an prevalence of 1 in 5000 births [14]. HSCR is characterized by an absence of enteric ganglia (i.e. aganglionosis) in the distal gut. The aganglionated bowel is tonically contracted due to the lack of active intestinal smooth muscle relaxation [13]. Fecal contents accumulate in the segment proximal to the aganglionated segment, causing the characteristic distended bowel (megacolon).

Intestinal muscle contractions are not exclusively evoked by neuronal innervation. Interstitial cells are part of the ENS circuitry as well. The term interstitial refers to the cells localization in narrow spaces in between other cells. A population referred to as interstitial cells of Cajal (ICC) is closely associated to ENS neurons and is electrically coupled to smooth muscle cells via gap junctions. These cells act as pacemakers [**TAKAYAMA.2002**] and are able to elicit muscular contractions.
A further major part of the ENS are enteric glial cells (EGCs). EGCs outnumber neurons by several fold in the human ENS in the human ENS [15, 16]. They are located in close proximity to neurons within the ganglia and along interganglionic connectives of the myenteric and submucosal plexus, but can also project into extraganglionic layers of the gut wall, forming a widespread network at all levels of the GI tract [17, 18]. EGCs are hence strategically located at the interface of neurons and their effector cells to modulate the regulation of intestinal motility, epithelial barrier stability and inflammatory processes. Their specific contributions to maintaining intestinal homeostasis are subject of current research.

1.3 Enteric glial cells as regulators of GI homeostasis

The term "enteric glia" was coined by Gabella as late as 1981 [15], before that, glial cells in the GI tract were considered to be Schwann cells because of their common ontogenetic descent from the neural crest. Electron microscopy studies performed by Gabella revealed, however, that enteric glia lack characteristics of Schwann cells and instead show unique features; they have extensive branching of their processes, contain bundles of gliofilaments and are surrounded by a single basement membrane [15, 19]. These features, together with their synaptic connections to neurons, rather make enteric glia reminiscent of CNS astrocytes. In 1983, Jessen and Mirsky analyzed whether the similarities between EGCs and astocytes are limited to a morphological resemblance or whether they extend to the molecular level. They found that enteric glia and astocytes express similar levels of Vimentin (high in immature cells, low when matured), glial fibrillary acidic protein (GFAP) (low in immature cells, high when matured) and glutamine synthetase [20]. It is important to note that GFAP expression is not constant but can be highly dynamic in individual EGCs but the functional relevance is currently not fully clear [21].
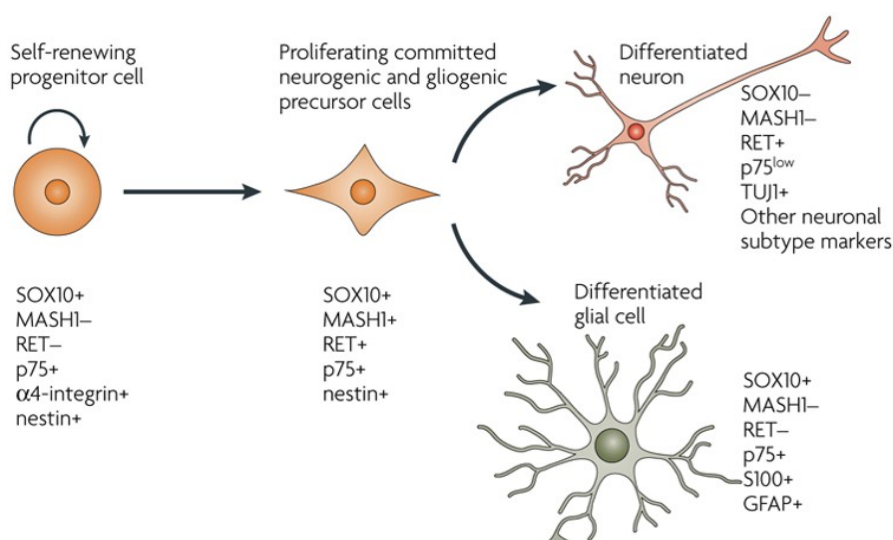
Figure 1.3: Self-renewing progenitor ENCCs express several markers characteristic of differentiated EGCs. Self-renewing progenitor ENCCs express SOX10, p75NTR, α4-integrin and Nestin, but not Ret or Mash1. When they commit to the neurogenic and gliogenic lineage, Ret and Mash1 expression is upregulated. Cells that differentiate to glial cell maintain SOX10 and p75NTR expression, downregulate Mash1 and RET and upregulate the glial markers S100B and GFAP. From [12]
.

Other markers that are expressed by differentiated EGCs are the transcription factor SOX10, brain-specific fatty acid binding protein (B-FABP), p75 neurotrophin receptor (p75NTR) and calcium binding protein S100B, see figure 1.3 [12][22]. Most interestingly, recent studies have

shown that mature EGCs can acquire a multipotent phenotype under certain conditions *in vivo* and *in vitro* and give rise to neurons and glia in the adult ENS [23, 24].

The structural and molecular similarities between EGCs and astrocytes are complemented by functional analogies. Astrocytes are closely associated with neuronal membranes, especially with synaptic regions, which makes them an integrative element in synaptic transmission. They maintain the extracellular environment by taking up excess extracellular potassium (K^+) ions and neurotransmitters released into the synaptic cleft upon neuronal activity [25]. Enteric glia have also been shown to express voltage-activated inward and outward K^+-channels, which are related to astrocytic K^+-channels [18] and suggested to be involved in K^+-uptake by EGCs [26]. EGCs furthermore express transporters and enzymes necessary for neurotransmitter uptake and re-synthesis, such as glutamine synthetase [20], γ-aminobutyric acid (GABA) transporter GAT2 [27] or the nucleotidase eNTPDase2 for the degradation of extracellular ATP [28].

Both glial cell types do not only provide a suitable microenvironment for neuronal activity, but they also secrete neurotrophic factors for the maintenance of neurons, in case of enteric glia reduced glutathione (GSH) has been identified to be produced and released by EGCs and to exert neuroprotective effects [29].

Glia are not only in functional contact with neurons, but also with endothelial cells. CNS-astrocytes can form a structural association with both neurons and endothelial cells, thereby creating the neurovascular unit [30, 31]. In this unit, the brain activity is functionally coupled to the blood flow rate. Further, astrocytes can induce endothelial cells to acquire the specialized phenotype of blood-brain-barrier (BBB)-associated endothelial cells, characterized by tight junction proteins, polarized location of transporters and specialized enzyme systems [32]. In the ENS, enteric ganglia are devoid of blood vessels, but EGCs contact capillaries with flat endfeet at the surface of ganglia and at extraganglionic sites. Interestingly, these capillaries are distinct from capillaries found elsewhere in the gut, they are much thicker walled and closely resemble cerebral capillaries of the BBB [18]. These findings suggest that enteric glia may also contribute to the regulation of endothelial permeability, but information on such mechanisms are scarce.

Barrier-stabilizing capacities of EGCs might be most relevant in the context of the mucosal epithelial barrier. The monolayer of intestinal epithelial cells (IECs) lining the GI tract forms a functional barrier that must be maintained by a tight control of the IECs' proliferation, differentiation and formation of tight junctions. Interestingly, EGCs have been shown to be in intimate association with epithelial cells, forming a dense network at the crypt base and extending along the crypt axis [33]. This morphology suggests a functional influence of glial cells on epithelial cells at the crypt base. Indeed, co-culture models with Caco-2 cells identified the release of transforming growth factor β1 and the prostaglandin 15d-PGJ2 by EGCs to inhibit IEC proliferation and to induce IEC differentiation [34, 35] and pro-EGF to promote wound healing [36]. *S*-nitrosoglutathione was furthermore identified to be released by EGCs *in vitro* and to increase intestinal barrier integrity *in vivo* [37].

Further support for the pivotal role of EGCs in maintaining GI homeostasis came from mouse models of glial ablation. Different approaches have been chosen to ablate glia in order to assess their functions *in vivo*, ranging from a coarse gliotoxin-mediated strategy [38] and autoimmune-mediated strategies [39, 40] to subpopulation-specific approaches targeting GFAP-expressing glia [37, 41]. Findings from these studies substantiate the tissue-protective effects of glia, since animals exhibited GI impairments ranging from reduced intestinal motility to severe inflammation caused by mucosal barrier disruption, vascular leakage and neuronal degeneration. However, as pointed out by Gulbransen, linking these observations to the absence of glia cannot be done without doubt: the inflammatory environment might also be fostered by ablation-induced activated glia and is not necessarily a result of ablated homeostatic functions [42]. This notion implies an important quality of EGCs, which is their responsiveness to changes in the microenvironment and their ability to acquire a reactive phenotype, another common feature with CNS astrocytes, termed reactive gliosis.

Reactive gliosis is a glial defense mechanism in response to axonal injury, that aims to protect stressed neurons, to isolate the area of injury and to remove pathogens, dying cells and cellular debris [43]. It is best studied in the CNS because it is a ubiquitous feature of a variety of CNS pathologies. Reactive gliosis is not an all-or-none phenomenon, but a finely gradated process ranging from subtle alterations in glial functions to scar formation [44]. Historically, reactive gliosis was negatively connotated, perceived as synonymous with scar formation, which inhibits axon regeneration and is thereby the main impediment to functional recovery after CNS injury. However, it is now clear that reactive CNS astrocytes can influence injury outcome also positively, by uptake or degradation of neurotoxic substances, by protection from oxidative stress, by facilitating BBB repair and by limiting spread of inflammatory cells into healthy tissue [44]. The phenotype of reactive glia is associated with hypertrophy and proliferation, along with an up-regulation of cytoskeletal components such as GFAP, vimentin or nestin [43].

In the GI-tract, changes in EGC phenotype have been observed in inflammatory disease conditions, particularly in patients with Crohn's disease (CD) or ulcerative colitis (UC), the most common forms of chronic inflammatory diseases of the bowel (IBD). Intriguingly, these changes particularly affected the expression levels of GFAP, the hallmark of reactive astrocytes. In UC-patient biopsies, the GFAP expression levels in the mucosa were significantly elevated in inflamed regions [39, 45]. In CD-patient biopsies, GFAP expression levels in inflamed samples were lower than in inflamed samples from UC-patients and even significantly reduced in non-inflamed mucosal biopsies compared to controls [39, 45]. An upregulation of GFAP in response to inflammatory stimuli was also confirmed in primary glial cell cultures *in vitro* [46] (see also section 1.5). These findings have been interpreted as (1) a sign for reactive gliosis in the ENS of UC-patients and (2) as an indication for the detrimental effect on tissue homeostasis when normal EGC function is lost, as it is the case in the CD-patients [47]. Consequently, this prompted studies on the interaction of EGC with the intestinal immune system and hopes to identify EGCs as therapeutically relevant targets to manage inflammatory bowel conditions.

1.4 The intestinal immune system

The intestinal immune system has to fulfill two somewhat conflicting functions; it has to tolerate commensal microbiota, which are essential for the digestive process, while at the same time eliminating pathogenic microbial agents. If the balance between tolerance and resistance is disturbed, inappropriate mucosal immune responses can lead to severe tissue damage as in IBD (see section 1.6). To understand how a dysregulated intestinal inflammation originates, it is necessary to shortly outline homeostatic intestinal immune processes.

The intestinal mucosa is equipped with several defense barriers to limit the intrusion of microbial products into the organism. These include (1) a mechanical barrier of mucus and epithelium, (2) an antimicrobial barrier of natural antimicrobial peptides such as defensins and immunoglobulin A (IgA) and (3) the immunological barrier of the innate and adaptive immune system [48]. The latter is organized in different tissue compartments that are structurally and functionally different.

The inductive sites of the mucosal immune system comprise organized lymphoid aggregates such as Peyer's patches (PP) and isolated lymphoid follicles (ILF) and are referred to as the gut-associated lymphoid tissue (GALT) [49]. Here, immune responses are initiated. Antigens are sampled from the mucosal surface and presented to naive lymphocytes by antigen-presenting cells (APC). Upon recognition of the antigen, lymphocytes become activated and differentiate into effector lymphocytes. Activated lymphocytes leave the inductive sites via the lymphatics, enter the blood stream and reenter the mucosal tissue at the effector sites [50, 51].

The effector sites of mucosal immunity comprise the lamina propria (LP) and the epithelium. Here, the activated lymphocytes can elicit an immune response. B cells mature into IgA-secreting plasma cells. T cells mature into different subtypes that elicit different responses dependent on the cytokines they secrete, both immunosuppressive responses/tolerance and pro-inflammatory responses can be induced. $CD4^+$ T cells that induce pro-inflammatory responses can be further divided into T-helper 1 (T_H1) cells that secrete interferon (IFN)-γ and T_H2 cells that secrete interleukin (IL)-4 [52]. The differentiation into T_H1- and T_H2-mediated inflammatory processes is relevant for IBD, CD is mediated by T_H1-cells, whereas UC is not [53, 54]. The different cytokine profiles released by effector T cells in CD and UC account for the differing disease patterns and their understanding is necessary for therapeutic approaches (see section 1.6).

In the healthy organism, the balance between immune activation and tolerance must be finely controlled. A variety of regulatory mechanisms are engaged in this control, such as the hormone-secreting endocrine system and also the ENS.

1.5 Interactions of the ENS with the intestinal immune system

One indication of an interaction between the ENS and the intestinal immune system is their interdependent embryonic development. The formation of PPs by a gut-infiltrating hematopoietic sublineage is dependent on RET signaling [55]. Likewise, RET signaling is crucial for migrating ENS precursor cells that colonize the intestine [56] (see figure 1.3). Recently, it was further shown that colonization of the mucosa by ganglionated glia depends on the presence of luminal microbiota [57].

The basis for a cross-talk between the GI immune and the nervous system is that many neurotransmitters and receptors are shared by both systems [58, 59]. One well-characterized systemic interplay is the "inflammatory reflex" [60]. This term refers to a mechanism, by which inflammatory mediators relay information to the brain via sensory pathways and trigger a reflexive release of neuromediators that dampen immune responses. Acetylcholine, released upon vagal nerve stimulation, has been shown to prevent post-surgical intestinal inflammation in a mouse model of postoperative ileus (POI) by inhibiting macrophage activation [61]. Cholinergic innervation of immune system components has subsequently been generalized to mediate anti-inflammatory effects [62]. But this neuro-immune cross-talk can also affect nervous system functions: the transient hypomotility characterizing POI is maintained by inhibitory neural pathways that are triggered by local inflammatory infiltrates arising from the bowel handling during surgery [63].

For this work, the interplay between glial cells and cells of the intestinal immune system is of interest. Observations on altered glial functions in inflamed intestinal tissue and possible mechanisms of interaction are introduced in the following section.

As pointed out in Section 1.3, EGCs of IBD-patients display abnormal features resembling activated CNS-astrocytes. In UC-patients these include elevated GFAP-expression levels. In CD-patients the hallmark of activated glia is the expression of major histocompatibility complex (MHC) class II antigens [64], which suggests a function of EGCs in antigen presentation to lymphocytes. Further glial alterations in the context of CD include increased glial cell numbers in areas of active inflammation (hyperplasia) and increased expression of receptors belonging to the TNF-receptor superfamily such as nerve growth factor receptor (NGFR) and CD27 [65], whose ligand $TNF\alpha$ is considered the prototypic pro-inflammatory cytokine.

These observations on EGC alterations in IBD-conditions were obtained about 20 years ago via immunohistochemial analyses of patient biopsies. They prompted *in vitro* studies on a molecular level to elucidate EGC-contributions to disease progression. Thus, activated EGCs were shown to release a range of inflammation-mediating factors.

In 2001, Anne Rühl showed the release of the proinflammatory cytokine IL-6 by rat EGCs upon stimulation with IL-1β, another proinflammatory cytokine, and provided evidence for a specific IL-1 receptor on EGCs [66]. IL-1β itself was found to be secreted by EGCs *in vitro* upon LPS-stimulation [67]. Von Boyen demonstrated an effect of IL-1β and other proinflammatory

mediators (TNF-α, LPS) on the expression level of GFAP, showing a significant upregulation of intracellular GFAP in EGCs after inflammatory stimulation *in vitro* [46]. Further studies confirmed the increase in GFAP expression in EGCs upon exogenous stimuli exposure, together with other signs of glial activation such as proliferation, MHC-II and cFos expression [68]. c-Fos is a transcription factor, which is rapidly expressed upon stimulation and hence is referred to as "immediate early gene". In CNS glia, cFos is known to influence the expression of inducible nitric oxide synthase (iNOS), IL-1, IL-6 and TNFα, all well-characterized mediators of the inflammatory responses in the CNS [69].

Furthermore, EGCs were shown to express the neurotrophin S100B in response to inflammatory stimulation *in vitro* [68, 70]. *In vivo*, increased levels of S100B protein expression and secretion were found to be elevated in biopsies from UC-patients, and this upregulation was associated with enhanced NO production by EGCs through the specific stimulation of iNOS [70]. NO is one of the most important signaling molecules involved in host-immune defense and a prominent pro-inflammatory mediator. This S100B-mediated increase in glial NO synthesis, triggered by inflammatory stimulation, proved EGCs as direct contributor to NO-mediated mucosal inflammation. Taken together, these studies confirmed the potential of EGCs to acquire an activated phenotype upon exogenous stimulation and to shape an inflammatory response in intestinal tissues at the interface of neural and immune systems.

However, none of these studies provided evidence for a direct response of EGCs to tissue-invading microorganisms, identifying them as interface between host and microbiota. Microorganisms are recognized based on conserved pathogen-associated molecular patterns (PAMPs) by Toll-like receptors (TLRs). Previously, it was shown that smooth muscle and myenteric plexus cells, but not epithelial cells, express TLR4, a subtype specifically recognizing the glycolipid lipopolysaccharide (LPS), an essential component of the cell wall of all gram-negative bacteria [71]. Later, TLR4 and other TLRs were explicitly shown on GFAP$^+$ EGCs [72]. Turco *at al* recently provided evidence that bacteria can activate EGCs by inducing the expression of cFos and MHC II proteins [73]. Bacteria are recognized by EGCs via TLRs, which are expressed at baseline and were shown to be upregulated in response to bacterial products. Interestingly, pathogens and probiotics differentially induced TLR subtype expression, implying a mechanism in EGCs to discriminate potentially pathogenic from commensal bacteria. Furthermore Turco *at al* found that TLR activation led to increased release of NO, and this increase was mediated via S100B, which was concomitantly increased, leading them to postulate a TLR/S100B signalling pathway interplay that regulates NO release.

These recent discoveries strengthen the role of EGCs in sensing and recognizing invading pathogens and in contributing to the inflammatory response in intestinal tissue.

1.6 Inflammatory bowel diseases (IBD)

Inflammatory bowel disease (IBD) is a chronic inflammatory disorder of the GI tract of unknown etiology. IBD mainly manifests as two diseases, CD and UC, with an estimated prevalence of 2.5-3 million people affected in Europe [74]. Industrialized countries, especially North America and Europe, have higher occurrence rates than non-industrialized countries, but a rise in previous low-incidence areas is currently being observed. The widely held hypothesis on IBD pathogenesis is that a dysregulated, overly aggressive mucosal immune response to commensal enteric bacteria develops in genetically susceptible individuals, with environmental factors favoring disease onset or progression [75]. Several disease features are shared in CD and UC, like a fluctuating chronic pattern, and acute as well as chronic inflammatory infiltrates within the LP [76]. But both conditions also display unique characteristics. Inflammation in UC-patients is confined to mucosa and submucosa and only affects the colon, starting from the anus and extending proximally. In CD, inflammation can affect any region and layer of the GI tract wall, often accompanied by fistula formation and weight loss [76] (see figure 1.4).

The basis for a chronic inflammation in IBD is the miscommunication between gut microbiota and the intestinal immune system at their contact interface, the intestinal epithelial barrier (IEB). In IBD, any of these three parties may be defective, leading to a breakdown of immune homeostasis. In the following paragraphs the IBD-specific alterations observed in these potential disease contributors are briefly described together with therapeutic strategies targeting these alterations.

Gut microbiota. Alterations in the microbial commensal flora have been documented in IBD-patients, including a decrease in diversity and changes in the relative proportions of bacterial phyla, collectively described as "dysbiota" [76]. Consequently, strategies have been developed to correct these abnormalities, leading from dietary changes, administration of antibiotics or probiotics to fecal microbiota transplantation. Even though these strategies are promising, limitations have been identified in the heterogeneity between CD and UC, different responsiveness of relapses and active disease and even region-specific differences along the GI tract. So far, these strategies have not yet achieved permanent effects [76, 79].

Intestinal immune system. Immune responses in IBD patients are dysregulated. As described in section 1.4, the mucosal immune system displays a constant low level of immune response by activated CD4-positive T cells in the healthy gut. In IBD patients, T cell responses are exaggerated, effector T cells (T_H1 and T_H2) predominate over anti-inflammatory Treg, and subsequently the cytokines released fuel a fulminant intestinal inflammation. The mechanisms leading to the imbalance towards effector T cells are diverse and vary in CD and UC. To achieve rapid remission from acute inflammatory flares, corticosteroids are usually administered, however, due to undesirable side effects prolonged use is not advised. Corticosteroids are anti-inflammatory
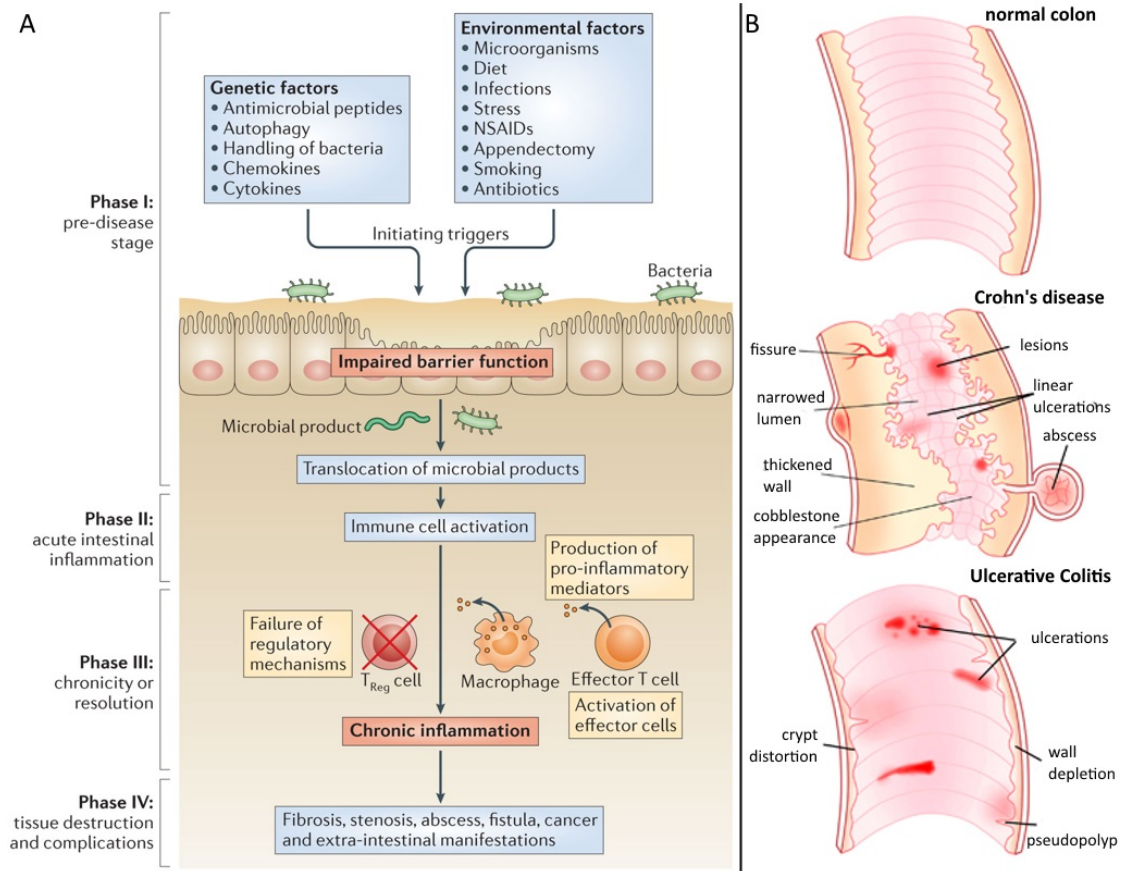
Figure 1.4: Conceptual pathogenesis and phenotypes of IBD. (A) Conceptual pathogenesis of IBD. Epithelial barrier function is impaired due to genetic and/or environmental factors. Bacteria and microbial products translocate into the bowel wall, wich leads to immune cell activation. If acute mucosal inflammation cannot be resolved, chronic inflammation manifests and can lead to tissue destruction. Adapted from [77]. (B) Schematic display of IBD phenotypes. Compared to healthy tissue (upper part), colonic tissue of CD-patients is affected in all layers of the gut wall (middle part), while inflammation in UC-patients only affects the mucosa and submucosa (lower part). Adapted from [78].

.

agents that act by downregulating the transcription of pro-inflammatory genes involved in cytokine production and inhibit the recruitment of immune cells [80]. A promising alternative to the administration of corticosteroids are biological agents. In IBD, the most widely used biological approach is an anti-TNF therapy with TNF-α-specific monoclonal antibodies, chiefly used in the treatment of CD and occasionally in UC. Anti-TNF-α antibodies neutralize soluble TNF-α, thereby altering cell signaling, and induce apoptosis of activated inflammatory cells expressing surface TNF-α [81]. Another recent therapeutic strategy in IBD is the cell-based approach, for which autologous stem cells are transplanted. The rationale is that the patient's immune system has a defect in self-tolerance, which might be restorable by immunosuppressive therapy followed by hematopoietic stem cell transplantation to restore the immune compartment [80].

First experimental and human studies yielded promising results but this strategy requires further testings.

IEB. The epithelial barrier is the contact interface between the host's immune system and the outside microbiota. Defects in the epithelium lead to increased intestinal permeability and are considered as an important contributor in the genesis of CD. It has been shown that not only do CD patients exhibit lowered epithelial resistance and increased permeability prior the clinical disease onset, but also healthy first-degree relative of a subset of IBD-patients [82]. As stated in section 1.3, EGCs are in intimate association with the epithelial cell layer and secrete factors that can increase barrier integrity. A contribution of EGCs to the initial barrier breakdown observed in IBD is currently not described. However, understanding strategies to stabilize the intestinal barrier further might be an important step in the management of IBD onset and progression and the beneficial effects of EGCs on epithelial impermeability are a promising starting point.

As pointed out earlier IBD is a multicausal condition, occurring in genetically predisposed individuals and triggered by environmental factors. The variety of disease contributors is reflected in a multitude of different strategies to experimentally induce an IBD phenotype. Animal models of IBD can be categorized into five broad groups: (1) gene knockout models, (2) transgenic rodent models, (3) spontaneous colitis models, (4) inducible colitis models and (5) adoptive transfer models [83, 84]. The choice of model is dependent on the scientific issue, however, chemically induced murine models are among the most commonly used models due to their immediate onset of inflammation, the controllability of duration and severity as well as the straightforward procedure. Several substances are well-established to induce intestinal inflammation, including dextran sulphate sodium (DSS) and trinitrobenzene sulfonic acid (TNBS). DSS is a sulfated polysaccharide that is administered in the drinking water, usually at a concentration of 2-5% (w/v). It can be administered continuously for a short period to induce an acute colitis or in a cyclical manner to evoke a chronic colitis. The resulting inflammation is caused by the toxic effect of DSS on gut epithelial cells that impairs the integrity of the mucosal barrier [85]. It is considered to be induced by innate but not acquired immunity [83].

TNBS, on the other hand, is a hapten, i.e. a small molecule capable of eliciting an immune response when bound to a carrier protein. Thus, TNBS haptenizes colonic proteins and renders them immunogenic to the host immune system, the resulting immune response in dependent on CD4-positive T_H cells [85]. Before TNBS is administered the mucosal barrier must destroyed with an ethanol enema.

To conclude, both DSS and TNBS can evoke a colon inflammation mimicking the phenotype of IBD. They vary in the mechanism of disease induction and the route of administration. A necessity for both chemically induced models is that the mouse strain is susceptible to the agents. [83, 85].

1.7 Sepsis as acute hyperinflammatory condition of the bowel

Sepsis is a systemic inflammatory response syndrome (SIRS) secondary to infection. It is one of the leading causes of death in critically ill patients due to organ failure and tissue hypoperfusion [86]. The intestine holds a special position in disease onset and progression, since it is both a source and target of the infection. It was long assumed that critical illness (caused by sepsis, trauma, burn or ischemia/reperfusion) leads to overgrowth of enteric pathogens and increased intestinal permeability, causing bacterial translocation over the gut wall, systemic spread and consequently multiple organ failure (MOF). This concept has recently been modified. Emphasis is no longer placed on bacterial translocation but on non-microbial tissue-injurious factors released from the intestine and spread systemically via the lymph [87, 88].

There is accumulating evidence that the pro-inflammatory mediators in lymph released from the GI tract influence gastrointestinal motility. Intestinal paralysis is a hallmark of sepsis that predisposes to luminal accumulation and bacterial translocation, potentiating the gut inflammatory response [89]. The mechanisms of how pro-inflammatory mediators lead to intestinal paralysis, also called ileus, are subject of research, since counteracting ileus might be highly beneficial in preventing life-threatening sepsis. In general, inflammatory mediators, mostly NO [90, 91] and prostaglandins [92], released by gut wall leukocytes can directly impair smooth muscle contractility. Importantly, such inflammatory mediators can also activate inhibitory neuronal pathways that dampen intestinal motility [93]. As described in section 1.5 the ENS and the gastrointestinal immune system are highly interconnected, the signaling molecules of one can convey information to the other and modulate its function. When inflammatory mediators activate vagal afferent fibers, the inhibitory reflex pathways triggered lead to a reduced gastrointestinal motility on the one hand and downregulation of the inflammatory activity of residential macrophages on the other hand [61, 94]. The strong interplay of intestinal immune and nervous system justifies further studies on the effect of the inflammatory milieu on ENS function. Importantly, previous studies have strongly focused on neuronal functions, whereas effects on the glial population is not understood yet.

1.8 Aim of the thesis

The regulation of principal GI-functions by the ENS such as motility, absorption and secretion has long been attributed to the actions of enteric neurons. Increasingly, regulatory functions of enteric glia are being recognized as well. These include modulation of synaptic transmission in neurons, of epithelial barrier integrity and of intestinal immune processes. The wide-ranging functions of EGCs have rendered them highly relevant for the study of intestinal tissue homeostasis and disruption thereof, as is the case in intestinal inflammatory diseases.

With increasing recognition of the fundamental role of EGCs comes the need to study the population in its complexity. Recent studies have revealed a considerable heterogeneity and phenotypic plasticity of EGCs. This heterogeneity covers site-specific subtypes along the luminal-serosal axis, including mucosal, ganglionic and interganglionic subtypes. There is also a heterogeneity in glial marker expression correlated to different functional states of EGCs, such as the cytoskeletal GFAP that is associated to a reactive phenotype.

For this reason, the overall aim of the thesis is to comprehensively study EGCs with focus on the reactive GFAP-expressing subpopulation under inflammatory conditions *in vitro* and *in vivo*. The following aspects will be addressed:

1. A novel *in vivo* rat model of acute systemic inflammation is employed to investigate rapidly occuring responses of EGCs to inflammation. Different segments along the rostro-caudal axis and the luminal-serosal axis are investigated to address region-specific differences.

2. The GFAP-expressing glial subpopulation is purified from hGFAP-eGFP mice that express an enhanced green fluorescent protein (eGFP) under the control of the human GFAP-promotor (hGFAP). The GFAP$^+$ population is expanded in 3D spheroids *in vitro*. The cultures are compared to the GFAP+ population *in vivo* and it is assessed how the transcriptomic and proteomic profiles of these cells change upon inflammatory stimulation.

3. The molecular inflammation-induced alterations in GFAP-EGCs found *in vitro* are correlated to findings obtained in an experimentally induced disease model of IBD in hGFAP-eGFP mice *in vivo*.

These studies aim to elucidate the mechanisms by which enteric glia influence intestinal pathophysiology. The results will allow the identification of crucial effector cell types that of EGCs. Knowledge on these interaction partners is crucial not only when considering therapeutic strategies to treat intestinal inflammation. They are further highly relevant when considering to build up *in vitro* test systems to model tissues *in vitro*. To be conclusive, these models need to incorporate the most relevant cell types to reflect the tissue's physiology accurately. To lay the basis for predictive *in vitro* models, a primary murine epithelial cell monolayer will be established on a suitable scaffold in co-culture with GFAP-EGCs.

2 Materials

2.1 Biological materials

For *in vivo* experiments male Sprague Dawley rats (obtained from Harlan Winkelmann, NM Horst, Netherlands), adult wildtype FVB mice (obtained from Charles River, Sulzfeld, Germany) and adult transgenice FVB/hGFAP-eGFP mice (kindly provided by Prof. Hirrlinger, University of Leipzig, Germany) [95] were employed. All animals were kept on a standard diet and water *ad libitum* at a 12 day and night cycle. Upon termination of the experiments animals were sacrificed in accordance with the ethical committee approval; rats received an overdose of isoflurane as approved (28/10, ethical committee of University Würzburg), mice received an overdose of carbon dioxide and cervical dislocation as approved (37/10, ethical committee of University Würzburg). Organs were removed from Lewis rats and early postnatal FVB/hGFAP-eGFP mice (postnatal day 7±2).

In vitro cell cultures were established from intestinal tissue digests obtained from early postnatal FVB/hGFAP-eGFP mice (postnatal day 7±2 days).

In preliminary experiments the human colorectal adenocarcinoma-derived cell line Caco2 was employed in passages P13 and P42. This cell line underwent spontaneous differentiation in culture displaying characteristics of mature enterocytes, which makes it a suitable alternative to primary IECs [96] and justifies their routine use in intestinal barrier transport studies [97].

2.2 Equipment and consumables

In table 2.1 all equipment is listed, in table 2.2 all laboratory materials and consumables are given.

Table 2.1: Laboratory equipment.

Designation	Specification	Manufacturer
Aspiration system	VACUSAFE	Integra Biosciences, Biebertal (G)
Autoclaves	Tecnoklav	Biomedis, Giessen (G)
	TableTop Autoclave	Systec, Wettenberg (G)
	Varioklav	H+P, Hackermoos (G)
Brush with magnet	Leica Brush	Leica, Wetzlar (G)
Cell culture safety cabinet	Safe2020	Thermo Fisher Scientific, Dreieich (G)
Cell incubator: 37 °C, 5%CO_2		Haraeus,Hanau (G)
		Continued on the next page

Table 2.1 Continued from the previous page

Designation	Specification	Manufacturer
Centrifuge	Multifuge X3R	Thermo Fisher Scientific, Dreieich (G)
Real-Time PCR Detection System	CFX96	Biorad,München (G)
Cold-storage room, 4 °C		Genheimer, Höchberg (G)
Cryostat	CM1850 UV Cryostat	Leica, Wetzlar (G)
Drying oven for microscopy slides	TDO 66	Medite, Dietikon (CH)
Experion Automated Electrophoresis Station		Biorad, München (G)
Experion Priming Station		Biorad, München (G)
Experion Vortex Station II		Biorad, München (G)
Freezers	-20 °C	Liebherr, Biberach (G)
	-80 °C	Kendro,München (G)
Fume hood		Prutscher Laboratory Systems, Neudörfl (AT)
Hand tally counter		neoLab, Heidelberg (G)
Horizontal gel system	PerfectBlue	Peqlab, Darmstadt (G)
Ice maschine	AF-80	Scotsman, Milan (I)
Immersion thermostat for water bath		Lauda, Lauda-Königshofen (G)
Medical pump	Asculap Microtron 60	B Braun, Melsungen (G)
Microbalance	SE2 Ultra	Sartorius Stedium Biotech, Göttingen (G)
Microcentrifuge	5417R	Eppendorf, Hamburg (G)
Microscopes	Biorevo BZ-9000	KEYENCE, Neu-Isenburg (G)
	Axiovert 40C	Carl Zeiss, Jena (G)
	AxioVision Observer.D1	Carl Zeiss, Jena (G)
	confocal TCS SP8	Leica Microsystems, Mannheim (G)
Microwave	NN-E205W	Panasonic
Minicentrifuge with strip rotor		Hartenstein, Würzburg (G)
Neubauer cell counting chamber		Hartenstein, Würzburg (G)
Orbital shaker	KM-2 Akku	Edmund Bühler, Hechingen (G)
PALM MicoBeam System		Carl Zeiss, Jena (G)
Paraffin Embedding Module	EG1150 H	Leica, Wetzlar (G)
PCR UV cabinet	Captair Bio	Erlab, Cologne (G)
pH meter		Mettler Toledo, Giessen (G)

Table 2.1 Continued from the previous page

Designation	Specification	Manufacturer
Pipets	0.5-10 μl, 10-100 μl, 100-1000 μl,	Eppendorf, Hamburg (G)
Pipetting aid Pipetboy		Brand, Wertheim (G)
Power supply for gel system		Peqlab, Darmstadt (G)
Precision balance	Kern PCB	Kern, Balingen-Frommern (G)
Real-time PCR detection system	CFX96	Biorad, München (G)
Rocking platform		neoLab, Heidelberg (G)
Septophag		Hesse, Emmerich (G)
SlideHolder 3x1.0		Carl Zeiss, Jena (G)
Sliding microtome	SM 2010R	Leica, Wetzlar (G)
Spin tissue processor	Microm STP 120	Thermo Fisher Scientific, Dreieich (G)
Stereo microscope	SteREO Discovery.V12	Carl Zeiss, Jena (G)
Thermocycler		SensoQuest, Göttingen (G)
Tissue float sbath	1052	Medax, Kiel (G)
Tissue Lyser	LT	Qiagen, Hilden (G)
Transilluminator		Vilber Lourmat, Torcy (F)
TubeCollector	2x500	Carl Zeiss, Jena (G)
Ultrapure water system		Millipore, Schwalbach (G)
Vortex shaker	Vortex-Genie 2	Scientific Industries via Carl Roth, Karlsruhe (G)
Water bath		Julabo Labortechnik, Seelbach (G)
Welding machine		Pro-System Verpackungstechnik, Schönnbrunn (G)

Table 2.2: Laboratory materials and consumables.

Designation	Specification	Manufacturer
Adhesive Caps	opaque, 200 μl	Carl-Zeiss Microscopy, Göttigen
Adhesive Seals	Microseal 'B'	Biorad, München (G)
Agarose gel combs		Peqlab, Darmstadt (G)
Agarose gel tray		Peqlab, Darmstadt (G)
Autoclaving Container	Stainless steel sterilization container	Fine Science Tools, Heidelberg (G)
Canule	Microlance	BD Biosciences, Heidelberg (G)

Table 2.2 Continued from the previous page

Designation	Specification	Manufacturer
Casting molds	Stainless steel	Labonord, Mönchengladbach (G)
Cell crowns		self constructed at TERM-department
Cell culture dish 35mm	Nunclon δ Surface	Thermo Scientific Nunc, Dreieich (G)
Cell culture multiwell plates	6 well, 12 well, 24 well	TPP, Trasadingen (G)
Cell Strainer EASYstrainer	40 μm, 70 μm, 100 μm	Greiner Bio-One, Frickenhausen (G)
Centrifuge Tubes	CELLSTAR 15 ml, 50 ml	Greiner Bio-One, Frickenhausen (G)
Cover slips for microscopy slides		Menzel-Gläser, Braunschweig (G)
Cryomolds	Tisssue-Tek Croymold	Sakura Finetek, Leiden (NL)
Embedding cassettes		Klinipath, Duiven (G)
Embedding filter paper		Labonord, Mönchengladbach (G)
Forceps	Standard, Dumont #3c, Dumont #5	Fine Science Tools, Heidelberg (G)
Humidity chamber		self constructed at TERM-department
Liquid repellent slide marker pen		DAKO, Jena (G)
Medical gloves	Nitril	Kimberly-Clark, Koblenz (G)
Membrane slide for LCM	NF 1.0 PEN	Carl-Zeiss Microscopy, Göttigen (G)
Microcentrifuge tubes	PCR clean 1.5 ml, 2 ml PCR soft tubes, 0.2 μl	Eppendorf, Hamburg (G) Biozym, Hessisch Oldendorf (G)
Microscopy slide racks	glass, stainless steel	Merceteo, München (G)
Microscopy slides	Super-Frost Plus	Langenbrinck, Emmerdingen (G)
Micro-spoon spatula		Hartenstein, Würzburg (G)
Multiplate for qPCR	Low-Profile 96-Well unskirted	Biorad, München (G)
PCR IsoFreeze Rack	with color indicator	LTF Labortechnik, Wassserburg (G)
PCR Tube Rack 96-Well with Cover		VWR, Darmstadt (G)

Table 2.2 Continued from the previous page

Designation	Specification	Manufacturer
Pipet tips	0.5-10 μl, 10-100 μl, 100-1000 μl	Nerbe plus, Winsen/Luhe (G)
Polyethylene foil tubing	30 cm x 0.2 mm	neoLab, Heidelberg (G)
Polysterene box		
QIAshredder spin columns		Biorad, München (G)
Scissors	Standard, Artery Scissors with Ball Tip	Fine Science Tools, Heidelberg (G)
Slide Box for microscopy slides		Hartenstein, Würzburg (G)
Staining dish with lid	105 x 85 x 70	Carl Roth, Karlsruhe (G)
Syringe	10ml Discardit II	BD Biosciences, Heidelberg (G)
Syringe filter	0.2 μm pore size, Minisart NML	Sartorius Stedium Biotech, Göttingen (G)
Tube clamps	up to 14 mmdiameter	Carl Roth, Karlsruhe (G)
Uncoated cell culture dishes	Petri dishes (94 mm, 145 mm)	Greiner Bio-One, Frickenhausen (G)

2.3 Chemicals and cell culture reagents

Table 2.3: Chemicals and cell culture reagents.

Designation	Catalog no.	Manufacturer
β-Mercaptoethanol	M31448	Sigma-Aldrich, München (G)
1,4-Dithiothreit	6908.4	Carl Roth, Karlsruhe (G)
2-Propanol	9866.6	Carl Roth, Karlsruhe (G)
Accutase solution	A6964	Sigma-Aldrich, München (G)
Acetic acid	6755.1	Carl Roth GmbH, Karlsruhe (G)
Agarose LE	840004	Biozym, Hessisch Oldendorf (G)
Albumin fraction V (BSA)	2834.4	Carl Roth, Karlsruhe (G)
Antibody Diluent Lab Vision OP Quanto	TA-125-ADQ	Thermo Scientific, Darmstadt (G)
B27-Supplement without Vitamin A	17504-044	Life Technologies, Darmstadt (G)
Benzyl alcohol	24122	Sigma-Aldrich, München (G)
Benzyl benzoate	B6630	Sigma-Aldrich, München (G)
Cell recovery solution (Corning)	734-0107	VWR, Darmstadt (G)
Chloroform	C2432	Sigma-Aldrich, München (G)

Table 2.3 Continued from the previous page

Designation	Catalog no.	Manufacturer
Collagenase NB IV 0,12 PZU/mg	17454	Serva Electrophoresis, Heidelberg (G)
Cresyl violet acetate	C5042	Sigma-Aldrich, München (G)
DAPI (1 mg/ml)	62248	Thermo Scientific, Darmstadt (G)
DeoxyribonucleaseI from bovine pancreas	DN25	Sigma-Aldrich, München (G)
Dextran Sulfate Sodium Powder 35-50 kDa	21011090	MP Biomedicals, Eschwege (G)
DMEM/F-12, GlutaMAX Supplement	31331-093	Gibco, Darmstadt (G)
DNA ladder plus 100-3000 bp	25-2020	Peqlab, Darmstadt (G)
Donkey serum	D9663	Sigma-Aldrich, München (G)
Ethanol, denatured, 96 %	T171.2	Carl Roth, Karlsruhe (G)
Ethylenediaminetetraacetic acid	431788	Sigma-Aldrich, München (G)
GelRed	M3199.0500	Genaxxon, Ulm (G)
GlutaMAX Supplement	35050-038	Life Technologies, Darmstadt (G)
Glycerin 85 % ("Babylax")		InfektoPharm, Heppenheim (G)
Heparin-Sodium 2500		Ratiopharm, Ulm (G)
Hepes (1M)	15630-080	Life Technologies, Darmstadt (G)
LPS from *E. coli* 0111:B4 potency 3 EU/ng	L2630	Sigma-Aldrich, München (G)
LPS from *E. coli* 026:B6 potency 3 EU/ng	L2654	Sigma-Aldrich, München (G)
n-hexane	139386	Sigma-Aldrich, München (G)
Matrigel matrix, Corning	FALC356231	Omnilab, Bremen (G)
MEM NEAA (100x)	11140035	Life Technologies, Darmstadt (G)
Minimal Essential Medium (MEM)	41090028	Life Technologies, Darmstadt (G)
Mounting media DAPI Fluoromount-G Entellan Mowiol	SBA-0100-20 1079610100 0713.1	Biozol, Eching (G) Merck, Darmstadt (G) Carl Roth, Karlsruhe (G)
N2-Supplement (100x)	17502-048	Life Technologies, Darmstadt (G)
N-Acetyl-L-cysteine	A9165	Sigma-Aldrich, München (G)
Na_2/EDTA	E5134	Sigma-Aldrich, München (G)
OCT compund Tissue-Tek	4583	LABART, Waldbüttelbrunn (G)
Ointment Bepanthen		Byer, Leverkusen (G)
Paraffin Roti-Plast	6642.6	Carl Roth, Karlsruhe (G)
PBS⁻	D8662	Sigma-Aldrich, München (G)
PBS⁺	D8537	Sigma-Aldrich, München (G)
Penicillin-Streptomycin (100x)	P4333	Sigma-Aldrich, München (G)
PFA 4 %	A3813	AppliChem, Darmstadt (G)
Picrylsulfonic acid (TNBS) 5 % in H_2O	P2297	Sigma-Aldrich, München (G)
recombinant proteins		

Table 2.3 Continued from the previous page

Designation	Catalog no.	Manufacturer
murine EGF	315-09	Peprotech, Hamburg (G)
murine FGF-basic	450-33	Peprotech, Hamburg (G)
murine Noggin	250-38	Peprotech, Hamburg (G)
murine R-Spondin	120-38	Peprotech, Hamburg (G)
RNAStabilization Reagent RNA*later*	76104	Qiagen, Hilden (G)
Roticlear	A538.5	Carl Roth, Karlsruhe (G)
Sodium Pyruvate (100mM)	11360039	Life Technologies, Darmstadt (G)
SsoFast EvaGreen supermix	172-5202	Biorad, München (G)
TE buffer pH 8.0	A2575	AppliChem, Darmstadt (G)
Tissue lysis reagent QIAzol	79306	Qiagen, Hilden (G)
TRIS (Trizma Base)	4855.1	Carl Roth, Karlsruhe (G)
Triton-X 100	3051.2	Carl Roth, Karlsruhe (G)
Trizma hydrochloride (Tris-HCl)	T5941	Sigma-Aldrich, München (G)
Tween 20	8.22184.0500	VWR, Darmstadt (G)

2.4 Composition of media and solutions

In table 2.4 the composition of all cell culture media are given, table 2.5 summarizes the composition of all other solutions employed.

Table 2.4: Composition of cell culture media.

Medium	Composition	
Caco-2 culture medium	80 %	Miminum Essential Medium (MEM)
	20 %	FCS
	1 %	Na-Pyruvat
	1 %	NEAA (100x)
	1 %	Penicillin-Streptomycin (100x)
Crypt culture medium	1 %	GlutaMAX Supplement
	10 mM	Hepes
	1 %	N2 (100x)
	1 %	B27 without Vitamin A (50x)
	1 %	Penicillin-Streptomycin (100x)
	1 μM	N-Acetyl-L-cysteine
		in Advanced DMEM
Complete crypt culture medium	50 ng/ml	murine EGF
	100 ng/ml	murine Noggin
	500 ng/ml	human R-spondin
		in Crypt culture medium
Glial basic culture medium	100 U/ml	penicillin
	10 μl/ml	N2 (100x)
	20 μl/ml	B27 without Vitamin A (50x)
		in DMEM/F-12 + GLUTAMAX

Table 2.4 Continued from the previous page

Medium		Composition
	40 ng/ml	murine EGF
Complete glial culture medium	40 ng/ml	murine bFGF
		in glial basic medium
	10 μl/ml	fibronectin
Surface coating solution	10 μl/ml	laminin
		in poly-ornithine

Table 2.5: Composition of solutions.

Solution		Composition
Antibody diluent for whole mount samples	20 % (v/v)	Permeabilization solution for whole mount samples in antibody diluent
Cell lysis buffer	10 μl/ml	β-Mercaptoethanol in RLT buffer (Standard or Plus)
Clearing solution	33.3 % (v/v) 66.6 % (v/v)	Benzyl benzoate Benzyl alcohol
Cresyl violet stain	10 mg/ml	Cresyl violet acetate in 50% EtOH filtered before use
DAPI staining solution	0.1 μg/ml	DAPI in PBS⁻ prepared freshly
DNase I incubation mix	10 μl 70 μl	Dnase I stock solution RDD Buffer mix by inverting
DSS solution	30 mg/ml	DSS powder in drinking water
Eosin	10 mg/ml	Eosin in deionized water
HCl/Ethanol	6.85 % (v/v)	HCl, 1M in 50 % (v/v) ethanol
Hemalaun(Mayer) after 4 weeks maturation	1.2 mg/ml 0.2 mg/ml 20 mg/ml 20 mg/ml 1 mg/ml	Hematoxylin NaI$_3$ Potassium alum Chloral hydrate Citric acid in deionized water
Permeabilization solution	0.2 % (v/v) 5 % (v/v)	Triton-X 100 donkey serum in PBS
Permeabilization solution for whole mount samples	0.5 % (v/v) 5 % (v/v) 1 % (w/v)	Triton-X 100 donkey serum BSA in PBS

Table 2.5 Continued from the previous page

Solution		Composition
TAE stock buffer (50x)	242 g	TRIS (Trizma Base)
	57,1 ml	acetic acid (100 %)
	100 ml	0.5 M Na_2/EDTA (pH 8.0)
	842.9 ml	deionized water
TBS stock, 0.5 M	78.8 g/l	Trizma hydrochloride
	87.66 g/l	NaCl
		in deionized water
TBS washing buffer 0.05 M	10% (v/v)	TBS stock
	0.5% (v/v)	Tween
		in antibody diluent
TNBS solution	300 μl	picrylsulfonic acid, 5 % in H_2O
	450 μl	H_2O
	750 μl	Ethanol
Washing buffer PBST	0.5 % (v/v)	Tween-20
		in PBS

2.5 Commercially obtained kits

Table 2.6: Commercially available kits.

Product name	Components	Manufacturer
Experion RNA HighSens Analysis Kit	RNA Highsens chips cleaning chips RNA gel RNA ladder RNA Highsens stain RNA Highsens loading buffer RNA sensitivity enhancer spin filters	Biorad, München (G)
iScript cDNA Synthesis Kit	iScript Reverse Transcriptase 5x iScript Reaction Mix Nuclease-Free Water	Biorad, München (G)
KAPA Mouse Genotyping Kit	10x KAPA Express Extract Buffer KAPA Express Extract Enzyme 2x KAPA2G Fast HotStart Genotyping Mix	Peqlab, Darmstadt (G)
RNeasy MinElute Cleanup Kit	RNeasy MinElute Spin Columns Collection Tubes (1.5 ml, 2.0 ml) Buffer RLT Buffer RPE Rnase-Free Water	Qiagen, Hilden (G)
RNeasy Micro Kit	Rneasy MinElute Spin Columns Collection Tubes (1.5 ml, 2.0 ml) Buffer RLT Buffer RW1 Buffer RPE Carrier RNA, polyA Rnase-Fre Dnase Set, including Rnase-Free Dnase I Buffer RDD Rnase-Free Water	Qiagen, Hilden (G)
RNeasy Micro Kit Plus	gDNA Eliminator Mini Spin Columns Rneasy MinElute Spin Columns Collection Tubes (1.5 ml, 2.0 ml) Buffer RLT Plus Buffer RW1 Buffer RPE Carrier RNA, polyA Rnase-Free Water	Biorad, München (G)

2.6 Oligonucleotides and resources for transcriptomic analyses

2.6.1 PCR primers for qPCR analysis and genotyping

Table 2.7: PCR primers employed in this work. TS = transcript size, bp = base pairs E = efficiency, AT = annealing temperature

Gene	NCBI RefSeq	Primer sequence	TS in bp	E. in %	AT. in °C
		Rattus norvegicus			
18S rRNA	M11188	GGGAGGTAGTGACGAAAAATAACAAT TTGCCCTCCAATGGATCCT	101	81.6	60
ACTB	NM_031144	GCAGGAGTACGATGAGTCCG ACGCAGCTCAGTAACAGTCC	74	92.9	60
Chat	NM_001170593	AAATGGCGTCCAACGAGGAT CCCGGTTGGTGGAGTCTTTT	114	n/a	60
Gfap	NM_017009.2	CCTGGAACAGCAAAACAAGGC TTTCATCTTGGAGCTTCTGCCTC	203	93.2	60
Nos1	NM_052799.1	AATCTCAGGTCGGCCATCAC ATCCCCCAAGGTAGAGCCAT	126	n/a	60
S100b	NM_013191.1	TTCAGGGAGAGAGGGTGACAA CTTCCTGCTCTTTGATTTCCTCC	104	85	60
Sod2	NM_017051.2	CCCAAAGGAGAGTTGCTGGAG CTGTAAGCGACCTTGCTCCT	144	n/a	60
Uchl1 (PGP 9.5)	NM_017237.2	TGAAGCAGACCATCGGGAAC GCCTGAATGGCCTCGTTCTT	178	n/a	60
		Mus musculus			
CIIta	NM_001243760	TGAACCACTTCCAGGCCATC AAGGCACAGTGGTATTCCCG	130	93.1	62.4
Hprt	NM_013556.2	GTTGGGCTTACCTCACTGCT TCATCGCTAATCACGACGCT	132	96.1	58
Il-1β	NM_008361	TGCCACCTTTTGACAGTGATG TGATGTGCTGCTGCGAGATT	138	89.2	60
Il-6	NM_031168.1	GCCTTCTTGGGACTGATGCT TGCCATTGCACAACTCTTTTCT	181	94.2	60
		Genotyping			
Gfap-eGFP		CAGGTTGGAGAAGGAGACGCATCA CCAGCTTGTGCCCCAGGATGT	157		60

2.6.2 nCounter Elements design

Table 2.8: Nanostring nCounter Codeset probes. Probes were designed to target the same genes at similar transcript positions as the Illumina probes of the microarray. The first 7 genes separated with a horizontal line were designed as reference genes. The colored background indicates the genes found to be most stably expressed in the dataset and were used as reference genes for data analysis.

Gene	Accession	Illumina ID	Target position	NanoString ID
B3gat1	NM_029792.1	ILMN_2724433	1552-1651	NM_029792.1:1551
Dctn5	NM_021608.3	ILMN_2732536	1220-1319	NM_021608.3:1219
Idh3b	NM_130884.4	ILMN_1235050	1296-1395	NM_130884.4:1295
Neu3	NM_016720.2	ILMN_2713763	2330-2429	NM_016720.2:2329
Nkiras1	NM_023526.3	ILMN_2649696	1030-1129	NM_023526.3:1029
Nupl1	NM_170591.1	ILMN_1245500	1439-1538	NM_170591.1:1438
Pdha1	NM_008810.2	ILMN_2679851	2280-2379	NM_008810.2:2279
Adam17	NM_009615.6	ILMN_2594718	4195-4294	NM_009615.6:4194
Agt	NM_007428.3	ILMN_1227398	1175-1274	NM_007428.3:1174
Bmp4	NM_007554.2	ILMN_1215252	1501-1600	NM_007554.2:1500
Bmp7	NM_007557.3	ILMN_2589662	1659-1758	NM_007557.3:1658
Camp	NM_009921.2	ILMN_2766604	376-475	NM_009921.2:375
Ccl11	NM_011330.3	ILMN_2647757	404-503	NM_011330.3:403
Ccl2	NM_011333.3	ILMN_1245710	199-298	NM_011333.3:198
Ccl5	NM_013653.3	ILMN_1231814	295-394	NM_013653.3:294
Cd40	NM_170702.2	ILMN_2502136	769-868	NM_170702.2:768
Cd82	NM_007656.5	ILMN_2747196	1410-1509	NM_007656.5:1409
Cdk5	NM_007668.3	ILMN_1216721	1736-1835	NM_007668.3:1735
Cebpb	NM_009883.3	ILMN_2756435	1148-1247	NM_009883.3:1147
Chil1	NM_007695.3	ILMN_2609813	1520-1619	NM_007695.3:1519
Csf1	NM_007778.4	ILMN_1254561	3970-4069	NM_007778.4:3969
Csf2	NM_009969.4	ILMN_2749412	798-897	NM_009969.4:797
Cxcl16	NM_023158.6	ILMN_2687586	1240-1339	NM_023158.6:1239
Cxcl9	NM_008599.4	ILMN_1215862	921-1020	NM_008599.4:920
Dag1	NM_010017.4	ILMN_2724585	4307-4406	NM_010017.4:4306
Fas	NM_007987.2	ILMN_2479290	419-518	NM_007987.2:418
Fgf5	NM_010203.5	ILMN_2642743	2179-2278	NM_010203.5:2178
Gfap	NM_010277.3	ILMN_1214715	1268-1367	NM_010277.3:1267
Glul	NM_008131.4	ILMN_2644496	2613-2712	NM_008131.4:2612
Gpc1	NM_016696.4	ILMN_2635784	3069-3168	NM_016696.4:3068
Hdac11	NM_144919.2	ILMN_2614912	2222-2321	NM_144919.2:2221
Hey2	NM_013904.1	ILMN_2657207	1853-1952	NM_013904.1:1852
Hgf	NM_010427.5	ILMN_2729117	2397-2496	NM_010427.5:2396
Hmga2	NM_010441.2	ILMN_2743802	3418-3517	NM_010441.2:3417
Id2	NM_010496.3	ILMN_1228557	625-724	NM_010496.3:624
Il13ra2	NM_008356.3	ILMN_1246284	1296-1395	NM_008356.3:1295
Il5	NM_010558.1	ILMN_2731160	1300-1399	NM_010558.1:1299
Il6	NM_031168.1	ILMN_1243601	647-746	NM_031168.1:646
Il6st	NM_010560.3	ILMN_2608184	5075-5174	NM_010560.3:5074
Irf5	NM_012057.3	ILMN_2621752	1827-1926	NM_012057.3:1826

Table 2.8 Continued from the previous page

Gene	Accession	Illumina ID	Target position	NanoString ID
Lama2	NM_008481.2	ILMN_2769479	8745-8844	NM_008481.2:8744
Lcn2	NM_008491.1	ILMN_2712075	420-519	NM_008491.1:419
Mmp2	NM_008610.2	ILMN_2678218	2666-2765	NM_008610.2:2665
Mmp9	NM_013599.3	ILMN_2711075	2986-3085	NM_013599.3:2985
Ncam1	NM_010875.3	ILMN_2722864	2434-2533	NM_010875.3:2433
Nfkb1	NM_008689.2	ILMN_2592476	3470-3569	NM_008689.2:3469
Nog	NM_008711.2	ILMN_2746870	1149-1248	NM_008711.2:1148
Olig1	NM_016968.4	ILMN_2760105	1909-2008	NM_016968.4:1908
Plp1	NM_011123.3	ILMN_1240381	2432-2531	NM_011123.3:2431
Pou3f1	NM_011141.2	ILMN_1233172	1386-1485	NM_011141.2:1385
Ptn	NM_008973.2	ILMN_2638114	1783-1882	NM_008973.2:1782
Rela	NM_009045.4	ILMN_2740859	2610-2709	NM_009045.4:2609
Reln	NM_011261.2	ILMN_2704257	11546-11645	NM_011261.2:11545
Ripk2	NM_138952.3	ILMN_2634970	1541-1640	NM_138952.3:1540
Runx1	NM_009821.3	ILMN_2589107	4143-4242	NM_009821.3:4142
S100b	NM_009115.3	ILMN_2634742	151-250	NM_009115.3:150
Socs3	NM_007707.3	ILMN_2618176	2376-2475	NM_007707.3:2375
Sox5	NM_011444.3	ILMN_1213910	2553-2652	NM_011444.3:2552
Tlr2	NM_011905.3	ILMN_2733733	2376-2475	NM_011905.3:2375
Tnc	NM_011607.3	ILMN_2485085	4883-4982	NM_011607.3:4882

2.6.3 GSE datasets employed in the comparative transcriptomic analysis

Table 2.9: GSE datasets employed in the comparative transcriptome analysis

Data set	Array Type	Array manufacturer	GSE	LPS
bladder	moex10stv1	Affymetrix	GSE15998	
BM derived neural crest cells	mouse430v2	Affymetrix	GSE30419	
cerebral cortex	moex10stv1	Affymetrix	GSE15998	
dorsal root ganglia	moex10stv1	Affymetrix	GSE15998	
embryonic and IPS cells	mouseRef8v2	Illumina	GSE36484	
embryonic and IPS cells	mouse430v2	Affymetrix	GSE10806	
embryonic and IPS cells	moex10stv1	Affymetrix	GSE36017	
endothelial progenitor cells	mouse430v2	Affymetrix	GSE29759	
epidermis	moex10stv1	Affymetrix	GSE15998	
GFAP-EGC-P7 in vitro	mouseRef8v2	Illumina	GSE78015	
GFAP-EGC-P7 in vitro +LPS	mouseRef8v2	Illumina	GSE78015	+
GFAP-EGC-P7 in vivo	mouseRef8v2	Illumina	GSE78015	
gut	moex10stv1	Affymetrix	GSE15998	
gut	moex10stv1	Affymetrix	GSE15998	
heart	mouse430v2	Affymetrix	GSE7196	
heart	moex10stv1	Affymetrix	GSE15998	
hippocampus	moex10stv1	Affymetrix	GSE15998	
kidney	moex10stv1	Affymetrix	GSE15998	

Table 2.9 Continued from the previous page

Data set	Array Type	Array manufacturer	GSE	LPS
liver	moex10stv1	Affymetrix	GSE15998	
lung	moex10stv1	Affymetrix	GSE15998	
MEF	mouse430v2	Affymetrix	GSE8024	
MEF	moex10stv1	Affymetrix	GSE26205	
MEF	moex10stv1	Affymetrix	GSE36017	
MEF	mouseRef8v2	Illumina	GSE30500	
MEF	mouseRef8v2	Illumina	GSE21516	
MEF	mouseRef8v2	Illumina	GSE36484	
mesenchymal stromal cells	mouse430v2	Affymetrix	GSE30419	
mesenchymal stromal cells	mouseRef8v2	Illumina	GSE31738	
NCSC	mouse430v2	Affymetrix	GSE11149	
neural progenitor cells	mouseRef8v2	Illumina	GSE36484	
neural progenitor cells	mouse430v2	Affymetrix	GSE8024	
neural progenitor cells	mouse430v2	Affymetrix	GSE10806	
neural progenitor cells	mouse430v2	Affymetrix	GSE29759	
neural progenitor cells	mouseRef8v2	Illumina	GSE30500	
olfactory bulb	moex10stv1	Affymetrix	GSE15998	
ovary	moex10stv1	Affymetrix	GSE15998	
placenta	moex10stv1	Affymetrix	GSE15998	
prostate	moex10stv1	Affymetrix	GSE15998	
sceletal muscle	moex10stv1	Affymetrix	GSE15998	
spinal cord	moex10stv1	Affymetrix	GSE15998	
stomach	moex10stv1	Affymetrix	GSE15998	
umbilical cord	moex10stv1	Affymetrix	GSE15998	
uterus	moex10stv1	Affymetrix	GSE15998	
astrocytes	mouseRef8v2	Illumina	GSE43808	-
astrocytes +LPS	mouseRef8v2	Illumina	GSE36089	+
GFAP-EGC-P7 in vivo	mouseRef8v2	Illumina	GSE78015	-
GFAP-EGC-P7 in vitro	mouseRef8v2	Illumina	GSE78015	-
GFAP-EGC-P7 in vitro +LPS	mouseRef8v2	Illumina	GSE78015	+
microglia 2	mogene1.0_st	Affymetrix	GSE49329	-
microglia 2 +LPS	mogene1.0_st	Affymetrix	GSE49329	+
microglia 1	mouseRef8v2	Illumina	GSE43808	-
sciatic nerve, adult	mouseRef8v2	Illumina	GSE44605	-
sciatic nerve	mouseRef8v2	Illumina	GSE16741	-

2.7 Antibodies

Table 2.10: Primary antibodies used in this study.

Antibody	Clone	Dilution	Host	Manufacturer	Cat. no.
α smooth muscle actin	1A4	1:100	mouse	Abcam, Cambridge (UK)	ab7817
ECad	36	1:100	mouse	BD Biosciences, Heidelberg (G)	610181
GFAP		1:600	rabbit	Dako, Hamburg (G)	Z0334
HuC/D	16A11	1:100	mouse	Invitrogen, Karlsruhe (G)	A-21271
p75NTR		1:250	rabbit	Promega, Mannheim (G)	G3231
S100B	SH-B1	1:100	mouse	Abcam, Cambridge (UK)	ab66028
SOX10	"3 gp"	1:700	guinea pig	provided by Prof. Wegner, University of Erlangen	
Vimentin	EPR3776	1:100	rabbit	Abcam, Cambridge (UK)	ab8069
AF 647 anti-mouse CD4	GK1.5	1:200	rat	BioLegend, San Diego (US)	100426

Table 2.11: Secondary antibodies used in this study.

Antibody	Dye	Dilution	Host	Manufacturer	Cat. no.
anti guinea-pig	AF 488	1:400	goat	Invitrogen	A-11073
anti mouse	AF 555	1:400	donkey	Invitrogen	A-31570
anti mouse	AF 647	1:400	donkey	Invitrogen	A-31571
anti rabbit	AF 555	1:400	donkey	Invitrogen	A-31572
anti rabbit	AF 647	1:400	donkey	Invitrogen	A-31573

2.8 Software

Table 2.12: List of software employed in this work.

Software	Application	Manufacturer
CFX Manager 3.1	recording of qPCR data	Biorad
Citavi 4	Reference mangement	Swiss Academic
Corel Draw X6	Graphic design	Corel
	Continued on the next page	

Table 2.12 Continued from the previous page

Software	Application	Manufacturer
Experion Software	Analysis of Automated Electrophoresis System	Biorad
FlowJo V10	FACS analysis	
GraphPad Prism	Graphic design	GraphPad
ImageJ v1.38	Pixel quantification Area measurements	NIH
Keyence BZ-II Viewer	Fluorescence microscopy	Keyence
LAS AF	Confocal microscopy	Leica
MegaCapt	Gel documentation	Vilber
NCBI Nucleotide BLAST	Primer design	NIH
NCBI Primer-Blast	Primer design	NIH
NCBI Probe Database	Primer design	NIH
nSolver 2.5	nCounter data analysis	Nanostring Technologies
RoboSoftware	Laserdissection	PALM
SPSS	Statistical analysis	IBM
Volocity	3D imaging software	PerkinElmer
Zen 2012	Fluorescence microscopy	Carl Zeiss

3 Methods

3.1 Establishment of disease models *in vivo*

3.1.1 Rat animal model of hyperinflammation

The hyperinflammation model was established by experienced anesthetists (Dr. Martin Schick & Dr. Jabob Wollborn) at the University Hospital Würzburg upon animal care committee approval (approval number 48/10) as published by the group [98, 99]. Briefly, 10 male Sprague Dawley rats (mean weight: 0.330±0.025 kg) were kept on a standard diet and water *ad libitum* at 12 h day and night cycles. A continuous intensive care set-up was chosen to closely monitor temperature and macrohemodynamic changes. Animals were anesthetized and randomized into a control and a LPS-treated group, n = 4 each. Control animals received a 0.5 ml intravenous bolus of NaCl as placebo, whereas LPS (E. coli O111:B4) was applied intravenously at a concentration of 2.5 mg/kg in the LPS-group. After 3.5 h laparotomy was performed and 4 h after LPS-injection animals were sacrificed via overdose of isoflurane.

Intestinal tissue samples of 1-2 cm length were taken from the duodenal, ileal and proximal colonic parts. For histochemical analyses samples from each animal and intestinal region were embedded in optimal cutting temperature (OCT) compound in cryomolds, frozen on dry ice and stored at -80 °C. For gene expression analyses samples were submersed with RNA stabilization reagent overnight at 4 °C, afterwards removed from the reagent and transferred to -80 °C until further use.

3.1.2 Murine animal model of acute IBD

The acute IBD animal model was induced in 4-6 months old FVB/N-mice with DSS and TNBS, two substances that trigger disease phenotype by different mechanisms (see section 1.6). In total 80 mice were incorporated in the study and assigned to one of the four treatment groups: DSS-treated, DSS control-treated, TNBS-treated and TNBS control-treated. Of the 20 animals per group, 10 animals (5 male, 5 female) were wildtype FVB/N-mice and the other 10 animals (5 male, 5 female) were hGFAP-eGFP transgenic animals. The study design is schematically presented in figure 3.1.
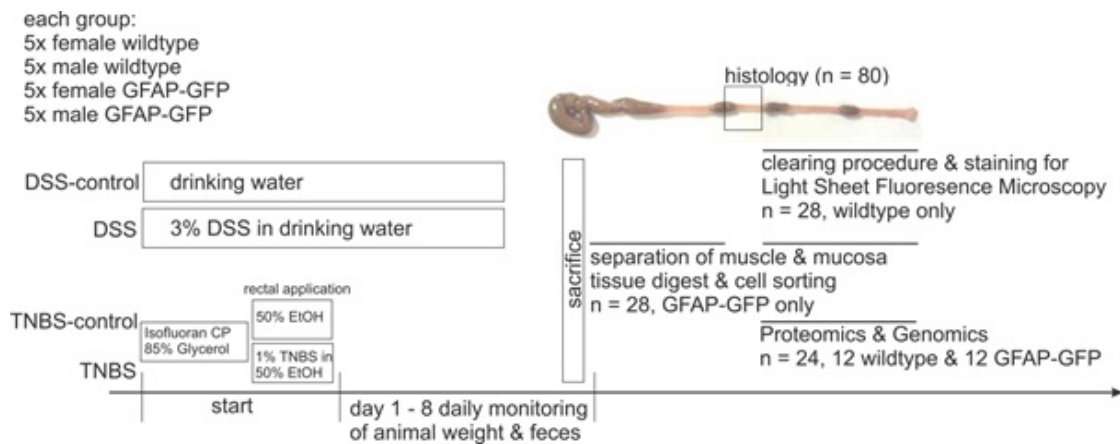

Figure 3.1: Study design of the acute IBD animal model For further illustration please refer to section 3.1.2. The processing of the tissue after animal sacrifice is explained in section 3.2.2.

On four starting timepoints (03.02., 04.02., 12.02., 13.02.2014), 5 animals of each group, either all males or all females, were launched, this way not all 80 animals had to be handled simultaneously. If same-sex animals of one group were littermates and had been sitting in one cage together, they were left together for the course of the experiment. On the starting date all animals were weighted. Animals of the DSS group were not further treated by received fresh drinking water supplemented with 3 % DSS solution, approx. 50 ml per animal in the cage. Animals of the DSS control-group received untreated drinking water. After four days the (DSS-supplemented) drinking water was replaced. Animals of the TNBS group received a rectal application of a 1 % TNBS solution. To do so animals were anesthetized with CO_2 and ointment (Bepanthen) was applied to the rectum with a cotton swab as lubricant. A self-constructed enema made from a syringe and a silicon tube was inserted and glycerin was injected to induce emtying of the bowel. Animals were put in a cage lined with paper until defecation occured. Afterwards, animals were anesthetized again and the cleaned enema was used to apply the TNBS-solution to the TNBS group or the solvent (50 % EtOH) to the TNBS control-group.

For the following 7 days of experiments, animals were weighted daily and assessed for their overall physiological and behavioral appearance. Further, every animals was separately placed in a cage

to defecate. Weight loss, feces consistency and fecal blood were assessed and scored with the scoring values given in table 3.1.

Table 3.1: Scoring system for the assessment of the IBD model.

Score	Parameter		
	Weight loss	**Feacal blood**	**Feacal consistency**
0	weight increase	no blood in feces	normal appearance
0.5		very little blood in feces	fawn, lightly smooth, dry
1	0%-5% weight loss	faintly red-colored feces	fawn, smooth, dry
1.5			smooth, moist, fibrous
2	5%-10% weight loss	distinctly red-colored feces	very smooth, very moist, mushy
3	$\geq 10\%$ weight loss		

3.2 Murine intestinal tissue preparation

3.2.1 Early postnatal small intestinal LMMP preparation

Small intestinal longitudinal muscle-myenteric plexus (LMMP) strips from early postnatal mice (postnatal day 7±2 days) were used to generate purified glial cell cultures. Briefly, transgenic FVB/hGFAP-eGFP were mated with transgenic FVB/hGFAP-eGFP mice or wildtype FVB mice. When a litter reached approx. postnatal day 7, all littermates were removed from the animal facility and placed in a polystyrene box filled with ice and covered with several layers of paper towel to induce anaesthesia by hypothermia. After approx. 10 minutes animal movement was significantly decreased and animals were decapitated swiftly with sharp scissors. The abdomen was torn off with forceps and the small intestines were removed and microscopically screened for GFP-positivity. Small intestines from transgenic pubs were transfered to a dish filled with cold PBS$^+$ and LMMP strips were peeled off of the remaining intestine with fine forceps (see figure 4.6). LMMP strips were transferred to a centrifuge tube and enzymatically digested in a sterile-filtered PBS$^+$-solution with 0.5 mg/ml collagenase and 0.5 mg/ml dispase at 37$°$C on an orbital shaker. The enzymatic digest was performed for 20 min, interrupted twice for vigorous trituation using 1000 μl tips. To terminate the digest, chilled DMEM/F-12 medium was added and the suspension was immediately centrifuged (1200 rpm, equivalent to 300 g, 5 min). The supernatant was discarded and the pellet resuspended in 5 ml fresh DMEM/F-12 medium. The cell suspension was filtered over a series of cell strainers placed on falcon tubes (100 μm, 70 μm, 40 μm pore size) to ensure homogenization. After a second centrifugation step the cells were resuspended in 500 μl of glial basic medium. At the core facility for cell sorting (IZKF Würzburg), the GFP$^+$ positive cell fraction was sorted and collected in 3 ml glial basic medium. To minimize the danger of bacterial contamination from the non-sterile sorting procedure, cells were washed with glial basic medium and seeded on cell culture dishes that had been coated with poly-ornithine, fibronectin and laminin for 1 h at RT and subsequently washed with DMEM/F-12

medium. Epidermal growth factor (EGF, 40 ng/ml) and basic fibroblast growth factor (bFGF, 40 ng/ml) were added to give complete glial medium (see table 2.4), and cells were cultured under hypoxic conditions (2 % O_2) in a humidified incubator at 37 °C. Cell culture dishes were placed in a PET tubing foil welded to generate a bag with a silicone tube inlet closed with a tube clamp. Via the tube inlet a gaseous mixture (5 % CO_2, 2 % O_2) was introduced to generate an oxygen-reduced atmosphere.

3.2.2 Adult colon tissue preparation

4-6 months old transgenic hGFAP-eGFP FVB/N mice were euthanized by carbon dioxide over-dose and cervical dislocation. Death was confirmed by cardiac arrest and negative pedal reflex. Organ removal procedure depended on the the further processing of the tissue (see also figure 3.1).

Tissue preparation from animals designated for light sheet fluorescence microscopy (n = 28) required whole-animal perfusion fixation to preserve the intestinal micro-architecture. Cervical discolation was not performed in these animals, instead the thorax was opened immediately after death to expose the heart. A cannula was inserted into the left heart ventricle and an outlet for blood and the fixative was created by an incision in the right atrium of the heart. Via the cannula first PBS$^-$ supplemented with heparin (0.2 %) was injected for approx. 2 min to clear out the blood and to prevent coagulation. Immediately afterwards 4 % paraformaldehyde (PFA) was injected as fixative. The cannula was connected to a self-constructed tubing system that was attached to two reservoir bottles, connected via a mechanical switch. This set-up allowed to inject the solutions successively without introducing air into the animal's vascular system. PFA was injected until the animal stiffened. Subsequently, the abdomen was opened, the colon was removed and a segment of the colon was processed in a whole-mount staining for light sheet fluorescence microscopy (3.5.6).

In the remaining animals the adomen was opened with scissors and the colon was removed by incisions posterior to the cecum and in the rectal segment. The tissue was transferred to a petri dish filled with PBS$^+$ and cleared of feces by flushing with a syringe filled with PBS$^+$. The tissue was opened longitudinally and a segment (approx. 1 cm) located at the center of the colon length was removed for histological analyses. To facilitate enzymatic digest of the remaining tissue, the muscle and the mucosal tissue layers were mechanically separated, minced and digested individually. Both fractions were enzymatically digested in sterile-filtered 0.5 mg/ml collagenase and 3 mg/ml dispase in a total volume of 5 ml PBS$^+$ at 37 °C on an orbital shaker for 20 min. The solution for the mucosal fraction was supplemented with mucolytic dithiothreitol (DTT, 1 mM). Following incubation, the suspension was triturated and filtered over a 100 μm cell strainer placed on a falcon tube and the flow-through was collected in cooled FACS-buffer (0.5 % BSA, 2 mM EDTA in PBS$^-$). The restrained tissue fragments were transferred to a fresh aliquot of digestion solution and the incubation was repeated. After the second filtration the remaining tissue fragments were transferred to another aliquot of digestion solution supple-

mented with 0.5 mg/ml DNase I to prevent cell clumping by free DNA fragments. The pooled flow-throughs from the three incubations were centrifuged (500 g), the pellet was resuspended in 500 μl cooled FACS-buffer and filtered over a 40 μm cell strainer to avoid blocking of the FACS nozzle. The two cell suspensions from the mucosal and the muscular digest were pooled and the GFP$^+$ positive cell fraction was sorted at the core facility for cell sorting (IZKF Würzburg), collected in lysis buffer see section 3.7.1 and stored at -80 °C until further use.

3.3 *In vitro* cell culture of GFAP-eGFP EGCs

Murine primary GFAP-EGCs were cultured after the isolation (P0) in adherent cell culture and after the first passage (P1) in free-floating neurosphere-like bodies, hereinafter called gliospheres [100]. To do so, the cell culture medium was removed, warmed cell detachment solution (Accutase) was added and incubated at 37 °C until cells had detached from the coated cell dish. The cell suspension was transferred to a centrifuge tube and pelleted (200× g, 3 min). To wash the suspension, the supernatant was removed, fresh DMEM/F-12 was added and centrifuged again. The cells were resuspended in fresh complete glial medium and seeded on uncoated cell culture dishes to promote spheroid formation. Due to the low yield of GFAP$^+$ cells, cells were splitted in a 1:1 or 1:2 ratio.
Cell culture medium was changed every 2-3 days by 50%. The growth factors EGF and bFGF were freshly supplemented every day if possible at full concentration (40 ng/ml each).

3.3.1 LPS-stimulation

For LPS-stimulation experiments, adherently expanded GFAP-EGCs (see section 3.2.1) were passaged after 2 weeks of culture. Cells from each animal preparation were split into two six well dishes. After gliospheres had formed, one subculture was stimulated with LPS (100 μg/ml, from E. coli O26:B6) dissolved in complete glial medium, the other subculture received fresh complete glial medium. After 48 h cell culture supernatants were collected for cytokine measurements (3.8) and cells were processed for total RNA isolation (3.7.1).

3.4 Establishment of 3D co-culture models of enteric neural cells and IECs *in vitro*

This section describes methods employed in preliminary studies and exemplary results are presented as an outlook on future studies. The methods employed to generate these data are hence only briefly outlined.

3.4.1 Generation of the decellularized small intestinal submucosal (SIS) biological matrix

The decellularization protocol employed here for producing a cell-free small intestinal submucosal (SIS) matrix relies on the dissolution of the cell membrane's lipid bilayer by sodium deoxycholate, which leads to complete cell lysis, and nuclease-mediated removal of residual nucleic acids. The

complete protocol has been published by our group, please refer to our publication for details [101]. Depending on the intended use, the SIS can be produced with a preserved mucosa (SIS-muc) or with the mucosa removed (SIS). The former is particularly suited for creating intestinal tissue models with a 3D tissue architecture closely resembling the native situation, the latter is rather suited for creating a barrier model, since the rather even surface facilitates the formation of a tight monolayer.

Figure 3.2: Decellularized small intestinal submucosa as biological matrix for 3D system systems. After decellularization the intestinal segment appears white and is free of any cells. For seeding experiments the intestinal tube is cut open and fixed between two metal rings with both the former serosal/muscular side and the former mucosal side accessible for seeding.

3.4.2 Seeding of cells onto the biological SIS-scaffold

To establish the mono-culture of primary murine epithelial cells on the SIS, organoids cultured in matrigel droplets (not described in this work) were dissolved out of the matrigel by addition of 500 μl cold cell recovery solution, thorough resuspension and incubation for 45 min on ice. Supernatants from all wells were pooled in a 50 ml tube, diluted with PBS$^-$ and centrifuged (350$\times$ g, 3 min). The supernatant was discarded, the organoids were further disaggregated by trituration and resuspended in crypt medium. The suspension was seeded on SIS fixed between two small rings and previously coated with matrigel (matrigel dilution 1:100 in Crypt culture medium). Wells were filled with Complete Crypt culture medium supplemented with 15 % Wnt3a-conditioned medium. After 3 days of static culture, the medium was replaced by Wnt3a-free medium and culture was continued under "dynamic conditions" on an orbital shaker in the incubator (80 rpm). Matrices were kept in culture for 2 weeks and afterwards fixed. To do so, medium was removed, matrices were washed with PBS$^-$, submersed with fixative for 2 h and paraffin-embedded as described in section 3.5.2

To establish the co-culture, enteric neural cells, isolated from early postnatal small intestinal LMMP preparation analogous to the isolation of GFAP-EGCs but without cell sorting (see section 3.2.1), were employed. Neurosphere-like bodies were dissociated as described in section 3.3 and a total of 1×10^5 cells in 500 μl glial basic medium (passage P2) were seeded on the former serosal/muscular side of the SIS fixed between two metal rings (area: approx. 1.2 cm^2). Cells were left to adhere for 3 h and afterwards wells were filled with glial complete medium (800 μl

in inner compartment of cell crown, 1.6 ml in outer compartment) and cultured under standard conditions.

After 3 days cell crowns were inverted so that the former mucosal side faced upwards. Caco-2 cells were seeded on the former mucosal side in a total cell number of 2.4×10^5 cells per cell crown in 100 μl Caco-2 medium. After 2 h for adherence, cell crowns were inverted and filled with glial basic culture medium supplemented with 2 % fetal calf serum (FCS). Cell crowns were cultured under standard conditions with medium change every 2-3 days for 2 weeks and afterwards fixed (see above).

3.5 Staining procedures

3.5.1 Preparation of cryosections

Intestinal tissue samples embedded in OCT compound were removed from the cryomolds and mounted onto specimen discs. At a working temperature of -20 °C, 12 μm sections were generated and mounted on microscopy slides. Samples were dried at RT for 10 min and stored at -80 °C. For laser capture microdissection, sections were placed on PEN-membrane coated slides that were previously UV-treated in a PCR UV cabinet for 30 min. The exposure to UV-light counteracts the membrane's hydrophobic character and destroys potentially contaminating nucleid acids.

3.5.2 Paraffin embedding and preparation of paraffin sections

Intestinal tissue segments from DSS-treated mice were embedded in paraffin for histological scoring. Segments of 1 cm length were cut open with a ball-tipped scissor and fixed on a cork plate before submersing the tissue in fixation solution (4% PFA). Tissues were fixed in 6 well plates for 6 h at RT, removed from the cork plate and transferred to embedding cassettes lined with filter paper with forceps. Embedding cassettes were placed in a beaker filled with tap water for 1 h and consequently transferred to the water compartment of the automated spin tissue processor. Tap water in the first station was changed before every run, the remaining solutions were changed once a month and paraffin pellets were refilled if necessary. Embedding was performed according to table 3.2.

Table 3.2: Paraffin embedding protocol of the spin tissue processor.

Solution	Time in h	Process
Tap water	1	Washing out of fixative agent
50 % (v/v) Ethanol	1	
70 % (v/v) Ethanol	1	
80 % (v/v) Ethanol	1	Dehydration
96 % (v/v) Ethanol	1	
2-Propanol I	1	
2-Propanol II	1	
2-Propanol/Roticlear 1:2	1	
Roticlear I	1	Removing of alcohol
Roticlear II	1	
Paraffin I	1.5	Infiltration with paraffin
Paraffin II	1.5	

Afterwards, the paraffin-infiltrated tissue was removed from the embedding cassette and transferred to a heated paraffin embedding module. Here, the tissue was placed in a preheated stainless steel casting mold filled with liquid paraffin. Using preheated forceps, the tissue was aligned with a longitudinal cutting edge facing the bottom of the mold and paraffin was allowed to completely harden at RT. Tissue sections of 5 μm thickness were generated with a sliding microtome and transferred to microscopy slides after straightening in a heated tissue float bath. Tissue sections were allowed to dry at 37 °C overnight and either stored at RT or directly processed for staining. Prior to staining, the sections had to be deparaffinized and rehydrated. To melt the paraffin, sections were incubated at 60 °C for 1 h and then processed as described in table 3.3

Table 3.3: Deparaffinization and rehydration of paraffin sections.

Solution	Time in min	Process
Roticlear I	10	Deparaffinization
Roticlear II	10	
96 % (v/v) Ethanol I	dip 3 times	
96 % (v/v) Ethanol II	dip 3 times	
70 % (v/v) Ethanol	dip 3 times	Rehydration
50 % (v/v) Ethanol	dip 3 times	
Deionized water	1	

3.5.3 Hematoxylin and eosin (H&E) stain

H&E-stains are a principal histological approach to gain an overview of a tissue's morphology. The two dying components employed are hemalaun and eosin. The former is prepared from hematoxylin, a basic (i.e. positively charged) compound that binds to the negatively charged phosphate backbone of nucleic acids and thereby stains a cell's nucleus blue. The structures

stained by hemalaun are referred to as basophilic. The latter is acidic (i.e. negatively charged) and binds to basic amino acid residues in eosinophilic cytoplasmic proteins, thereby staining the cytoplasm red.

After deparaffinization (see table 3.3) the staining procedure was performed, given in table 3.4. Sections were subsequently mounted with rapid mounting medium for microscopy.

Table 3.4: H&E staining procedure.

Solution	Time in min	Process
Hemalaun	8	Staining of basophilic structures
Deionized water	until clear	Rinsing off excess hemalaun
HCl/Ethanol	dip 3 times	Differentiation of hemalaun
Deionized water	1	Rinsing off HCl/Ethanol
Tap water	5	Blueing
Eosin	1	Staining of eosinophilic structures
Deionized water	until clear	Rinsing off excess eosin
70 % (v/v) Ethanol	dip 3 times	
96 % (v/v) Ethanol I	2	
2-Propanol I	5	Dehydration
2-Propanol II	5	
Roticlear I	5	
Roticlear II	5	

3.5.4 Cresyl violet stain for laser capture microdissection

Samples mounted on PEN membranes for LCM were quickly stained with 1 % cresyl violet acetate, a basic stain that visualizes cell nuclei. Cresyl violet is dissolved in ethanol, which is a great advantage in sample preparation for LCM, since it inhibits the activity of endogenous RNases. The staining protocol of samples prior to LCM is given in table 3.5. The storage of solutions and the staining procedure were done at $4\,^{\circ}$C to further limit RNase activity.

Table 3.5: Cresyl violet staining procedure.

Solution	Time in min	Process
RNase-free water	dip into solution	Removal of excess OCT compount
70 % EtOH	2	Fixation
1 % Cresyl violet stain	0:30	Staining
		Remove excess stain
70 %	dip into solution	Dehydration
100 %	dip into solution	
	1-2	air-dry under fume hood

3.5.5 Immunohistochemistry

Immunohistochemistry (IHC) refers to the detection of macromolecules based on the specific binding of an antibody to its antigenic determinant. Antibodies are proteins synthesized by the immune system that identify foreign compounds to initiate their neutralization. In immunohisto-chemistry, this specific recognition and binding is used for visualization of the macromolecule of interest. An antibody bound to its specific antigenic determinant with its Fab region (fragment antigen-binding) can act as an antigenic determinant itself: its species-specific crystallibsable fragment (Fc) can be recognized and bound by so-called secondary antibodies directed against the species in which the primary antibody was produced. The secondary antibody is conjugated to a labeling agent, either to an enzyme that catalyzes a chromogenic substrate reaction or to a fluorescent dye. Both detection techniques have advantages, the former incorporates an additional signal amplification step by the enzymatic catalysis, the latter allows to differentiate antibodies raised in different species by differently conjugated secondary antibodies. In this work the fluorescent dye-based detection was chosen. Detection via a chromogenic substrate was only employed in preliminary experiments using the the IHC-Kit "'"DCS SuperVision 2 HRP" (DCS Innovative Diagnostik-Systeme).

Immunohistochemistry was performed on cryosections, small intestinal longitudinal muscle-myenteric plexus (LMMP) strips and gliospheres. Samples were fixed with 4 % PFA, the duration of fixation depended on a sample's thickness: cryosection were fixed for 10 min, LMMP strips and gliospheres for 30 min. Cryosections on slides were quickly dipped into deionized water to remove access OCT compount and circling of samples with a liquid repellent slide marker pen was done to limit the reagents' required volume. All incubation steps were performed in a darkened humidity chamber at RT, if not indicated otherwise in table 3.6, all washing steps were performed on a rocking platform in darkened staining dishes. Prior to antibody incubation, samples were incubated with a permeabilization solution to ensure access of the antibody to its antigen. This solution was supplemented with serum from the species in which the secondary antibody was raised to saturate unspecific binding sites. Following this permeabilization and blocking, the antibody dilutions as given in table 2.10 were applied. The staining protocol is given in table 3.6.

Table 3.6: Immunohistochemical staining procedure.

Solution	Time in min	Process
Permeabilization solution	30	Permeabilization and blocking
Primary antibody dilution	overnight at 4 °C	Incubation
TBST	3×5	Washing
Secondary antibody dilution	60	Incubation
TBST	3×5	Washing

False-positive staining results due to unspecific antibody bindings were tested and excluded in negative controls in the absence of primary antibodies. Cryosections were mounted with an aquaous mounting medium supplemented with DAPI, an intercalating agent that stains nuclei blue. Gliospheres were incubated in DAPI staining solution prior to microscopy.

3.5.6 Whole-mount staining for light sheet fluorescence microscopy (LSFM)

After whole-animal perfusion fixation (3.2.2) colon tissue was removed, cleared from feces and postfixed overnight in 4 % PFA at 4 °C. The fixation and staining procedure was performed in 24 well plates at 4 °C on a rocking platform. The final steps involving the clearing solution were conducted in small sealable glass containers, since the clearing solution degrades the polystyrol-plates. The protocol was adapted from the collaborating laboratory of Prof. Beilhack [102] and is given in table 3.7. After immunohistochemical staining and dehydration, an optical clearing of the tissue was performed. The technology relies on the immersion of a sample in a medium with a refractive index similar to that of lipids to reduce the scattering of light. Thereby the sample becomes transparent and a thin plane of light (i.e. a light sheet) can optically section the sample. The advantage of this technique is that it allows a fast, nondestructive scanning of a thick tissue segment that can be reconstructed into a three-dimensional representation [103]. Microscopy was performed in collaboration with Prof. Beilhack's group from the center for Experimental Molecular Medicine (Department of Medicine II, University Hospital Würzburg) at a multicolor LSFM self-constructed by the group. Briefly, samples were co-stained with a mouse anti-CD4 antibody directly conjugated to Alexa Fluor (AF) 647 and a rabbit anti-GFAP antibody detected with secondary antibody conjugated to an AF 555. After clearing, samples were fixed to a home-built glass rod and placed in a homebuilt coverglass chamber filled with clearing solution and positioned with a motor-controlled stage [102]. The microscopic set-up involved a commerical inverted microscope, an objective inverter and a telescope for the expansion of the laser excitation beams. The light sheet was created by focusing the excitation beam in a cylindrical lens. The respective excitation and emission filter combination were used sequentially plane by plane and images were taken at 5 μm increment. All hardware and data acquisition were controlled and synchronized with the software package LabView (for complete methodology see [102]).

Following data acquisition by Prof. Beilhack's staff, resulting multicolor stacks were processed with ImageJ and de-interleaved into single-color stacks that were subsequently projected to a two-dimensional presentation (using maximum intensity Z-projection). To yield a three-dimensional projection the software Volocity was employed.

Table 3.7: Staining procedure for whole mount samples following fixation.

Solution	Time in hours	Process
PBS⁻	3 × 0.5	Washing
Permeabilization solution for whole mount samples	overnight	Permeabilization and blocking
Primary antibody (GFAP) in diluent for whole mount samples	overnight	Incubation
PBS⁻	3×0.5	Washing
Secondary antibody or directly conjugated antibody in diluent for whole mount samples	overnight	Incubation
PBS⁻	3 × 0.5	Washing
50 % (v/v) Ethanol	2	
70 % (v/v) Ethanol	2	
80 % (v/v) Ethanol	2	Dehydration
96 % (v/v) Ethanol	2	
100 % (v/v) Ethanol	overnight	
n-hexane	2	Clearing process
Clearing solution	3 × 0.5	

3.6 Laser capture microdissection

Laser capture microdissection is a technique to site-specifically collect cells of interest from tissue sections under microscopic visualization for downstream analysis. It relies of a focused laser beam that cuts out a user-defined shape and subsequently applies a laser pulse to catapult the tissue fragment into a collection device. In this work the PALM MicroBeam system was employed to separate the myenteric tissue region, the submucosal tissue region and the mucosal tissue region from one another from rat intestinal tissue sections. To separate these segments, multiple oval-shaped tissue segments were excised from each tissue layer that contained the plexus structures and surrounding extra-ganglionic cells (see 4.5).

Following quick cresyl violet stain, the PEN membrane slide was mounted on a slide holder and inserted into the holding frame of the computer-controlled motorized PALM RoboStage. Stage movements were controlled with the PALM RoboSoftware. Specimens were visualized at 20× magnification with the AxioCam MRc camera. Laser energy and laser focus were tested and calibrated if necessary with the software-implemented "Cut Laser Adjustment Wizard". Cut laser energy of 54±2 and cut laser focus of 73±2 were found suitable for 20× magnification. To collect tissue regions of interest, AdhesiveCaps were employed as collection device. The tube's cap was inserted in a TubeCollector and mounted onto the PALM CapMover device. With the RoboSoftware the collection device was aligned above the sample. The RoboSoftware offers different laser cutting functions. Here, a shape was drawn with the Freehand tool and cut in the RoboLPC-mode, which automatically positions the laser pulse along the cutting line and thereby catapults the entire cut area intactly into the cap. For the myenteric and submucosal regions a

total area of on average $2.1{\times}10^6$ μm^2 was collected per intestinal region (i.e. duodenum, ileum, proximal colon) and per animal. For mucosal regions a total area of on average $2.8{\times}10^6$ μm^2 was collected. The tissue fragments were dry-collected in the AdhesiveCaps and cell lysis buffer was added to proceed with RNA isolation when sufficient material was collected.

3.7 Transcriptomic analyses

3.7.1 RNA isolation

Total RNA was isolated from intestinal tissue, laser-dissected tissue sections, gliospheres and single cells.

For tissue samples, rigorous disruption and homogenization of the starting material was necessary. RNA*later*-protected tissue were transferred to a round-bottomed microcentrifuge tube, submersed with Lysis Reagent (1 ml/100 mg tissue) and a stainless steel bead was added. Tissue was lysed by vigorous shaking for 3 min at 50 Hz. Consequently, 400 μl Lysis Reagent and 200 μl were added and vortexed for 15 sec until suspension became foamy. Suspension was left on ice for 15 min and subsequently centrifuged (15 min, 4 °C). The upper aqueous RNA-containing phase was transfered to a new tube and processed with the RNeasy MinElute Cleanup Kit. This process relies on the high-affinity binding of RNA to silica membranes, from which contaminants can be washed off. Briefly, the sample was mixed with the same volume of 70% EtOH (500 μl) and transferred onto a RNeasy MinElute spin column. Columns were centrifuged (8000× g, 1 min), flow-through discarded and columns transferred to new collection tubes. Columns were washed with RPE buffer, 80% EtOH and dried by centrifugation. RNA was eluted into fresh collection tubes with 20 μl RNase-free water and diluted 1:10 with H_2O. Quantity and quality were spectrophotometrically determined. Samples yielded on average 614 ng/μl in the diluted samples with a 260/280 ratio of 1.96 on average.

Laser-dissected tissue sections were incubated with 350 μl cell lysis buffer upside-down at RT in AdhesiveCaps, quickly vortexed, centrifuged and further processed with the RNeasy Micro Kit. Briefly, lysates were mixed with the same volume of 70% EtOH, transferred onto a RNeasy MinElute spin column and quickly centrifuged (8000× g, 30 sec). Flow-through was discarded and columns were washed with 350 μl RW1 buffer. 80 μl DNase I incubation mix was added to the column membrane and incubated (30min, RT), followed immediately by a washing step with RW1 buffer (350 μl, 8000× g, 30 sec). Columns were washed with RPE buffer (500 μl, 8000× g, 30 sec) and 80% EtOH (500 μl, 8000× g, 2 min). Subsequently, columns were dried by centrifugation at fullspeed (i.e. > 20.000×g, 5 min) and RNA was eluted with 14 μl RNase-free water into a fresh centrifugation tube. RNA quality from randomized representative samples was assessed with the Experion Automated Electrophoresis System and yielded consistently satisfying results (RNA integrity number (RIN) $\geq$ 7.4).

Gliospheres and cells directly collected after FACS were lysed in 350 μl Cell lysis buffer prepared with RLT Plus, a component of the RNeasy Plus Micro Kit. In addition to all components included in the standard RLT buffer, the RLT Plus buffer contains detergents to support efficient

binding of RNA to gDNA Eliminator columns. Briefly, cells were homogenized with QIAshredder spin columns by loading of the lysate onto the column followed by centrifugation (> 20.000×g, 2 min). The flow-through was transferred to gDNA Eliminator spin columns and centrifuged (8000× g, 30 sec). Flow-through from this step was mixed with the same volume of 70% EtOH and further processed with the RNeasy Plus Micro Kit analogous to the RNeasy Micro Kit described above. 2 μl of the eluates were assessed with the Experion Automated Electrophoresis System and yielded consistently satisfying results (RIN $\geq$ 8). RNA was stored at -80 °C and sent to AG Niesler (nCounter core facility, Heidelberg) on dry ice for nCounter analysis.

3.7.2 cDNA synthesis

RNA from tissue and laser-dissected samples was transcribed to copyDNA (cDNA) with the iScript cDNA Synthesis Kit. All pipetting steps were performed on ice. For tissues 500 ng RNA was used, for laser-dissected samples the complete eluate was used and all samples were filled with RNase-free water to a final volume of 15 μl. To each sample, 4 μl of 5x iScript Reaction mix and 1 μl of iScript Reverse Transcriptase were added to achieve a final reaction volume of 20 μl. The reaction of primer annealing, elongation and denaturing of double-strands was carried out in a thermocycler following the protocol given in table 3.8. After transcription, cDNA samples generated from tissue lysates were diluted 1:2 by addition of 20 μl TE-buffer, all samples were stored at -20 °C until further use.

Table 3.8: Reaction protocol for the conversion of mRNA to cDNA.

Temperature in °C	Time in min	Process
25	5	Primer annealing
42	30	Elongation of cDNA strand
85	5	Denaturing of double strand
4	∞	Cooling until further use

3.7.3 Quantitative real-time PCR analysis

Quantitative real-time polymerase chain reaction (qPCR) is a technique to measure amplification of a specific DNA sequence based on the incorporation of a fluorescent dye that intercalates in double-stranded DNA. The process relies on the hybridization of a pair of primers to a complementary oligonucleotide sequence of the targeted DNA sequence and subsequent polymerization of a complementary strand by a DNA polymerase. Primer annealing, elongation and double strand denaturation are repeated in a cyclic manner. With each cycle the amount of PCR product increases and hence also the fluorescence intensity. Once the signal reaches a pre-defined threshold significantly above the background signal, this threshold cycle (Ct or Cq) is used to conclude the original relative expression level of the gene of interest, since the Cq-value is inversely proportional to the starting amount.

A prerequisite for qPCR analysis is the use of specific primer pairs that anneal to the target transcript. Suitable primers of 70 - 200 bp length were designed with Primer-BLAST software. If possible, primer pairs were designed to span an exon-exon junction of the transcript to exclude amplification of genomic DNA. Sequences and efficiencies of all primers are given in table 2.7. Upon delivery, lyophilized primers were diluted in nuclease-free water to a stock concentration of 100 μM and further diluted to working concentrations of 10 μM. Analyses were performed in duplicate with 0.4 pmol/μl of each primer. For cDNA from tissue lysates, 1 μl (12.5 ng) were employed, for cDNA from laser-dissected samples 2 μl of unknown concentration were used. 2xSsoFast EvaGreen Supermix (containing dNTPs, polymerase, MgCl$_2$, Evagreen dye and stabilizers) was used 1:2 in a total volume of 25 μl, adjusted with RNase-free water. As a negative control, the mastermix without any cDNA was analyzed to exclude contamination.

The themperature profile is given in table 3.9. For laser-dissected samples the number of cycles was increased to 49 repetitions to ensure complete signal detection in low-amount samples.

Table 3.9: Reaction protocol for qPCR analysis.

Step	Temperature in °C	Time in min	Process
1	95	3	Activation of polymerase
2	95	0:10	Denaturation
3	primer-specific	0:30	Annealing
4			Pleate Read
			Go to step 2, repeat 39 cycles
5	65-95	0:05	Melt Curve
			increment 0.5 °C with Plate Read
	4	∞	Cooling until further use

Data acquisition and subsequent analysis using the efficiency-corrected $\Delta\Delta$Cq method were performed with the Bio-Rad CFX Manager. These analyses were performed with the following equations:

Calculation of the efficiency based on the slope of a standard curve from dilution series of the amplified PCR-product:

$$E = 10^{(\text{-1/slope})}$$

Calculation of the expression levels of a gene of interest (GOI) normalized to the reference genes (Ref):

$$Normalized\ Expression_{sample(GOI)} = \frac{RQ_{sample(GOI)}}{\left(RQ_{sample(Ref1)} \times RQ_{sample(Ref2)}\right)^{\frac{1}{2}}}$$

with the relative quantity defined as:

$$Relative\ Quantity_{\text{sample(GOI)}} = E_{GOI}^{C_{\text{q(MIN)}} - C_{\text{q(sample)}}}$$

47

The quality of amplified PCR products was proven by melting curve analysis and agarose gel electrophoresis.

3.7.4 Genotyping

Genotyping is a technique used to identify transgenic offsprings of a breeding pair with at least one transgenic parent animal. To do so, a PCR is performed with a primer pair that is complementary to short sequences of the transgenic genomic sequence. In this work genotyping of hGfap-eGfp transgenic mice was done with the forward primer annealing to a sequence in the hGfap-promotor and the reverse primer annealing to a sequence that codes for eGfp (see table 2.7 for sequences). The process of genotyping involves extraction of genomic DNA from mouse tissue, amplification of the transgenic sequence and subsequent analysis of reaction products by gel electrophoresis. DNA extraction and amplification were done with the KAPA Mouse Genotyping Kit following the manufacturer's instructions. Briefly, ear punches were transfered to 0.2 μl nuclease-free microcentrifuge tubes and a total volume of 100 μl extraction mix was added, consisting of 10 μl 10x KAPA Express Extract buffer, 2 μl 1U/μl KAPA Express Extract Enzyme and 88 μl nuclease-free water. The mix was lysed for 10 min at 75 °C with a subsequent enzyme inactivation for 5 min at 95 °C in a thermocycler. The lysates were vortexed and centrifuged to pellet cellular debris. 1 μl of the extract were directly employed in the PCR reaction. The PCR mastermix contained 1.25 μl of each primer (10 μM), 12.5 μl of the 2xKAPA2G Fast HotStart Genotyping Mix with dye and 9.5 μl nuclease-free water. 24 μl of the mix were added to the template DNA and amplified in a PCR reaction with the protocol given in table 3.10. A positive control with DNA from a previously genotyped sample and a negative control without template DNA were always included in the analysis.

Table 3.10: Reaction protocol for the KAPA2G Fast Hotstart Genotyping PCR.

Step	Temperature in °C	Time in min	Process
1	95	3	Initial denaturation
2	95	0:15	Denaturation
3	60	0:15	Annealing
4	72	0:15	Extension
			Go to step 2, repeat 39 cycles
5	72	1	Final extension
	4	∞	Cooling until further use

PCR products were visualized by gel electrophoresis. Agarose gels were produced by heat-dissolving 2 % agarose in Tris-acetate-EDTA (TAE) buffer at 600 W in a microwave oven. 5 μl GelRed per 100 ml agarose gel were added and the liquid gel was poured into a suitable gel tray with comb. After the gel solidified, the tray was transferred to a horizontal gel system filled with TAE buffer and the PCR products and the DNA ladder were given in the well produced by

the comb. Voltage was applied so that the negatively charged DNA fragments moved through the gel pores to the positive pole. For a 7×8 cm gel, a voltage of 90 mV (with 50 W) was applied and the gel was run for at least 45 min. Subsequently, the gel was transferred to a gel documentation system and analyzed under UV-light.

3.7.5 Transcriptomic profiling by microarray

Total RNA was extracted from three independent preparations of murine hGFAP-eGFP$^+$ cells expanded *in vitro* as gliospheres with LPS-stimulation ("GFAP+LPS *in vitro*") prepared as described in section 3.3.1, without LPS-stimulation ("GFAP *in vitro*") and from transgenic cells directly lysed after cell isolation and purification ("GFAP *in vivo*").

Sample preparation and RNA integrity control (RIN $>$ 7) was performed at the Translational Centre for Regenerative Medicine (TRM) Leipzig. Illumina BeadChip analysis was conducted at the microarray core facility of the Interdisciplinary Center for Clinical Research (IZKF) of the University of Leipzig. Briefly, 250 ng RNA per sample were ethanol precipitated and dissolved at a concentration of 100-150 ng/μl prior to producing biotin-cRNA. 750 ng were hybridized to MouseRef-8 v2.0 Expression BeadChips and scanned on the Illumina HiScan instrument according to the manufacturer's specifications.

Data analysis was performed at the IZKF Core Facility and the Department of Bioinformatics (University of Würzburg). Briefly, raw data was background-corrected (normexp method) and normalized (VSN method). Microarray probes referring to unexpressed genes (detection p-value $>$ 0.05 in all samples, known as bad assay performance) or with no assigned genes were removed from the dataset. Moderated t-tests were used for detection of differentially expressed genes. Analyses were performed in the R environment (Version 3.3.1) [104] with Bioconductor extension packages "svn", "made4", "limma" and "illuminaMousev1p1.db.".

Data have been deposited in NCBI's Gene Expression Omnibus (GEO) [105] and are accessible via the GEO accession number GSE78015.

To deduce biological meaning from the list of significantly differentially expressed genes (SDEGs), the following approaches were taken:

(1) For the comparison of LPS-treated gliospheres and untreated controls, each of the 70 SDEGs were subjected to a database query via QIAGEN's Ingenuity Target Explorer (https://targetexplorer.ingenuity.com/) or NCBI Gene (http://www.ncbi.nlm.nih.gov/gene/) to gain information on the biological function and cellular component of a gene's product. These information were used to create a graphic display of SDEGs with biological functions and subcellular localization indicated (see figure 4.9).

(2) Enrichment analyses were performed with the bioinformatics ressource DAVID [106]. For the comparison of LPS-treated gliospheres and untreated controls (GFAP+LPS *in vitro*/GFAP *in vitro*) all 70 SDEGs were integrated in one analysis. Significant enrichment of a Gene Ontology (GO) term [107][108] was postulated when the Benjamini-corrected p-value was below 0.05. For data presentation the p-values are given as the base 10 logarithm to indicate the smallest p-value

with the greatest bar in a bar diagram (see figures 4.9 and 4.10).

For the comparison of directly sorted GFAP-EGCs to gliospheres expanded *in vitro* (GFAP *in vivo*/GFAP *in vitro*) 2705 SDEGs were identified and the up- and downregulated genes were analyzed separately. For each category, the terms significantly enriched (Benjamini-corrected p-value < 0.05) were selected, and among these, the top 5 with the greatest Fold Enrichment were selected. Fold Enrichment is the ratio of the count of genes associated to the term in the list of SDEGs relative to the statistically expected count of the term (Count/ExpCount).

(3) A color-coded Voronoi diagram [109] was created to visualize the SDEGs with respect to the relative expression change. Calculation of the Delaunay triangulation and the subsequent calculation of Voronoi tessellation was done in R by application of the deldir package (Version 0.1-9) [110].

3.7.6 Comparative transcriptome analysis

The global transcriptional datasats generated in this study were compared with data from previous studies deposited in the GEO database. The datasets are given with their GEO series (GSE) accession numbers in table 2.9. This meta-analysis was conducted by Andreas Heider (TRM Leipzig). Briefly, R/Bioconductor and the software "virtualArray" were used to combine data into one dataset (i.e. virtual array) [104][111]. The resulting new array was exported and analyzed in TM4 MeV [112] and Archaeopteryx [113], which was further used to employ hierarchical clustering analysis to show similarities or differences to cells of related identity or other cells of interest [114].

3.7.7 Transcriptomic profiling by nCounter technology

The nCounter technology (Nanostring Technologies) was employed to validate microarray data. It's suitability as validation tool has been investigated before [115] and is also discussed in this work (see section 5.3.1.1).

A customized CodeSet was designed to quantitatively assess 60 target genes including 7 reference genes. The choice of target genes was based on multiple transcriptomic profiles of enteric neural samples, including but not restricted to those presented in this work. From these multiple datasets genes were selected that either showed highly stable expression in multiple conditions (reference genes) or that showed significantly differential expression in multiple conditions (target genes).

The nCounter technology relies on the hybridisation of two different, non-overlapping probes to the target mRNA, the reporter probe and the capture probe (see figure 3.3 and section 5.3.1.1 for detailed explanation). The binding sequence is defined by the design of the probes. It is recommended to design the nCounter probes complementary to sequences that were also bound by the oligonucleotide in the microarray. To identify the exact Illumina-probe's binding sequence (which is not given in the microarray design), data were retrieved from publicly accessible NCBI databases. In a first step the Illumina ID of a target gene was entered into the NCBI Probe-

Database to retrieve its 50 bp sequence. The sequence was then entered into to NCBI Nucleotide Blast together with the target's accession number to find the position of the sequence. These information were sent to Nanostring Technologies' customer support for the design of matching nCounter Elements probes. Information on the resulting Elements probes are given in table 2.8.
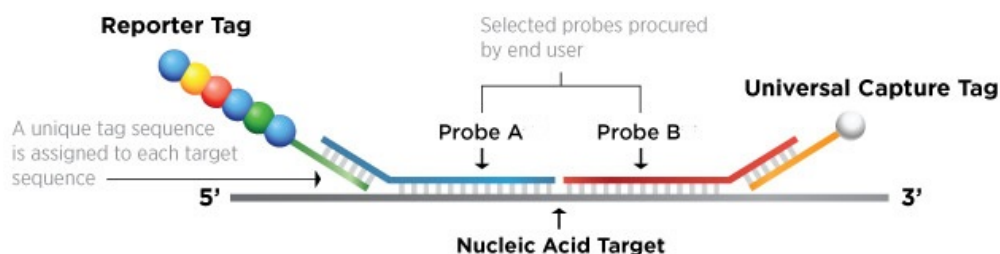

Figure 3.3: nCounter Elements TagSets chemistry. Quantification of a nucleic acid target relies on the binding of two probes, a reporter probe with a fluorescent barcode signal and a capture probe to immobilize the complex for data collection. The probes bind to a nucleotide sequence of the target defined by the end user. Adapted from [116]

Target genes were selected based not only on the transcriptomic profiles of GFAP-EGCs presented in this work, but on further microarray profiles of enteric neural samples. The reference genes were selected because of their highly stable expression over multiple microarray profiles and the remaining 53 genes were selected because of their differential expression over multiple microarray profiles. In the nCounter analysis 4 of the 7 genes previously selected as reference genes proved to be very stably expressed over all groups and were used as references in subsequent data analyses (see table 2.8).

Due to the low yield of GFAP$^+$ cells from murine early postnatal intestinal tissue, it was not possible to use the same RNA samples in both the microarray and the nCounter analyses. Thus, cell lysates had to be generated exclusively for the nCounter analysis. In order to yield sufficient amounts of RNA, isolates from different litters were pooled and measured in three technical replicates. The RNA samples were sent on dry ice to the nCounter Core Facility in Heidelberg that performed the analysis. Raw data processing was done with the nSolver analysis software.

3.8 Proteomic analysis with BeadArray technology

The quantitative multiplexed profiling of cytokines and chemokines in gliosphere culture supernatants (see section 3.3.1) was performed by our collaborators at the University hospital Würzburg. Briefly, the Cytokine Mouse 20-Plex Panel by Invitrogen was employed following the manufacturer's instructions. Analyses were done in triplicates as previously described [117][118] employing the StarStation Software.

Several of the 20 cytokines could not be quantified in at least two of the three replicates. These cytokines (FGF basic, GM-CSF, IL-1a, IL-17, KC, MIG, VEGF) were excluded from the analysis.

3.9 Data analyses

3.9.1 Analysis of immunohistochemical and histological staining

For quantification of stained nuclei 10 representative images with 20x magnification were taken with constant exposure time per intestinal region (duodenum, ileum, proximal colon) of each sample (n = 5 per group), counted by the experimentator in a blinded procedure and averaged. For area measurements of immunohistochemical stainings microscopic images were taken accordingly. For measurement of muscle thickness pixel information were translated into a length specification (1388 pixel corresponded to 30.6 cm). For GFAP quantification individual pictures were taken from the muscular and mucosal compartment because of the differing staining intensities (exposure time for muscular compartment: 1/50 sec for duodenum and ileum, 1/25 sec for colon; exposure time for mucosal compartment: 1/15 sec for duodenum and ileum, 1/7 sec for colon). Pictures were imported into ImageJ, image type was changed to 8 bit grayscale and threshold levels were adjusted to remove background (20-255 for muscular samples, 25-255 for mucosal samples). The stained area was subsequently measured.

3.9.1.1 Histological scoring

Histological scoring was performed on H&E stains. For this histological scoring alterations in the epithelium, the mucosa and submucosa were assessed and scored as given in table 3.11.

Table 3.11: Histological scoring parameters for the IBD model.

	Finding	Scoring value
	normal morphology	0
	loss of individual goblet cells	1
Epithelial damage	extensive loss of goblet cells	3
	disturbances in cryt architecture	3
	crypt loss	4
	no infiltrates	0
	minor infiltrates at the crypt base	1
Immune cell infiltrates	infiltrates between crypts und muscularis mucosae	2
	edema within the mucosa	2
	dense infiltrates	3
	infiltrates into the submucosa	4
	no granulocytes	0
	infiltration of the epithelium by granulocytes	1
	erosions of the epithelium	2
Granulocytic infiltrates	ulcers	3
	crypt abscesses	3
	destruction of the entire mucosa	4
	spread into the submucosa	5

3.9.2 Statistical analyses

Statistical analysis was performed with the nonparametric Mann-Whitney-U-Test or, if the criterion of normal distribution was met, with univariate ANOVA. Results are given as mean±standard deviation. The level of statistical significance was set at $p < 0.05$, indicated with an asterisk (*). Grading in significance is indicated as follows: * $p < 0.05$, ** $p < 0.01$, ** $p < 0.001$. A p-value between 0.05 and 0.10 was considered as moderate evidence for statistical significance and biological relevance and is indicated with a hash (#).

4 Results

The following experimental strategy was chosen to identify cellular and molecular effects of intestinal inflammation on glial cells. First, the overall ENS was studied in an *in vivo* model of an acute intestinal hyperinflammation. Next, for a specific analysis of EGCs with focus on the GFAP-expressing glial population, transgenic hGFAP-eGFP mice were employed [95]. From these animals, primary cultures of GFAP$^+$ EGCs-derived gliospheres were established and exposed to inflammatory stimuli *in vitro*. Additionally, the GFAP$^+$ population was studied in a well-established disease model of IBD *in vivo* to elucidate its contribution to disease manifestation.

4.1 Acute hyperinflammatory model *in vivo*

To unravel the effects of a systemic inflammatory insult on the ENS, a LPS-mediated hyperinflammation was induced in rats *in vivo*. At the University hospital Würzburg this rodent model was established to study the pathogenesis of systemic inflammation in critically ill patients, with emphasis on alterations in microcirculatory flow [98]. To continuously monitor microcirculatory flow in mesenteric postcapillary venules and other parameters, rats were kept in an intensive care setup including vascular access, tracheotomy with mechanical ventilalation as well as median laparotomy to expose the mesentery. Even though this complex setup is not required to merely induce a systemic inflammation via intravenous LPS-injection, it mimicks the situation in critically ill patients very well, which are often dependent on life sustaining measures. Additionally, manual handling of the mesentery necessary for intravital microscopy resembles the manual bowel handling during abdominal surgery, which is often followed by bowel inflammation. Hence, many aspects of this complex model make it highly suitable to study the effects of a systemic inflammation on the intestinal tissue.

4 hours after LPS-injection animals were sacrificed. To validate the induction of systemic inflammation by intravenous LPS-injection, our collaborators measured plasma cytokine levels and found significantly elevated levels of IL-1β, IL-2, IL-4, IL-6, IL-12 and IFN-γ in LPS-treated rats compared to sham-treated controls [99]. From the intestinal tissue duodenal, ileal and colonic parts were removed and processed either for histology, immunohistochemistry or gene expression analysis. Histometric parameters of the muscular layer were assessed to detect effects of the inflammation on tissue architecture. These analyses were performed by measuring the thickness of the muscle layer and myenteric plexus morphology in histochemically stained tissue sections (figure 4.1A). 4 h after LPS injection significant alterations were neither observed in the thickness of the intestinal muscle nor in the number or area size of myenteric plexi. Instead, hematoxylin and eosin (H&E) stains of tissue segments revealed extensive immune cell infiltrates in the mu-
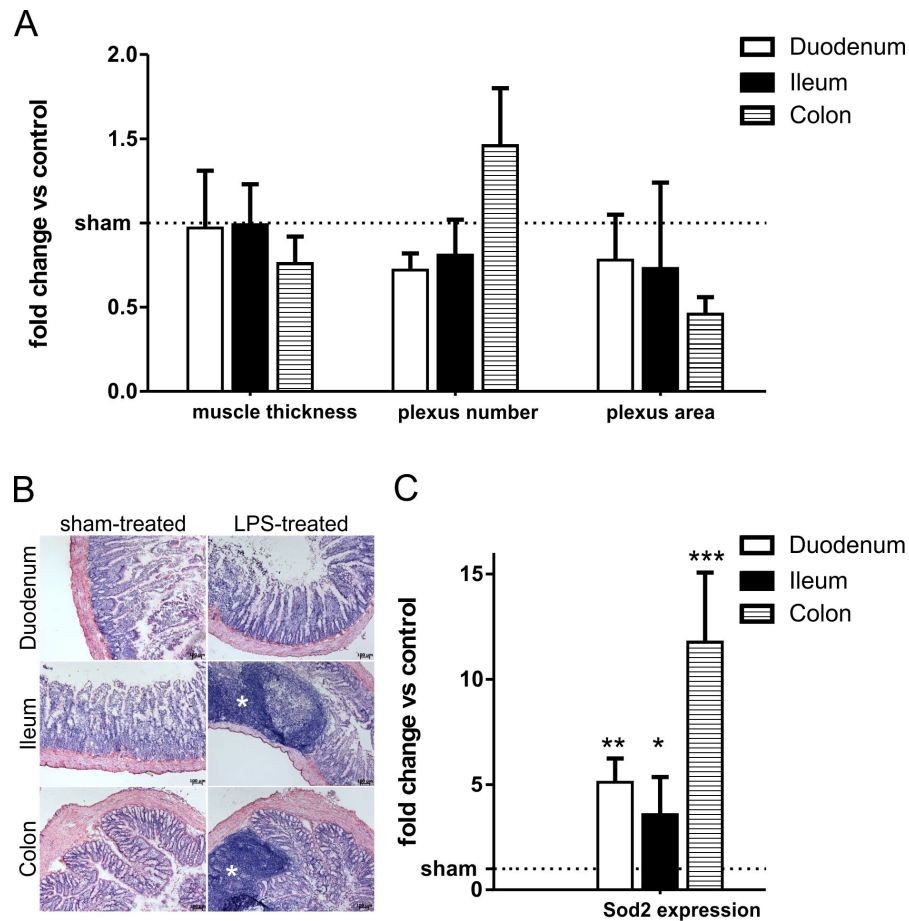
Figure 4.1: Inflammation-induced alterations in the overall intestinal tissue. (A) Histometrical analysis of muscle thickness, number of plexi and area of plexi measured in p75/DAPI stained tissue sections. No significant alterations are detected 4 h after LPS injection. (B) Representative hematoxylin and eosin stains of duodenal, ileal and colonic segments from a sham-treated (left) and a LPS-treated (right) animal. In the latter extensive immune cell infiltrates (white asterisks) are present in the ileum and colon. (C) qPCR analysis of Sod2 gene expression in whole gut wall samples reveals significant inflammation-induced Sod2 mRNA increase in all tissue segments. Results (mean $\pm$ SD) are given as fold change relative to sham group set to 1, as indicated by the horizontal line. Scale = 100 μm, n = 3, p $<$ 0.05, ** p $<$ 0.01, *** p $<$ 0.001.

cosa of LPS-treated animals, especially in ileal and colonic segments (figure 4.1B). To assess the level of inflammation-induced oxidative stress in the intestinal tissue, gene expression levels of the oxidative stress biomarker superoxide dismutase 2 (Sod2) were measured by qPCR in the different intestinal regions (figure 4.1C). This analysis revealed significant increases in Sod2 expression along the entire intestinal length, in duodenal tissue by 5-fold (p $<$ 0.01), in the ileum by 4-fold (p $<$ 0.05) and up to 12-fold (p $<$ 0.001) in the colon, indicating inflammation-associated oxidative stress.

4.1.1 ENS-alterations along the rostro-caudal axis

Alterations of ENS neurons and glia were analyzed on mRNA and protein level by quantitative PCR (qPCR) and immunohistochemical analysis of duodenal, ileal and colonic rat tissue (figure 4.2). In qPCR analysis mRNA levels of the overall glial marker S100b as well as the glial subpopulation marker Gfap were measured and normalized against the reference genes Actb and 18srRNA. Samples from five animals per group were analyzed and the mean normalized expression of each gene from the LPS-treated group was calculated as a ratio of the sham-treated control to give the treatment-induced fold change. It was found that 4 h after LPS injection levels of Gfap mRNA were significantly increased in duodenal (6.8±1.7-fold, p < 0.01) and colonic (5.5±1.6-fold, p < 0.01) whole intestinal wall segments (figure 4.2A). However, this increase did not coincide with an overall glial marker expression increase, since S100b mRNA expression decreased after LPS treatment to 0.6-fold in duodenal and ileal, and to 0.4-fold (p < 0.01) in colonic segments (figure 4.2A). In contrast to duodenal and colonic samples, Gfap expression levels in ileal segments showed no significant LPS-mediated increase. Noteworthy, as shown in figure 4.2B, the total Gfap mRNA levels normalized against the reference genes in sham-treated animals were about 3-fold higher in ileal samples than in duodenal or colonic tissue segments. Hence, the inflammation-induced net change in Gfap transcript levels is less pronounced. In preliminary experiments, the expression levels of Gfap in intestinal segments of sham- and LPS-treated rats of the hyperinflammatory model were compared to untreated Lewis rats to assess the impact of the surgical procedure that was identical in both groups (figure 4.3). In this analysis Gfap expression levels in ileal samples from untreated controls were not as elevated as in the animals from the hyperinflammatory model. Instead ileal Gfap levels of untreated animals were highly similar to Gfap expression levels in duodenal and colonic samples from sham-treated rat.

To correlate these findings to protein expression levels, immunohistochemical stainings of glial markers were quantified. The transcription factor SOX10 was chosen as a selective and complete marker for postnatal glial nuclei (figure 4.2D). SOX10$^+$ nuclei were counted in the myenteric plexus only, because cell counting within the submucosal plexus was impeded by nuclear fluorescence signals from infiltrating immune cells in inflamed submucosal areas. To gain representative cell numbers 10 tissue section per animal and per intestinal region were counted and averaged. The analysis revealed a tendency for inflammation-induced reduction of SOX10$^+$ glia by 38% in the duodenum (p < 0.1) and by 29% in the ileum and colon. This is in line with glial S100b mRNA level reduction upon LPS treatment. The decrease in overall glial marker positivity was again not observed in the GFAP-expressing glial subpopulation, on protein level no reduction but also no increase was measured for intramuscular GFAP-staining (figure 4.2D). Since GFAP is not a nuclear but a cytoplasmic marker, counting of positive cells was not feasible and instead area measurements of positive stainings were taken. Staining intensities varied in muscular and mucosal parts of the tissue, so that both were recorded individually with attuned exposure times
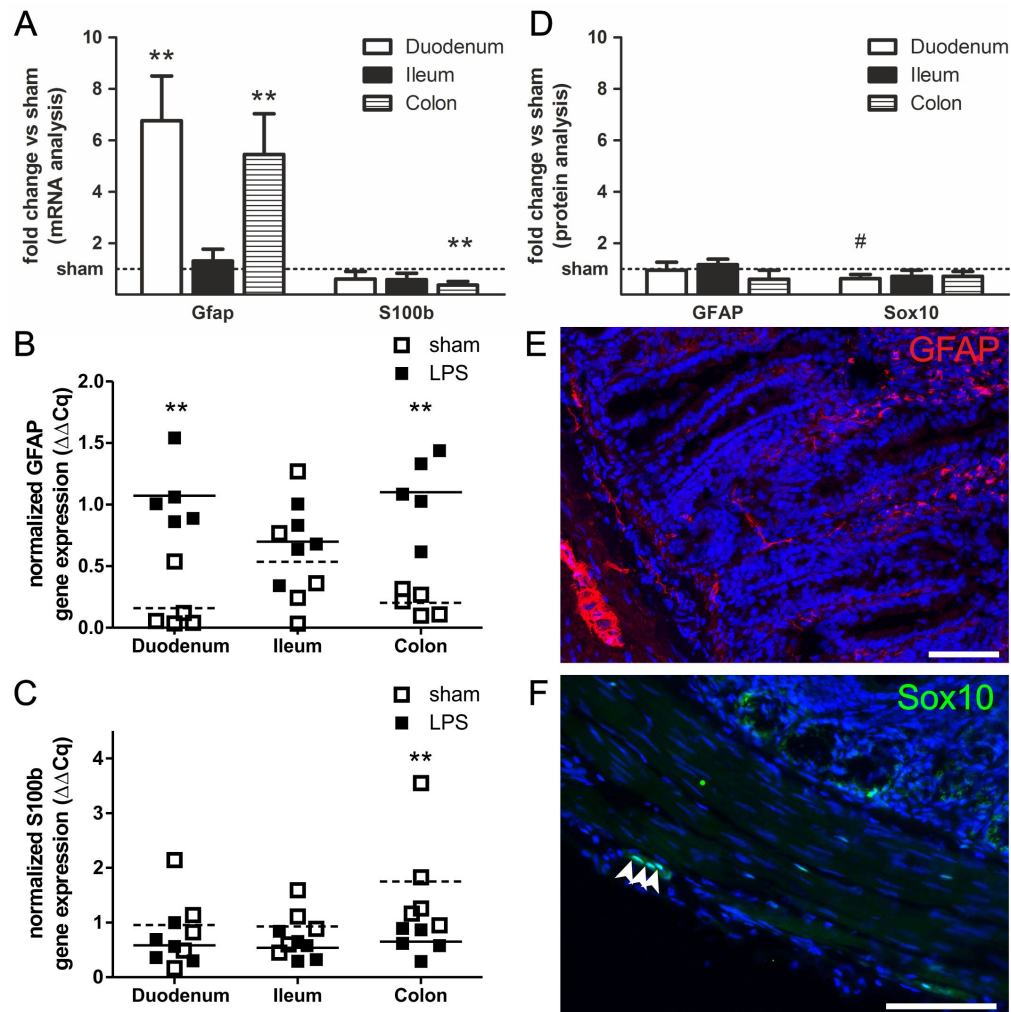
Figure 4.2: Glial-specific LPS-induced ENS alterations in hyperinflamed intestinal rat tissue. (A) Quantitative PCR analysis of glial marker expression in whole intestinal wall preparations from duodenal, ileal and colonic segments shows that Gfap gene expression but not S100b expression is upregulated in hyperinflamed gut tissue. In ileal samples no significant change is observed. Absolute gene expression of Gfap and S100b normalized to the reference genes ($\Delta\Delta$Cq) are given in (B) and (C), respectively. Means of LPS-treated samples (filled symbols) are indicated with lines, means of sham-treated samples (empty symbols) are indicated with dashed lines. (D) Quantification of immunohistochemical stainings for intramuscular GFAP (E, representative duodenal staining) and the glial transcription factor SOX10 (F, representative duodenal staining). 4 h after LPS injection protein levels are not significantly altered. Results (mean $\pm$ SD) are given as fold change relative to sham group set to 1, as indicated by the horizontal line. Scale = 100 μm, n = 5, # p < 0.10, ** p < 0.01. [119]

and measurement values were averaged. It is worth mentioning that no significant alterations in GFAP-positivity were detected in neither the muscular or the mucosal compartment alone.

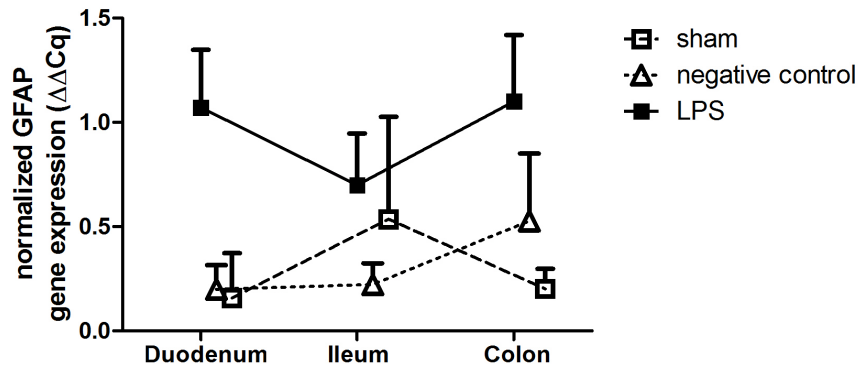In accordance with glial cell quantifications, inflammation-mediated effects on neuronal marker

Figure 4.3: Effect of sham-treatment on Gfap expression in hyperinflammatory model *in vivo*. Absolute Gfap gene expression levels normalized to the references genes ($\Delta\Delta Cq$) are given. In ileal samples from untreated rats (empty triangle with dotted line) Gfap mRNA levels are comparable to Gfap mRNA levels in duodenal and colonic samples from sham-treated rats (empty squares with dashed line). Means+SD, n = 5 for sham- and LPS-treated animals (Sprague Dawley rats), n = 4 for untreated animals (Lewis rats).

expression were assessed on mRNA and protein level (figure 4.4). No significant alterations were observed by qPCR analysis of normalized Uchl1 (PGP 9.5) expression level as a total neuronal marker, nor of the cholinergic (Chat) and nitrinergic (Nos1) neuronal subpopulations (figure 4.4A). On protein expression level neuronal cell counts positive for the HuC/D RNA binding protein in the myenteric plexus were neither significantly affected (figure 4.4B). Merely a tendency for decreased cell numbers in the small intestine is observed in the small intestine by 30% at most, similar to the glial SOX10 quantification.

Taken together, these results indicate that systemic inflammation caused a severe immune cell infiltration of the intestinal mucosa, accompanied by a strong increase in oxidative stress biomarker expression. However, neither the overall myenteric architecture was significantly affected nor the basic cellular composition of myenteric ganglia, as analyzed on protein level. However, a significant increase in Gfap mRNA expression level was detected by qPCR analysis of whole gut wall samples, inconclusive on the localization of the GFAP-expressing glia within the intestinal tissue.
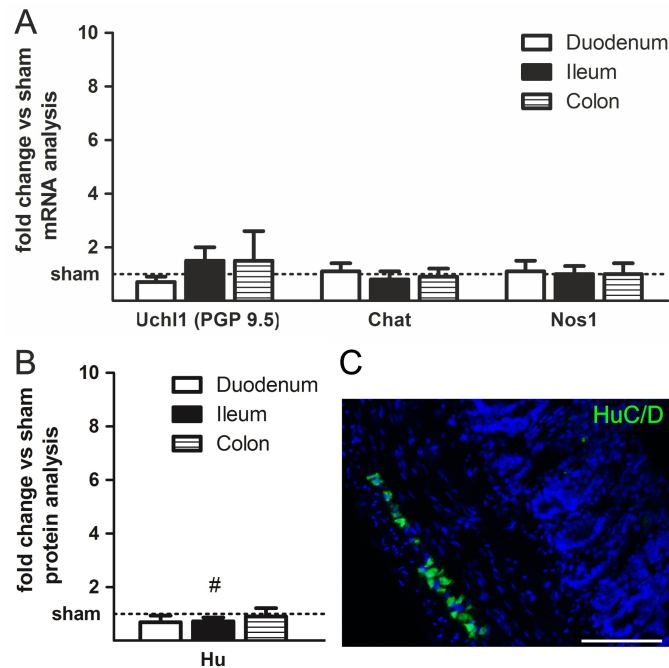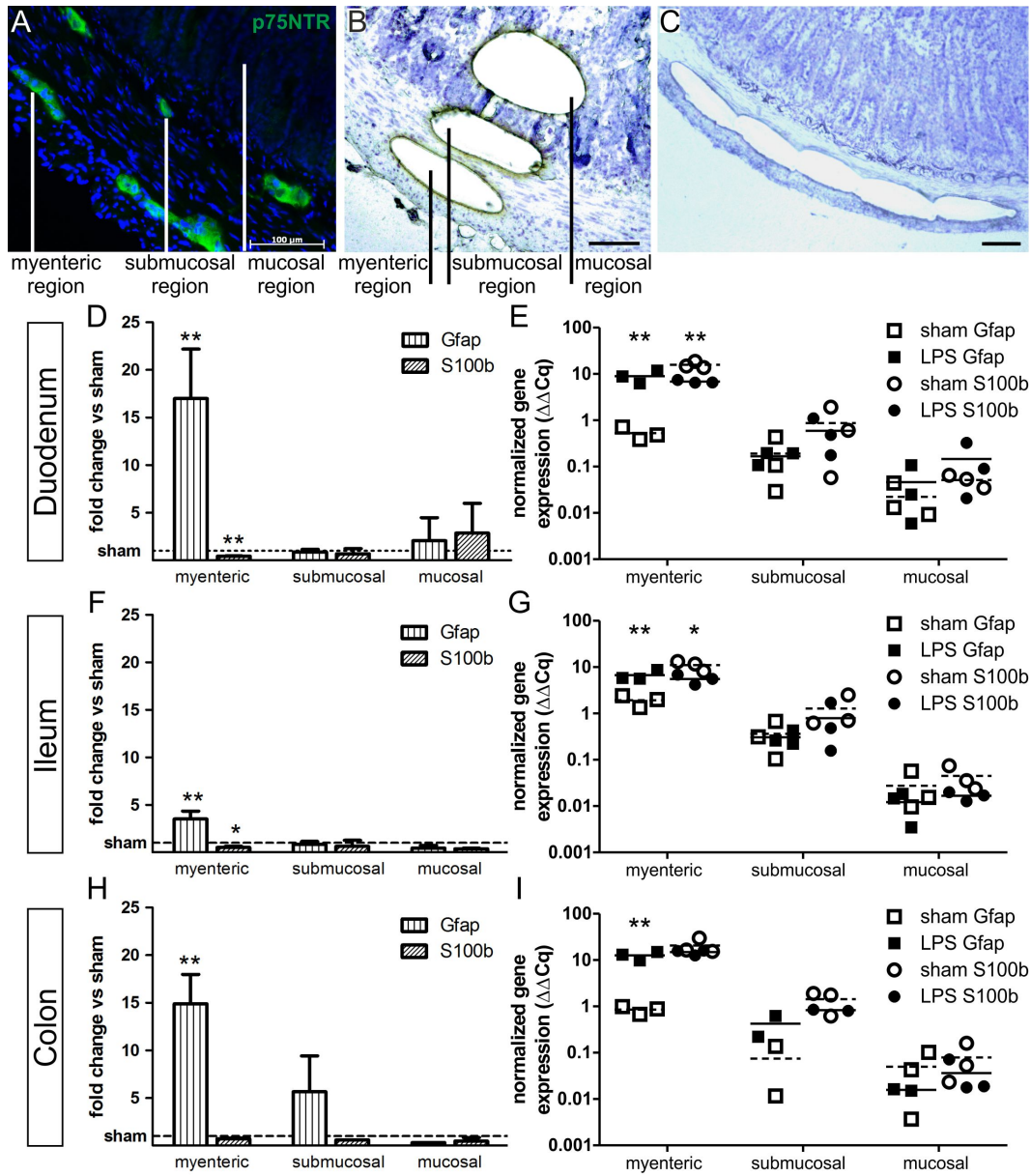
Figure 4.4: Neuronal cells do not show alterations 4 h after LPS injection. (A) Quantitative PCR analysis of neuronal marker expression in whole intestinal wall preparations from duodenal, ileal and colonic segments shows no alterations in normalized mRNA expression levels of the overall neuronal marker Uchl1 (PGP 9.5) or cholinergic (Chat) and nitrinergic (Nos1) subpopulations. (B) Quantification of immunohistochemical staining for HuC/D RNA binding protein in the myenteric plexus (C, representative staining). 4 h after LPS injection no significant alterations on protein level were observed, but a tendency for reduced numbers in ileal segments. Results (mean ± SD) are given as fold change relative to sham group set to 1, as indicated by the horizontal line. Scale = 100 μm, n = 3-5, # p < 0.10. [119]

4.1.2 Analysis of EGCs along the luminal-serosal axis

To analyze the region-specificity of LPS-responsive GFAP-glia, laser capture microdissection (LCM) followed by qPCR analysis was performed (figure 4.5). LCM is a laser-assisted method to excise tissue fragments under microscopic visualization and to collect them for further analysis. In principle, unfixed tissue cryosections are transferred onto membrane-coated slides and quickly stained in preferrably non-aqueous solutions to avoid exposure to RNases. The slides are microscoped and with a software interface it is possible to select clusters of cells. An ultraviolet laser subsequently cuts along the lines drawn around these regions of interest and a second, defocussed laser pulse is used to catapult the tissue fragments into a capture device. These fragments can then be further processed, in this project RNA was isolated. In the process of optimizing the LCM procedure for the rat intestinal tissue, RNA amount and quality, given as a RNA quality indicator (RQI) value, were regularly assessed with a chip-based automated electrophoresis system. An RQI value ≥ 7 indicates acceptable quality, and samples acquired from rat tissue yielded on average an RQI of 7.4. However, since the amount of RNA isolated

Figure 4.5: LPS-induced gene expression alterations are confined to the myenteric plexus.
(A) Immunohistochemical staining of p75NTR indicates the position of myenteric and submucosal plexus structures. (B-C) Cresylviolet-stained tissue section showing exemplary myenteric, submucosal and mucosal tissue segments cut and catapulted for mRNA transcript level analysis (B) and sequential excision of segments (C). (D, F, H) qPCR analysis of laser-dissected myenteric, submucosal and mucosal tissue segments of duodenal (D), ileal (F) and colonic (H) samples as fold change relative to the sham group set to 1 (horizontal line). (E, G, I) Absolute normalized gene expression of Gfap (squares) and S100b (circles) in duodenal (E), ileal (G) and colonic (I) segments, plotted on a logarithmic scale. Means of LPS-treated samples (filled symbols) are indicated with lines, means of sham-treated samples (empty symbols) are indicated with dashed lines. n = 3, * $p < 0.05$, ** $p < 0.01$. [119]

from tissue fragments was very low, this quality testing was no longer performed once the method was established.

For the spatial analysis of Gfap-expressing glia, myenteric, submucoal and mucosal tissue segments were excised (figure 4.5B-C) from duodenal, ileal and colonic tissues and analyzed for Gfap and S100b gene expression levels (figure 4.5D-I). Interestingly, the LPS-group revealed a highly significant Gfap mRNA increase in the myenteric plexus regions of duodenal samples by 17.2 ± 5.2-fold, of ileal samples by 3.5 ± 0.8-fold and of colonic samples by 15.0 ± 3.1-fold ($p < 0.01$ each). As in whole gut wall specimens, S100b expression was concurrently decreased, reaching significant values in the small intestine to the 0.4-fold in the duodenum ($p < 0.01$) and to the 0.5-fold in the ileum ($p < 0.05$). No significant effects on Gfap or S100b expression were detectable within the submucosal and whole mucosal regions.

In summary, systemic LPS application caused inflammation-induced oxidative stress in intestinal tissue within 4 h in our hyperinflammation model. In this time frame, no cellular alterations are observed in the largest division of the ENS, the myenteric plexus, except for the gene expression level of the glial-specific cytoskeletal GFAP. The inflammation-induced Gfap-expression is limited to the myenteric plexus and varies in intensity along the intestinal rostro-caudal axis.
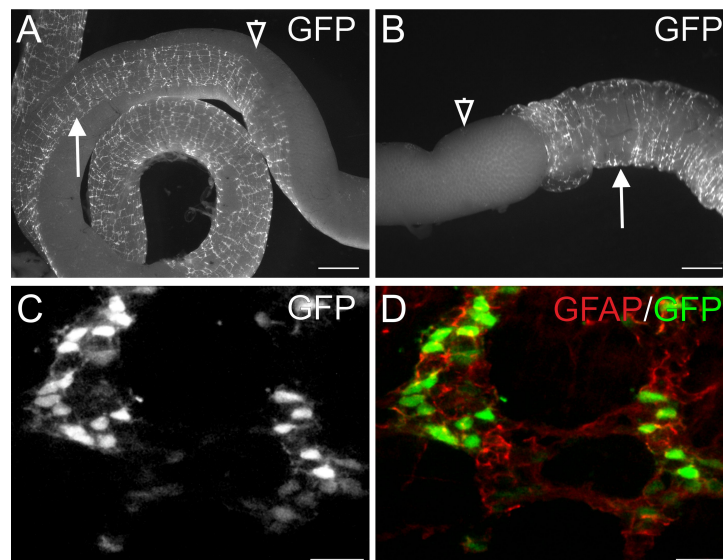

Figure 4.6: GFP-expression in the myenteric plexus of hGFAP-eGFP mice. (A-B) Fluorescence microscopy of eGFP-expression in the native intestine of hGFAP-eGFP mice. LMMP can be removed in strips (A) or peeled off (B). Filled arrows indicate gut regions with the muscle strip still attached, empty arrowheads indicate gut regions with the LMMP peeled off. Scale = 1000 μm. (C) Endogenous GFP fluorescence and (D) overlay with GFAP antibody staining in LMMP strips visualizes that only cells within the plexus structures express GFP in varying intensities. Scale = 100 μm

4.2 *In vitro* culture of myenteric GFAP-glia as gliospheres

In order to specifically study the GFAP-expressing glial subpopulation *in vivo* and *in vitro*, transgenic eGFP-hGFAP mice were employed, which express an enhanced green fluorescent protein under the human GFAP promotor. To establish cell cultures, postnatal day 7 mice were employed. Small intestinal longitudinal muscle-myenteric plexus (LMMP) strips were mechanically separated from the mucosa and enzymatically digested (figure 4.6A-B). As shown in figure 4.6C-D all GFP-positive cells in LMMP-preparations from hGFAP-eGFP mice coexpress GFAP. The cell suspension resulting from the LMMP digest contained appromixately 4% GFAP-expressing glia, which were enriched by flow cytometry (figure 4.7A-C).
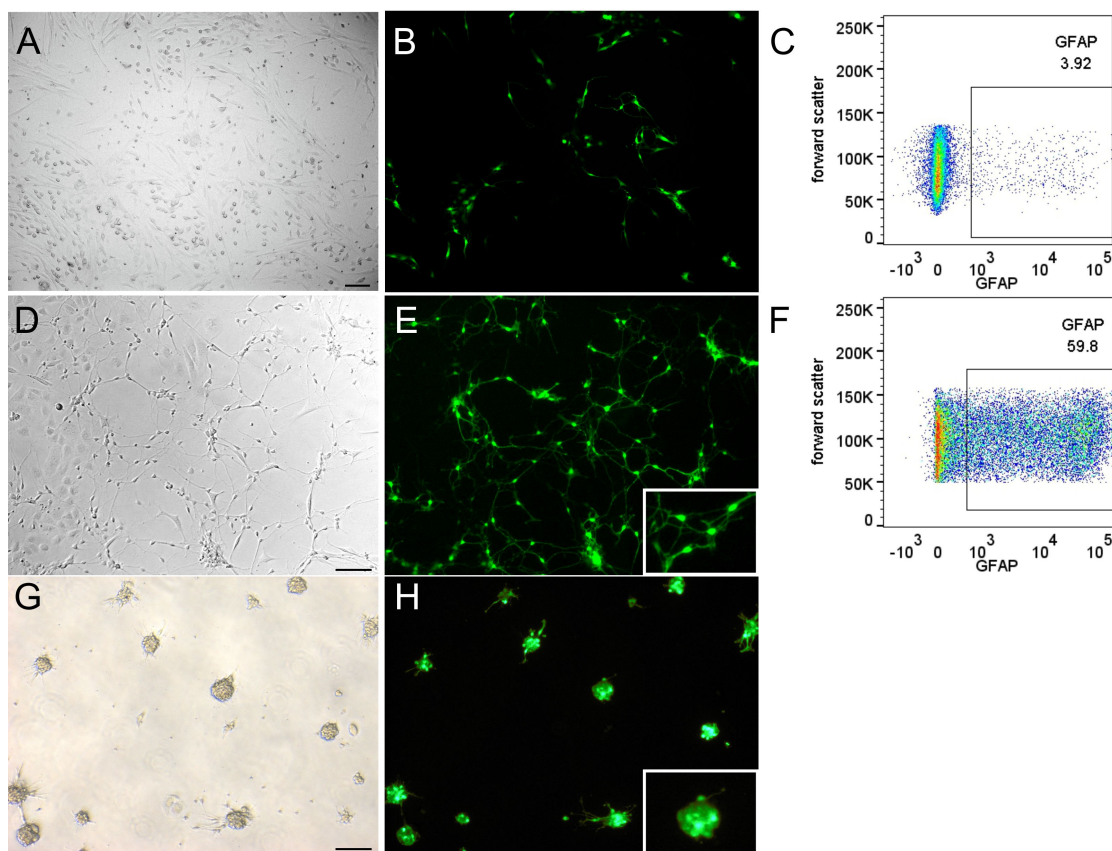

Figure 4.7: GFP-expressing glia can be sorted to establish enriched adherent or spheric cultures. Representative brightfield (A,D,G) and fluorescence (B,E,H) microscopy images of EGC cultures. (A-C) Enzymatic digest of murine LMMP strips generated a heterogeneous culture containing 4% GFP-expressing GFAP-glia as quantified by flow cytometry. (D-H) After 2 weeks in culture, sorted GFP$^+$ cell population was propagated to a heterogenous glial population containing 60% GFP-positive cells, either as adherent (D-E) or spheroid culture (G-H). Scale = 100 μm. [119]

The resulting GFAP$^+$ glial population was propagated as either adherent (figure 4.7D-E) or spheroid (figure 4.7G-H) cultures and contained approximately 60% GFAP$^+$ cells after three weeks of expansion. Gliospheres expanded *in vitro* showed strong immunohistochemical staining for the glial markers GFAP (figure 4.8A) and S100B (figure 4.8B). Spheres also contained a proportion of α-smooth muscle actin-positive (figure 4.8E) but no prominent Vimentin-positive (figure 4.8D) cells.
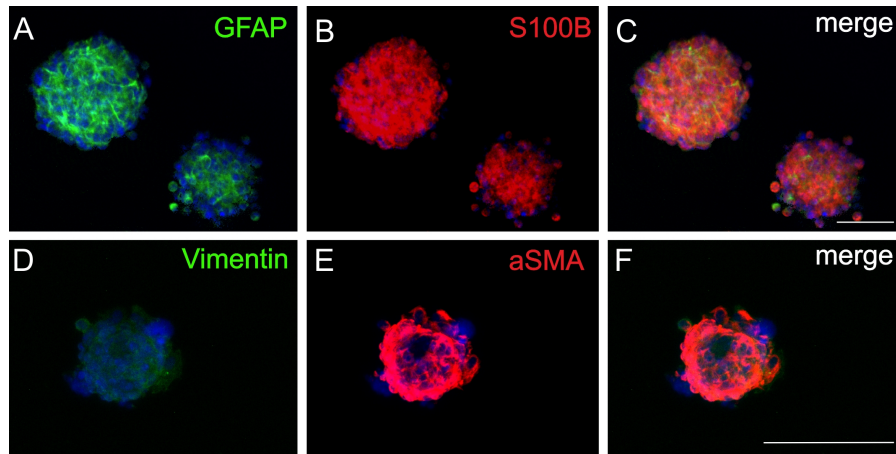

Figure 4.8: Characterization of marker expression in expanded gliospheres. Immunohistochemistry reveals that the major proportion within gliospheres are glial cells positive for GFAP (A) and S100B (B) but spheres also contain cells expressing α-smooth muscle actin (αSMA) (E) but are devoid of strongly Vimentin-positive cells. Scale = 100 μm. [119]

4.3 Inflammatory stimulation of gliospheres *in vitro*

To investigate the potential role of GFAP-expressing glia in onset and maintenance of intestinal inflammation, gliospheres were stimulated with the bacterial cell wall component LPS *in vitro* to mimic a direct exposition of GFAP-EGCS to bacteria. LPS-stimulation was performed for 48 h at a final concentration of 100 μg/ml LPS. From the LPS-challenged gliospheres total RNA was extracted and a transcriptome analysis was performed to detect LPS-induced alterations in gene expression profiles. In this analysis 70 significantly differentially expressed genes (SDEGs) were identified, given in table 4.1.

To approach this list several methods were employed. In a first step each protein coded for by a SDEG was assigned its predominant subcellular localization (nucleus, cytoplasm, plasma membrane, extracellular space) and its key biological function (e.g. transcription factor, enzyme, receptor, cytokine) manually by database search (figure 4.9A). Even though this approach gives a first impression on the biological processes that might be affected by differential expression of the respective genes, it is not feasible for more extensive lists of SDEGs. Further, it gives no indication of the upstream or downstream processes that might be differentially effected. Even

though the information is given that a gene codes for an extracellular enzyme, its substrates and the products of the enzymatic reaction are unknown. Also, this analysis does not indicate if the one protein class is over- or underrepresented in the dataset. To give an example, 10 out of 70 genes differentially expressed upon LPS-treatment code for nuclear transcriptional regulators, but this information does not imply whether this ratio is high or low.

A broader analysis can be performed by more complex database queries that integrate multiple interlinked attributes of each gene product. The most commonly used and freely accessible database is the Gene Ontology (GO) database [107, 108]. This bioinformatics resource provides information on the molecular functions of a gene product, the biological processes it contributes to, and the cellular compartments where these occur. If several gene products in the list of SDEGs are annotated to the same quality, the respective GO-term is given as enriched by the database query. The level of significance of a term's enrichment depends on the number on gene products within the list that are linked to this term. In addition to the statistical significance of an enrichment the magnitude of this enrichment can be given. This magnitude depends on the expected enrichment of a term, which is in turn based on the number of all genes in the genome associated with the term. If a term is assigned to x% of all genes in the genome (the expected count) and to y% of all genes in the list of SDEGs (the actual count), the ratio of y to x gives the magnitude of enrichment, also referred to as the fold enrichment.

To use this bioinformatics resource, the list of SDEGs upon LPS-treatment was first analyzed for enriched terms describing the molecular function and cellular compartment of the gene products (figure 4.9). This analysis identified 6 terms describing cellular compartments to be enriched (figure 4.9B), all associated to the extracellular region. The genes annotated to these cellular compartments encompass different cytokines, secreted enzymes and receptors (figure 4.9A). Correspondingly, the overrepresented molecular functions were associated with signaling processes such as cytokine and chemokine activity (figure 4.9C). A limitation of this analysis is that the GO-terms have different hierarchical levels with child terms that are more specialized but largely redundant to the parental terms. To exemplify, the most significantly enriched terms describing the cellular components in this data set are "extracellular region part" and "extracellular region". "Extracellular region part" is a child term of "extracellular region"; while the first describes constituent parts of the extracellular region (e.g. basal lamina and extracellular matrix (ECM) proteins), the latter rather describes functional properties of the extracellular regions (e.g. transport processes). All gene products that are annotated to the child term "extracellular region part" (e.g. matrix metalloproteinases that degrade ECM proteins) are equally annotated the the parental term "extracellular region", while the parental term includes additional annotations that are not annotated to the child term (e.g. the chaperone clusterin that aids protein folding of secreted proteins). Despite this redundancy, the GO analysis gives a good overview of the cell's functions the LPS-affected genes are associated with.

Table 4.1: SDEGs in LPS-treated gliospheres *in vitro* compared to untreated controls. The official gene symbol, the logFold Change, the average expression, the p-value and the full gene name are given.

Gene	LogFC	AveExpr	p-Value	Full Gene Name
Ccl5	2,48	7,41	4,2E-10	chemokine (C-C motif) ligand 5
Mmp9	2,50	8,00	8,1E-10	matrix metallopeptidase 9
Ripk2	1,31	7,89	1,2E-09	receptor (TNFRSF)-interacting serine-threonine kinase 2
Cx3cl1	2,36	7,95	1,4E-09	chemokine (C-X3-C motif) ligand 1
Vmn1r181	2,43	7,99	1,7E-09	vomeronasal 1 receptor 181
Tnfaip2	1,69	7,52	1,0E-08	tumor necrosis factor, alpha-induced protein 2
Cebpb	2,58	10,59	1,1E-08	CCAAT/enhancer binding protein, beta
Ms4a6d	1,48	7,16	1,5E-08	membrane-spanning 4-domains, subfamily , member 6D
Ccl2	3,62	8,38	2,5E-08	chemokine (C-C motif) ligand 2
Tlr2	2,02	8,11	2,7E-08	toll-like receptor 2
Tnfaip3	1,51	7,61	4,3E-08	tumor necrosis factor, alpha-induced protein 3
Cxcl16	1,86	7,49	8,8E-08	chemokine (C-X-C motif) ligand 16
Csf2	1,24	7,06	1,0E-07	colony stimulating factor 2
Bcl3	1,42	7,70	1,1E-07	B cell leukemia/lymphoma 3
Dcn	2,73	8,82	1,6E-07	decorin
Gbp5	0,92	7,05	2,0E-07	guanylate binding protein 5
Nxn	1,29	12,08	9,3E-07	nucleoredoxin
Pdlim4	2,38	10,39	1,2E-06	PDZ and LIM domain 4
Rgs8	2,13	7,76	1,6E-06	regulator of G-protein signaling 8
Sox7	1,53	7,31	1,6E-06	SRY-box containing gene 7
Nfkbie	0,99	7,67	1,7E-06	nuclear factor of kappa light polypeptide gene enhancer in B cells inhibitor, epsilon
Fcgr2b	1,62	7,98	2,1E-06	Fc receptor, IgG, low affinity IIb
Car13	1,60	7,67	2,5E-06	carbonic anhydrase 13
Casp4	1,81	8,15	3,6E-06	caspase 4, apoptosis-related cysteine peptidase
P2ry6	1,29	10,80	4,1E-06	pyrimidinergic receptor P2Y, G-protein coupled, 6
Slc11a2	0,83	8,33	6,2E-06	solute carrier family 11 (proton-coupled divalent metal ion transporters), member 2
4933426M11Rik	1,32	10,99	9,2E-06	RIKEN cDNA 4933426M11 gene
Sbno2	0,86	7,80	1,0E-05	strawberry notch homolog 2 (Drosophila)
Gxylt2	0,93	7,24	1,1E-05	glucoside xylosyltransferase 2
Lcn2	4,53	8,98	1,2E-05	lipocalin 2
Mmp3	0,90	7,20	1,2E-05	matrix metallopeptidase 3
Gpr17	-2,49	10,18	1,2E-05	G protein-coupled receptor 17
Crispld2	0,78	7,34	1,4E-05	cysteine-rich secretory protein LCCL domain containing 2

| Gene	LogFC	AveExpr	p-Value	Full Gene Name
Trf	1,02	11,04	1,4E-05	transferrin
Relb	1,10	7,76	1,8E-05	avian reticuloendotheliosis viral (v-rel) oncogene related B
Itga7	1,48	7,69	1,8E-05	integrin alpha 7
Mmp10	2,31	8,01	2,0E-05	matrix metallopeptidase 10
Cxcl5	1,89	7,37	2,1E-05	chemokine (C-X-C motif) ligand 5
Cd82	1,59	8,35	2,2E-05	CD82 antigen
Cd14	1,46	7,51	2,3E-05	CD14 antigen
Slc2a6	1,26	9,44	2,6E-05	solute carrier family 2 (facilitated glucose transporter), member 6
Map3k8	1,17	7,35	2,8E-05	mitogen-activated protein kinase kinase kinase 8
Kcnn2	-0,54	7,37	2,8E-05	potassium calcium-activated channel, subfamily N, member 2
Il13ra1	1,54	8,32	3,0E-05	interleukin 13 receptor, alpha 1
Nr1h3	0,84	7,19	3,7E-05	nuclear receptor subfamily 1, group H, member 3
Ramp1	-1,51	9,09	4,0E-05	receptor (calcitonin) activity modifying protein 1
Csf1	1,52	8,36	4,9E-05	colony stimulating factor 1 (macrophage)
Saa3	4,17	8,83	5,0E-05	serum amyloid A 3
Ms4a6d	0,63	7,05	6,1E-05	membrane-spanning 4-domains, subfamily A, member 6D
Irf1	1,08	9,25	8,2E-05	interferon regulatory factor 1
1110008P14Rik	1,28	10,85	8,6E-05	RIKEN cDNA 1110008P14 gene
Socs3	1,87	9,84	9,3E-05	suppressor of cytokine signaling 3
Fas	1,58	7,80	9,8E-05	Fas (TNF receptor superfamily member 6)
Col28a1	-2,53	8,59	9,9E-05	collagen, type XXVIII, alpha 1
Dram1	1,43	8,11	1,1E-04	DNA-damage regulated autophagy modulator 1
Junb	1,53	9,96	1,2E-04	Jun-B oncogene
Nfkbiz	2,18	9,34	1,2E-04	nuclear factor of kappa light polypeptide gene enhancer in B cells inhibitor, zeta
Gadd45g	1,24	8,32	1,3E-04	growth arrest and DNA-damage-inducible 45 gamma
Mmp13	1,48	7,35	1,3E-04	matrix metallopeptidase 13
Ccrn4l	1,23	8,99	1,3E-04	CCR4 carbon catabolite repression 4-like (S. cerevisiae)
Chi3l1	2,44	8,13	1,3E-04	chitinase 3-like 1
Casp8	0,73	8,31	1,4E-04	caspase 8
Hspb3	-0,93	7,45	1,5E-04	heat shock protein 3
Nrarp	-0,79	8,44	1,6E-04	Notch-regulated ankyrin repeat protein
Cst3	-1,10	13,51	1,6E-04	cystatin C
Cyp7b1	1,50	7,96	1,7E-04	cytochrome P450, family 7, subfamily b, polypeptide 1
Enpp1	-1,15	8,81	1,8E-04	ectonucleotide pyrophosphatase/ phosphodiesterase 1
Rassf10	0,84	7,31	2,1E-04	Ras association (RalGDS/AF-6) domain family (N-terminal) member 10
Clu	1,80	8,83	2,1E-04	clusterin
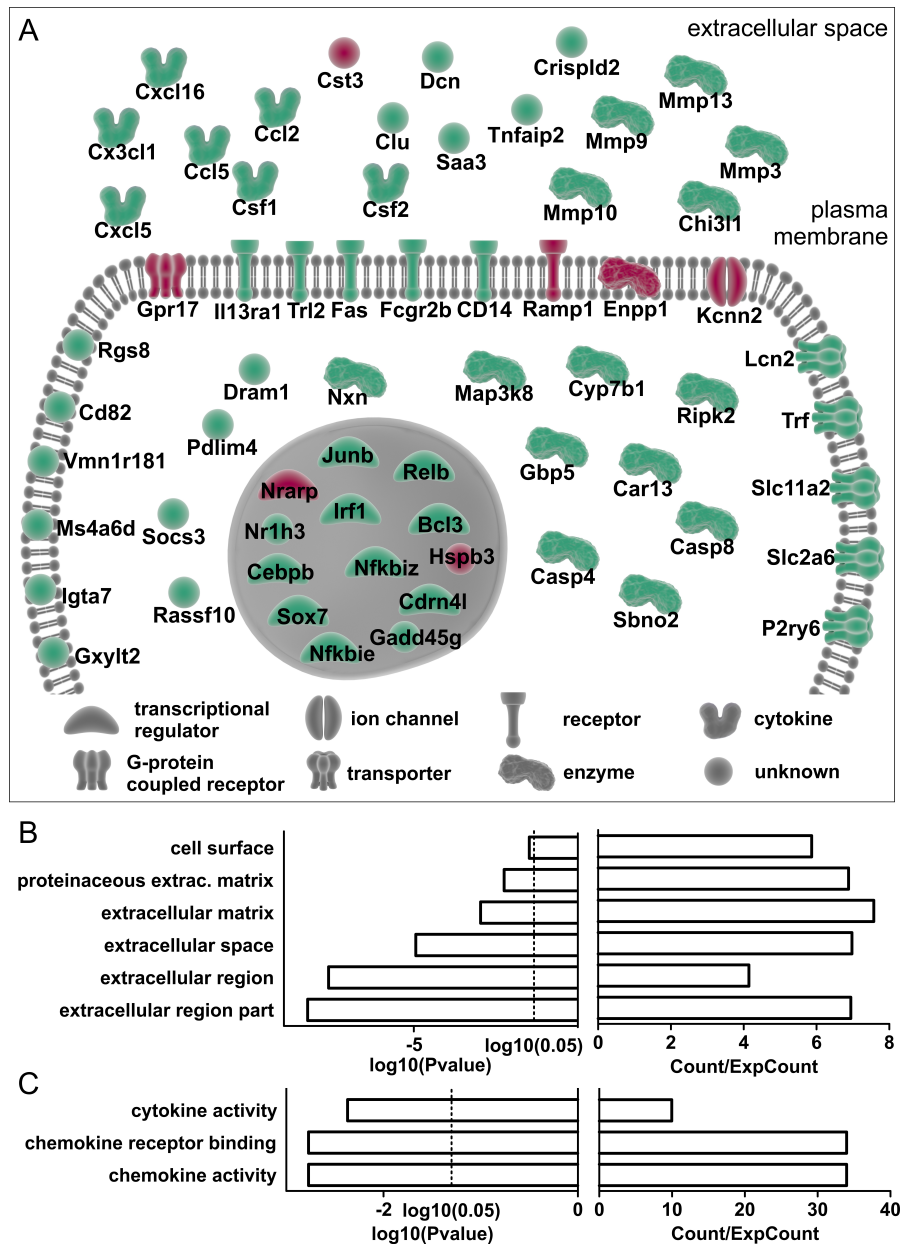
Figure 4.9: Differentially expressed genes upon LPS stimulation. (A) Graphic display of SDEGs with biological functions of the gene products and subcellular localization indicated. Green coloring indicates upregulation of expression, red color indicates downregulation. Significant enrichment of annotations to cellular compartments (B) in the dataset and to molecular functions (C). Enrichment is given as the count of genes associated to the term in the dataset relative to the expected count (Count/ExpCount). The level of significance is given as the base 10 logarithm of the p-value calculated using the Benjamini correction.
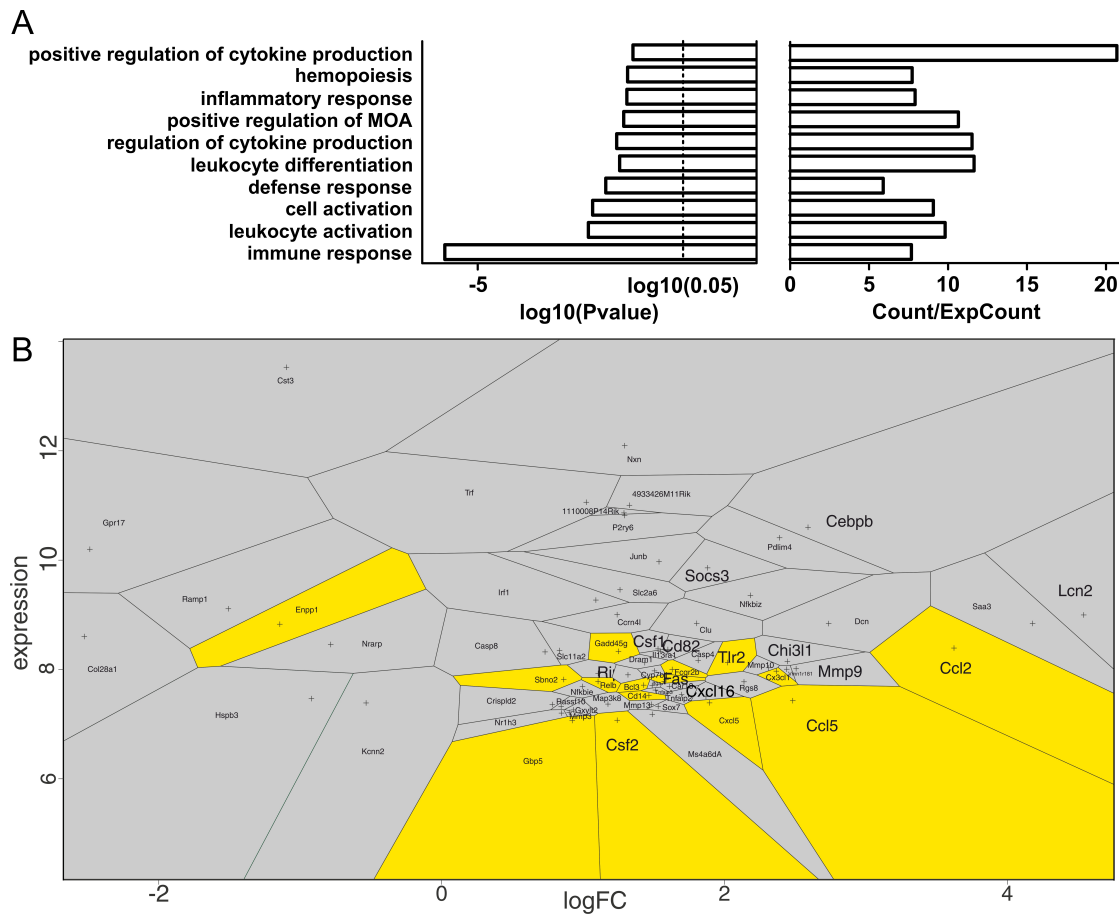
Figure 4.10: Biological processes associated with SDEGs upon LPS stimulation. (A) Top ten most significantly enriched annotations to biological processes of the LPS-affected genes. Enrichment is given as the count of genes associated to the term in the dataset divided by the expected count (Count/ExpCount). The level of significance is given as the base 10 logarithm of the p-value calculated using the Benjamini correction. The term "immune response" is enriched with the highest significance. (B) Voronoi-diagram displaying each significantly differentially expressed gene. Genes are plotted based on their absolute expression level and the relative expression change in response to LPS treatment given as fold change. The plotting area is segmented and a field is assigned to each gene, its size represents the unique character of the expression parameters. Yellow coloring indicates the association of a gene product to the GO-term "immune response". [119]

The GO analysis additionally gave an extensive list of statistically over-represented biological processes the 70 SDEGs were associated with (figure 4.10A) The most significantly enriched term is "immune response" (p < 2.6E-6), and other terms in the list have a similar biological context, such as "leukocyte activation", "defense response", "leukocyte differentiation" and "inflammatory response". However, the mere enrichment of the annotation does not imply the degree of differential expression of the respective genes. To gain a better understanding of the expression parameters of the genes associated to the "immune response"-term, a voronoi diagram was created (figure 4.10B). Here, each gene is plotted based on the absolute expression level and the relative

expression change in the response to LPS treatment, given as the logarithmic fold change. This results in a diagram with the distance from one gene's coordinates to its neighboring indicating the uniqueness of its expression parameters. For an easier display, the diagram is segmented into fields, and each field belonging to a gene consists of all points closer to the gene coordinates than to any other. In a next steps these fields were colored to indicate the association to the "immune response"-term (yellow) or any other term (grey). The resulting diagram displays that the "immune response"-associated genes include those genes with the highest fold-change increases in expression upon LPS-stimulation, such as chemokine (C-C motif) ligand 2 and 5 (Ccl2 and Ccl5).

Taken together, the microarray data reveal that upon LPS-stimulation GFAP-EGCs-derived gliospheres show a shift in gene expression profiles affecting 70 genes. Among these 70 SDEGs, a statistically enriched percentage of the respective gene products is associated with biological functions mediated at the extracellular site, predominantly signaling processes.

To validate these transcriptomic results, the nCounter technology was employed. This technique, like the microarray technology, relies on the hybridization of mRNA to a complementary probe and subsequent detection of the double-stranded complex. But unlike in microarrays, mRNA does not need to undergo any processing such as *in vitro* transcription prior to the assay, which minimizes potential biases in input samples. In a microarray application, this processing is necessary to label input RNA for detection of probe-bound RNA. In an nCounter assay, not the RNA is labeled but each probe is conjugated to a barcode consisting on a unique sequence of fluorescent dyes. When a barcoded probe binds to its complementary nucleotide sequence in input RNA, each resulting complex is digitally counted, which yields a higher accuracy on absolute transcript numbers than the microarray technology. However, with this barcoding approach it is not possible to reliably differentiate more than several hundred probes in one assay, which limits the number of genes to be assessed per array.

The accurate expression analysis of individually selected genes makes the nCounter technology highly feasible as validation method for microarray data. The strategy is hence to custom-design oligonucleotides to target genes that either showed differential expression in different conditions investigated, or genes that showed highly consistent expression over all conditions as reference genes. For this study 60 genes were selected: 7 reference genes with robust expression over all groups and 53 differentially expressed genes in multiple comparisons, 14 of which were SDEGs in the dataset of LPS-treated and untreated gliospheres analyzed in the microarray.

Other than the samples from LPS-treated and untreated gliospheres *in vitro*, both the microarray and the nCounter assay included an additional group, i.e. RNA from GFAP-expressing glia isolated directly after cell sorting without *in vitro* culture ("GFAP *in vivo*"). For these 60 genes nCounter probes were designed to bind to an overlapping nucleotide sequence as the original Illumina probes (see table 2.8).

Figure 4.11 displays the expression data of three of the groups investigated: *in vitro*-cultured gliospheres with and without LPS-stimulation and GFAP-glia analyzed directly after cell sorting.

As shown by the dendrogram in figure 4.11B technical replicates within each condition yielded highly similar results. Across all groups the gliospheres cultured *in vitro* with and without LPS-stimulation were more similar to each other than GFAP-glia *in vivo*. When comparing the relative expression changes measured with both techniques, highly significant correlations were found. In the comparison of *in vitro* cultures with and without LPS-stimulation (figure 4.11C) the correlation of relative expression data showed a Spearman correlation coefficient of r=0.74 (p < 0.0001). When comparing microarray and nCounter data on the comparison of GFAP-glia *in vivo* and *in vitro* (figure 4.11D), they again correlated significantly (r=0.40, p < 0.002). Hence it can be concluded that the shifts in transcriptomic profiles detected by the microarray were highly robust and reproducible in an entirely independent experimental approach.

4.3.1 Transcriptomic meta-analysis of gliospheres

An interesting aspect of the transcriptomic analysis was that culturing of cells *in vitro* induced a shift in gene expression profiles. To further assess this observation, the data on whole genome transcription were compared to those of other cell and tissue types deposited in a database repository (figure 4.12). Such a meta-analysis allows to group different cell types based on the resemblance of their transcriptomic profiles. It revealed that GFAP-glia *in vivo* showed high transcriptomic resemblance to other nerve cell entities, both from PNS and CNS and neural embryonic progenitors (figure 4.12A). These nerve cell types were grouped together but were dissimilar from all other cell types investigated, GFAP-glia cultured *in vitro* included. Concerning the latter, there was a high similarity between gliospheres with and without LPS-treatment, and from there the closest resemblance was to a heterogeneous group including different neural and non-neural precursor cell types. Interestingly, the cluster of *in vitro* cultured GFAP-glia showed a higher similarity to a number of inner organs (e.g. reproductive organs, lung heart) than to GFAP-glia *in vivo*, from which they had been generated. Taken together, the meta-analysis confirmed that the degree of similarity of the three test groups observed in the nCounter array on the basis of only 60 genes was valid when taking the whole genome into account. Additionally, it showed that prolonged *in vitro* culture led to a shift in expression of genes shared by different nerve cell entities towards a less differentiated phenotype.

To investigate glial-specific aspects of the genetic profiles further, a second meta-analysis was conducted incorporating different CNS- and PNS-derived glial cell types (figure 4.12B). This analysis revealed a high transcriptomic resemblance of enteric GFAP-glia *in vivo* to CNS astrocytes. GFAP-glia cultured *in vitro*, however, showed more similarities to peripheral glia derived from sciatic nerves. Both enteric cell types were rather dissimilar to microglia. Interestingly, while LPS-stimulation affected the transcriptomic profile of CNS astrocytes severely, the LPS-mediated effect on enteric glia was far less pronounced.

To summarize, the transcriptomic profiling revealed that GFAP-EGCs are transcriptionally sim-
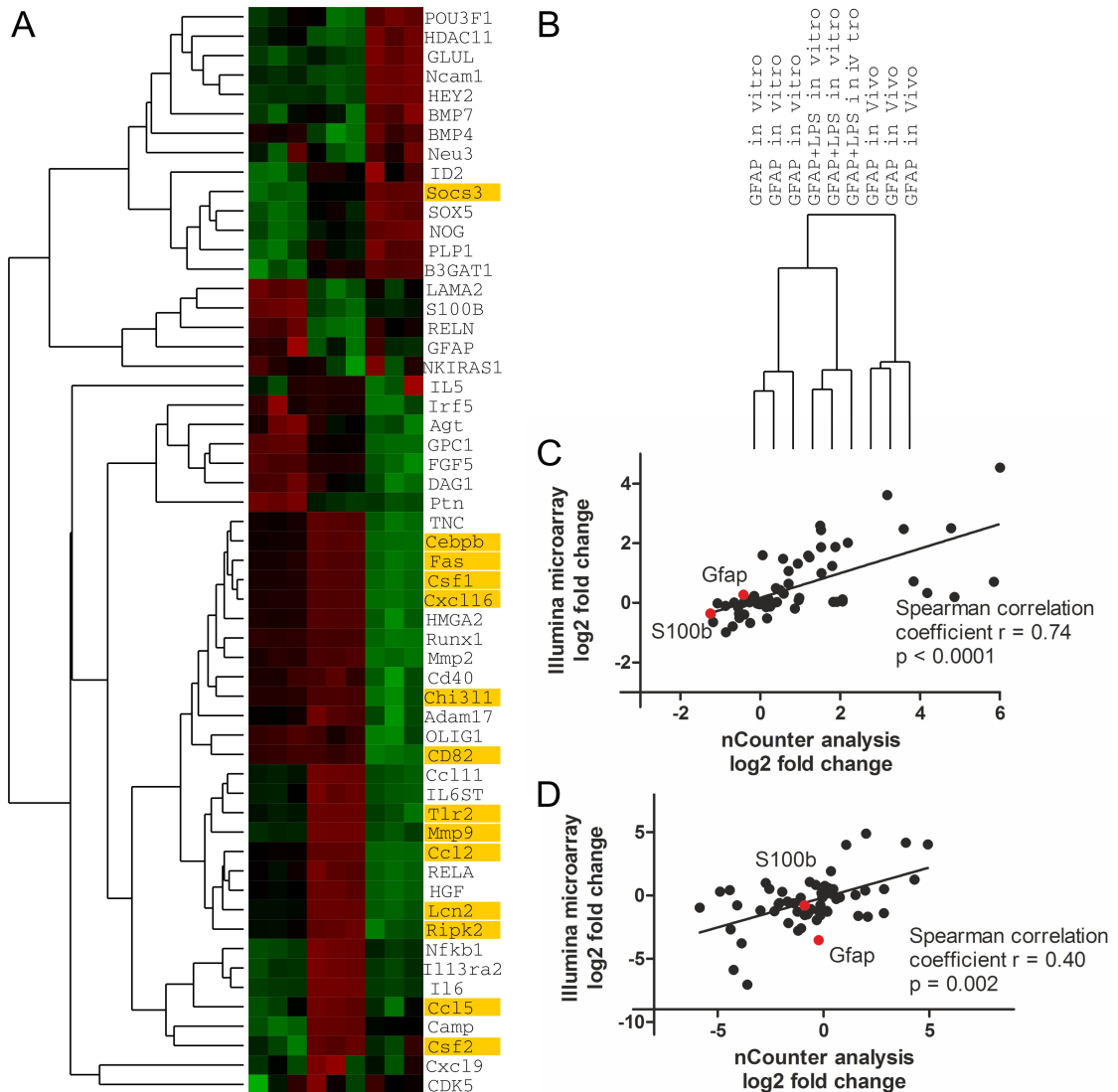
Figure 4.11: Validation of microarray data with the nCounter technology. (A) Heatmap displaying transcriptomic data on GFAP-glia *in vivo* and *in vitro* with and without LPS-stimulation acquired with nCounter technology. Lane labels are given in (B). Yellow highlighting indicates significant upregulation in the LPS-microarray dataset. (C-D) Correlation of the gene expression data acquired with the nCounter and Illumina microarray technologies. (C) Correlation of data on the comparison of GFAP *in vitro* versus GFAP+LPS *in vitro*. (D) Correlation of data on the comparison of GFAP *in vivo* versus GFAP *in vitro*. Data obtained with both technologies correlate highly significantly in both comparisons.
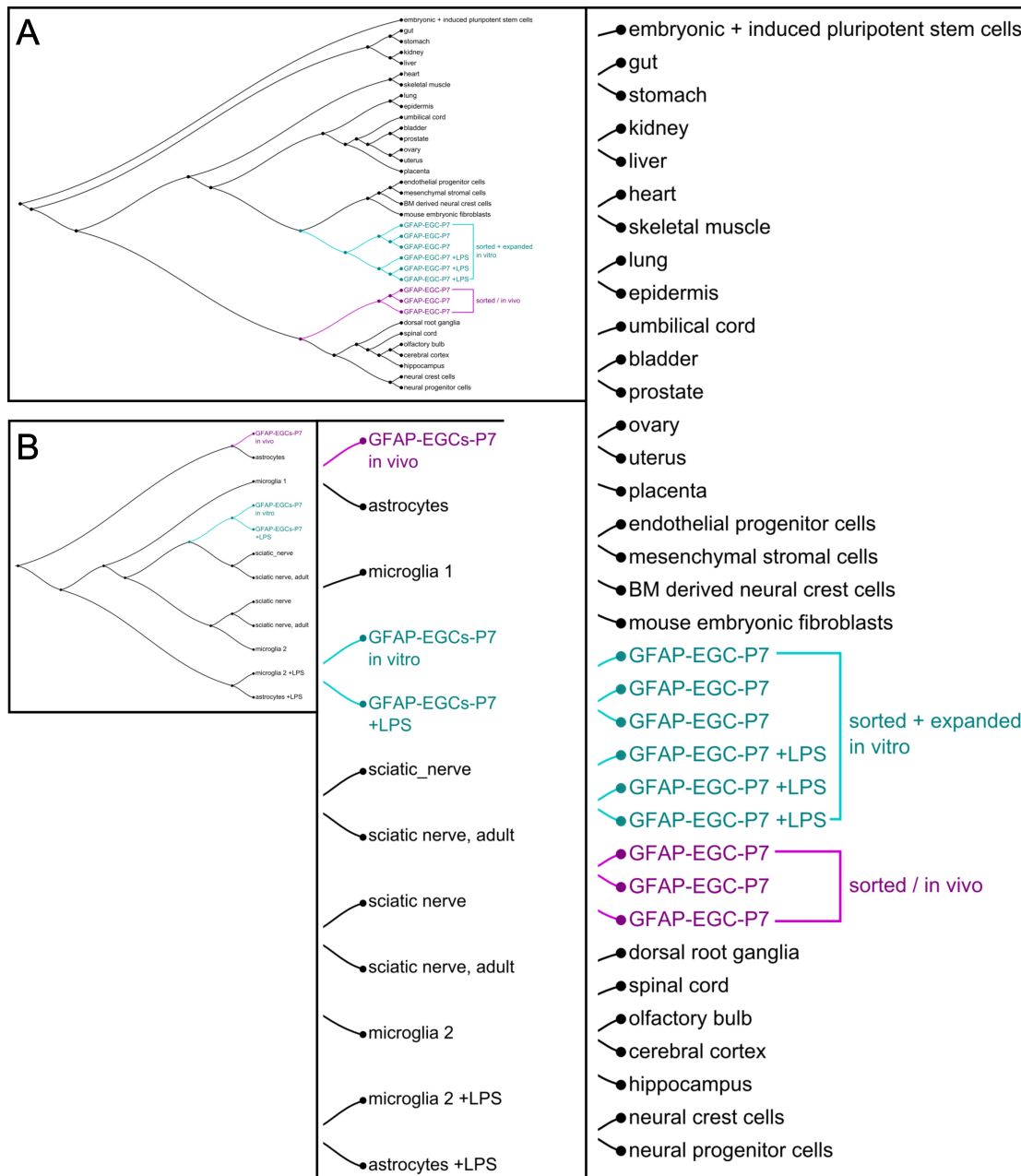
Figure 4.12: Comparative transcriptomic meta-analyses reveal genetic similarities among different tissue and cell types. The length along the line connecting two datasets in the dendrogram indicates the degree of similarity; the shorter the distance of connecting lines, the more similar these datasets are. For better legibility the list of datasets are enlarged right of the dendrogram overview. (A) GFAP-glia *in vivo* are highly similar to CNS and PNS nerve cell types and show a much lower similarity to GFAP-glia expanded *in vitro*. Gene expression profiles of the latter show similarities to mesenchymal cell types. (B) GFAP-glia *in vivo* transcriptionally resemble astrocytes *in vivo*. If cultured *in vitro*, the GFAP-glia genetic profile has higher similarity to PNS sciatic nerve cells and CNS microglia. [119]

ilar to other nerve cell types, especially astrocytes. When cultured *in vitro* for several weeks, GFAP-EGCs loose the transcriptomic resemblance to differentiated nerve cell types. However, they are responsive to LPS-stimulation *in vitro* and show differential expression of genes associated predominantly with immunologic processes mediated by secreted signaling molecules.

4.3.2 Signaling molecules secreted by gliospheres

From the LPS-challenged gliosphere cultures (see 4.3) supernatants were used to measure the secretion of different pro- and anti-inflammatory cytokines by multiplex protein profiling (figure 4.13). Elevated levels of different pro- but also anti-inflammatory signaling molecules were detected upon LPS-stimulation. Secretion of the pro-inflammatory cytokine interferon (IFN)-γ was found to be robustly increased to the 2-fold (p < 0.001) (figure 4.13A). The other pro-inflammatory cytokines were not consistently increased in the different independent experiments, but showed a clear tendency for increased secretion following exposure of gliospheres to LPS, except for tumor necrosis factor (TNF)-α, which showed no such increase. The most prominent increase in LPS-induced secretion was measured for interleukin (IL)-1β (figure 4.13C), however, severe divergences were detected among the individual replicates, making this increase not statistically relevant.

Interestingly, anti-inflammatory cytokines were measured in elevated levels after LPS-treatment as well, IL-4 showed a significant increase to the 2.6-fold (p < 0.05). These findings indicate a complex regulatory role of EGCs in contributing to the inflammatory intestinal environment.

Taken together, the inflammatory stimulation of murine gliospheres *in vitro* led to a shift in gene expression profiles affecting a number of genes associated with inflammatory response processes. Gene products of the affected genes were largely associated with chemokine and cytokine activity. An increased secretion of signaling molecules could be validated on protein level by analyzing the supernatants of LPS-treated gliospheres. These results clearly indicate that GFAP-expressing glia have the potential to respond to a bacterial invasion with secretion of inflammatory signaling molecules and modelling of the inflammatory intestinal environment.

4.4 Acute inflammatory bowel disease model *in vivo*

The results on immunomodulatory capacities of GFAP-expessing EGCs *in vitro* legitimated an analysis of these cells under acute inflammatory conditions *in vivo*. To specifically study GFAP-expressing EGCs, transgenic hGFAP-eGFP mice were employed to set up chemically induced mouse models of intestinal inflammation. Several strategies using different chemical agents have been published to induce an IBD-like phenotype in mice [85]. In the present study dextran sodium sulfate (DSS) and 2,4,6-trinitro benzene sulfonic acid (TNBS) were chosen. As intro-
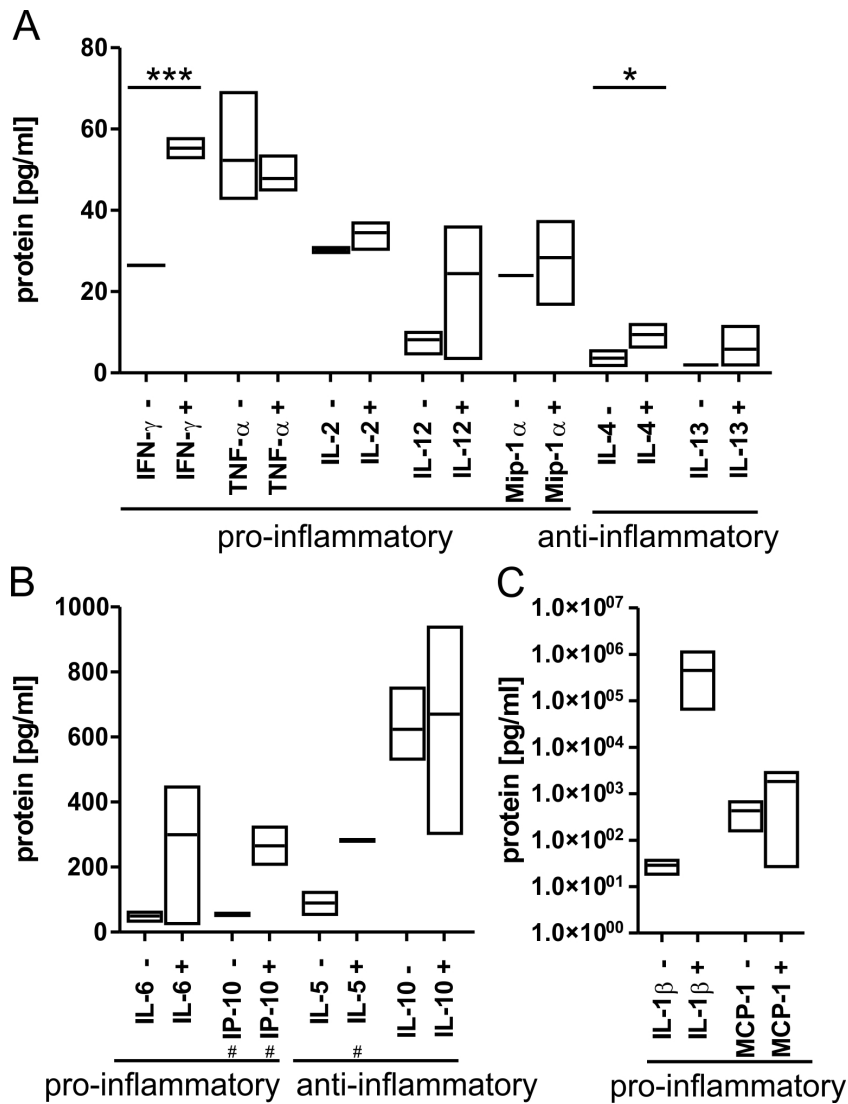
Figure 4.13: Signaling molecules secreted by gliospheres. (A) Secretion of pro- and anti-inflammatory signaling molecules in the range of 0 - 80 pg/ml secreted by gliospheres derived from GFAP-expressing EGCs. All signaling molecules measured but TNF-α were measured in increased concentrations after LPS-stimulation. (B) Secretion of signaling molecules in the range of 0 - 1000 pg/ml. (C) Secretion of signaling molecules in the range of 0 - 1$\times$ 10^{07} pg/ml plotted on a logarithmic scale Each box displays the maximum, minimum and mean value of three independent experiment, if not indicated otherwise. (+) and (-) indicate the presence or absence of LPS-stimulation. n = 3, * p < 0.05, *** p < 0.001, # indicates that one of the three replicates was not measurable. [119]

duced in section 1.6 TNBS and DSS employ different modes of action: TNBS haptenizes colonic proteins rendering them immunogenic to the host immune system [85], whereas DSS acts toxic on epithelial cells and causes a breakdown of the epithelial barrier. Since these two agents affect the intestinal tissue via different mechanisms, employing both might provide complementary

information on the role of EGCs in intestinal inflammation. However, an essential prerequisite for inducing colitis with chemicals is the susceptibility of the mouse strain employed for the respective chemical. In the present study transgenic mice of the FVB/N background were used, for which there is only scarce information on the susceptibility to TNBS and DSS, respectively. Thus, it was essential to assess the potency of these agents to induce an acute intestinal inflammation. This assessment included daily monitoring and endpoint analysis of different parameters described in the following section.

4.4.1 Disease activity index (DAI) scoring of the IBD model

During the 7-day test period all 80 animals were scored each day for different parameters of disease activity. These included body weight, consistency of feces and feacal blood but also the overall physiological and behavioral appearance of the animals. Figure 4.14 shows the progression of scorings for body weight loss, for stool consistency and for fecal blood. A detailed study design and composition of the groups is given in section 3.1.2. Interestingly, there was no sub-
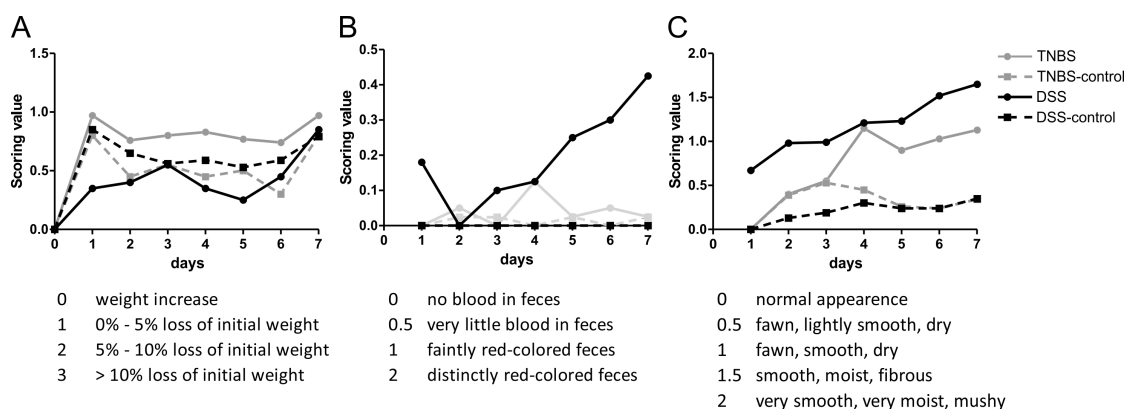

0	weight increase	0	no blood in feces
1	0% - 5% loss of initial weight	0.5	very little blood in feces
2	5% - 10% loss of initial weight	1	faintly red-colored feces
3	> 10% loss of initial weight	2	distinctly red-colored feces

0	normal appearence
0.5	fawn, lightly smooth, dry
1	fawn, smooth, dry
1.5	smooth, moist, fibrous
2	very smooth, very moist, mushy

Figure 4.14: Daily scoring of disease activity parameters. Criteria for scoring values are given below the respective diagrams. Scoring results for animals of the DSS-group are colored in black, those for animals of the TNBS-group are colored in grey. Results on substance-treated animals are indicated with circular symbols connected with a solid line, results on the respective control-treated animals are indicated with rectangular symbols connected with a dashed line. (A) Daily scoring of weight loss. (B) Daily scoring of blood in feces. (C) Daily scoring of feces consistency. n = 20

stantial loss of body weight observed in either of the groups (figure 4.14A) . None of the groups reached a mean scoring value above 1, which is equivalent to a loss of 0% to 5% of the initial body weight, indicating that a groups's average weight loss on each day was below 5% of the initial body weight. DSS-treated animals showed on average less weight loss than the untreated control group during the first five days, but showed an increased weight loss during the last two days of experiment. In contrast, animals of the TNBS-treated and TNBS-control groups reached a peak in weight loss scoring on the day after substance injection, that subsided in the following

days but reached a second peak on the final day of experiment. The early peaks observed in TNBS- and TNBS-control groups are likely due to the glycerin enema performed prior to ethanol and TNBS injection. This glycerin enema was performed to induce bowel emptying and hence to ease the application of test substances. However, on the final day of experiment both the DSS- and the TNBS-treated groups as well as their respective control groups reached similar scoring values.

In contrast to body weight, daily scoring of feacal blood yielded treatment-specific differing results (figure 4.14B). A scoring value of 0.5 was assigned when feacal blood was not apparent, but became evident when feces was lightly squeezed between clean tissue towels. A scoring value of 1 was assigned when feces showed a reddish color and of 2 when feces was distinctly colored red. DSS-treated animals showed the highest mean scoring value among the groups on the first day after initial substance administration. Especially within the last days of the test period, the DSS-treated group yielded the highest scoring values of up to a mean value of 0.43.

DSS-treated animals additionally reached the highest scoring values on changes in feces consistency (figure 4.14C). For this parameter the color, the softness and the moisture of feces was analyzed. The DSS-group's score increased consistently throughout the experiment, so did the TNBS-treated group but to a lesser extend than the DSS-treatd animals.

In addition to parameters recorded daily, further scoring data were obtained from colonic tissue after the intestine was removed. The length of the colon was measured as one scoring parameter. Subsequently, a segment was excised and haematoxylin and eosin stains were performed to assess histological indications of tissue inflammation. For this histological scorings alterations in the epithelium, the mucosa and submucosa were assessed. For the epithelium, reduction in goblet cells and disruptions in crypt architecture were considered. Density and depth of immune cell infiltrates were assessed, ranging from minor infiltrates at the crypt base or between crypts and muscularis mucosae to infiltrates into the submucosa. Also, erosions of the epithelium, ulcers and abscesses caused by granulocytic infiltrates were scored. A complete list of the histological parameters and their assigned scoring value is given in table 3.11.

Figure 4.15A summarizes all scoring results; for those parameters collected daily the scoring value taken on the final day of experiment is given. DSS-treated animals reached significantly higher values in the histological scorings and scorings of feces qualities as well as significantly reduced colon lengths. Unaffected by the DSS-treatment was the weight of the animals and neither were changes in behavior and physical appearance observed. TNBS-treated animals, on the other hand, developed less severe signs of inflammation. Only two scoring parameters reached significantly different values in TNBS-treated animals compared to untreated controls, those were scorings of the histology and of feces consistency. Figure 4.15B shows representative histological stainings of the colon tissues of all groups. The majority of DSS-treated animals showed disruptions in the epithelial crypt architecture and infiltrates of immune cells in the epithelial layer or as far as the submucosa. These histological indications of inflammation resulted in the highest mean scoring value for DSS-treated animals among all groups assessed. A further
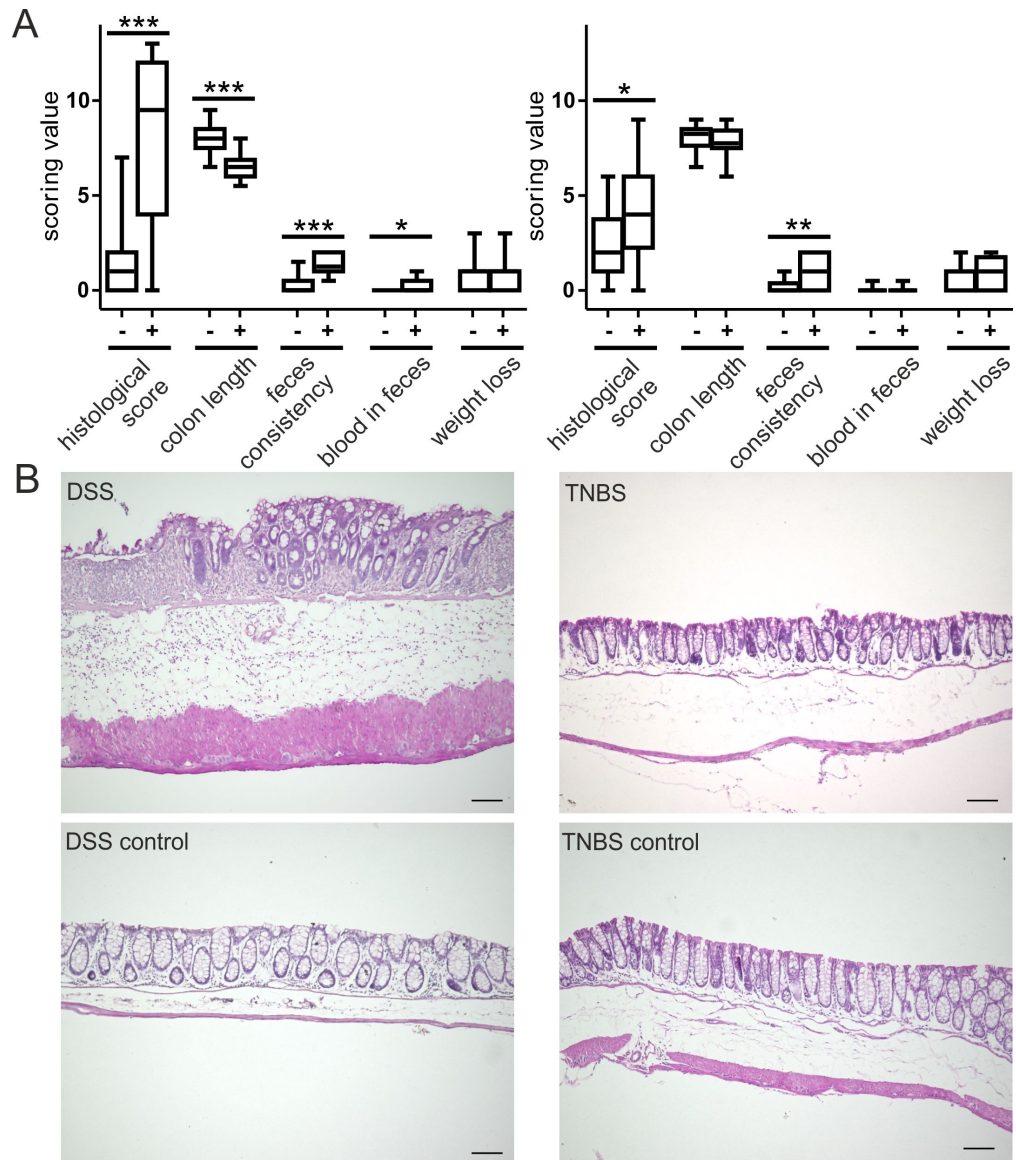
Figure 4.15: Endpoint scoring data of DSS- and TNBS-treated animals. (A) Endpoint scoring data of DSS-treated animals (left) and TNBS-treated animals (right). DSS-treated animals (+) show significant alterations in scoring values on histological scoring, feces qualities and colon length compared to control-treated animals (-). TNBS-treated animals (+) display less pronounced alterations in fewer categories. (B) Representative hematoxylin and eosin stains of colonic tissue from a DSS-treated animal (upper left) and respective control (lower left) . Tissue from DSS-treated animal shows severe disruption of epithial crypt architecture due to immune cell infiltrates, which infiltrate mucosa and submucosa densly. Tissue from TNBS-treated animal (upper right) or respective control (lower right) do not show severe inflammation. Scale = 100 μm, n = 20, * p < 0.05, ** p < 0.01, *** p < 0.001.

prominent feature of tissue sections obtained from DSS-treated animals was a thickening of the muscle layer. In consultation with a pathologist from the university hospital Würzburg, this feature was not integrated in the histological scoring, since the appearance of the muscle depends on the stretching of the tissue by intestinal contents and is not a histological feature.

In summary, the disease activity index, that is the sum of the different scoring values, is a tool to quantify the symptoms evoked by the chemical treatment of mice. It identified the administration of 3% DSS better suited to induce an acute inflammation in the colon of FVB/N-mice than an injection of TNBS. Noteworthy, male mice in the DSS-treated group scored on average higher DAI values in all categories assessed except for the histological score; here, males and females reached identical mean scores. The increase in scoring values in males was most prominent for occult blood, but did not reach statistical significance in any category.

4.4.2 Transcriptomic analysis of isolated GFAP-EGCs from the IBD model

Next, the effects of the intestinal inflammation on GFAP-expressing glia within the colon tissue were assessed (4.16). For this, the colon was removed and to facilitate the tissue digest the muscle layer was peeled off of the mucosa and both were digested in enzyme solutions (see section 3.2.2). The resulting two cell suspensions were pooled and sorted via flow cytometry to specifically select the GFAP-expressing glia via their GFP expression. In a first step, the cells were analyzed for morphological criteria (i.e. volume and by granularity) by how they scattered light in the laser beam detected as forward- and side-scattered light. Based on these morphologic parameters viable cells were distinguished from debris, dead cells and duplets. A positive selection of the viable cell population is of special importance in the context of tissue digests, since debris can have a high autofluorescence that might impact the sorting efficiency. The events recorded for an intestinal tissue digest contained on average only about 15% viable cells (data not shown). This population is shown representatively in figure 4.16A in a two-color fluorescence dot plot. Only a minor fraction ($\leq 1\%$) was prominently GFP-positive and was collected for further analysis. Worth mentionioning, induction of inflammation had no effect on the number of GFP-positive glia extracted from the tissue.

From those cells RNA was isolated and mRNA levels of the inflammatory signaling molecules IL-1β and IL-6 as well as the transcriptional activator of the class II major histocompatibility complex (CIITA) were measured and normalized against the expression level of the reference gene HPRT. Optimal annealing temperature and efficiency of each primer pair were determined beforehand and are given in table 2.7. As shown in figure 4.16B RNA isolates from DSS-treated mice contained on average higher levels of the inflammatory mediators IL-1β and IL-6. However, samples from DSS-treated animals showed considerable variations in RNA levels of these interleukins, which rendered the increase not statistically significant but a tendency. For CIITA mRNA levels, the increase in DSS-treated animales was more consistent and hence statistically
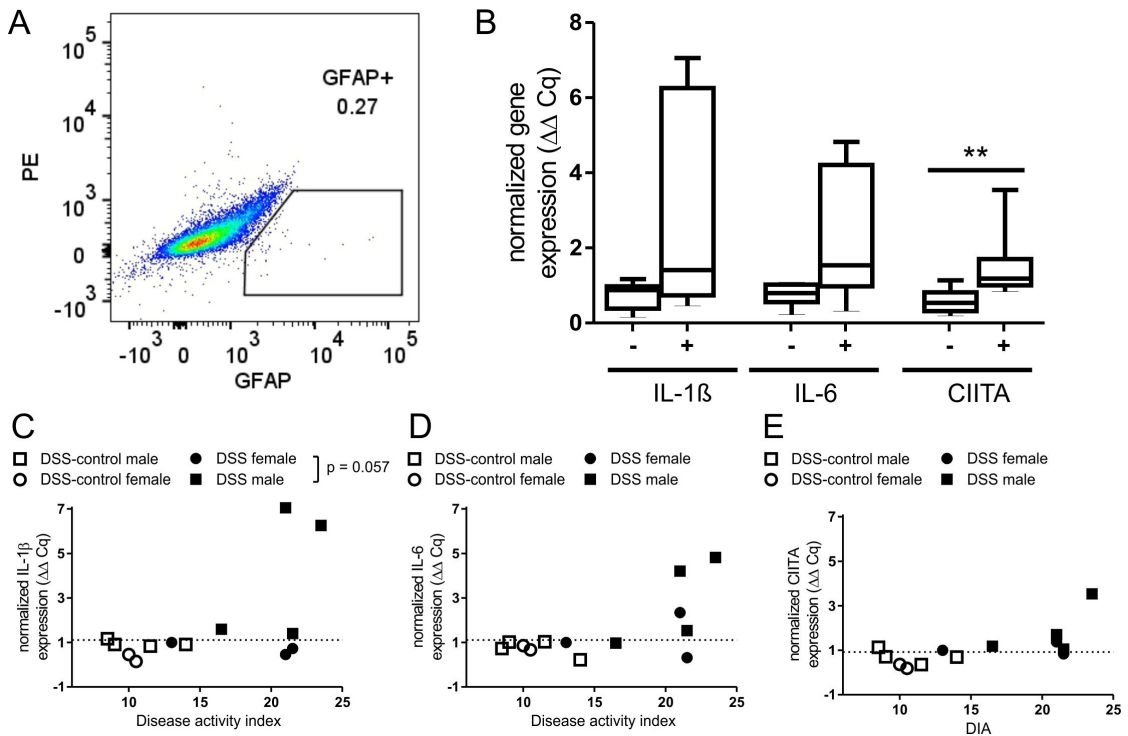
Figure 4.16: GFAP-expressing glia isolated from DSS-treated animals express inflammatory mediators. (A) Representative dot plot displaying flow cytometry data of the cell suspension obtained after colon tissue digest. Cells displayed have been identified as the viable population by morphologic gates (not shown). Less than 1% of the population is prominently GFP- (i.e. GFAP) positive. (B) Box and whisker plot displaying qPCR results of the GFAP-positive subpopulation (see A). On average, DSS-treated animals (+) express higher levels of IL-1β, IL-6 and CIITA mRNA compared to untreated controls (-) For CIITA the difference reaches statistical significance (p = 0.008). (C-E) Correlation of expression levels for the different genes (IL-1β, IL-6 and CIITA, respectively) to the disease activity index of the animal from which RNA was isolated. Filled symbols represent DSS-treated animals, empty symbols represent untreated controls. Circles represent females, squares represent males. Dashed lines indicate the mean expression plus SD of the control-treated group. n = 6-7, ** p < 0.01.

significant (p = 0.08).

Interestingly, the dispersion of normalized expression levels of interleukins was only detected in the DSS-treated group, the untreated control group yielded much more consistent expression levels. It is conceivable that expression of inflammatory mediators is correlated to disease manifestation. Since this varied among individual animals considerably (see fig. 4.15), normalized expression levels of the inflammatory markers were correlated to the disease activity index of the respective animal (fig. 4.16C-E). It was found that the animal with the highest DAI value expressed highly elevated levels of all three inflammatory markers. However, some animals that scored high in DAI values showed non-elevated normalized mRNA expression levels, so that a clear correlation of DIA value to inflammatory marker expression cannot be postulated. For IL-1β and IL-6, only four of the seven DSS-treated animals exhibited expression levels higher

than the mean value of the control group plus the group's standard deviation. Most interestingly, for IL-1β these four animals were all males, whereas the non-elevated samples were all from females. When statistically comparing the normalized expression levels of IL-1β in DSS-treated males to DSS-treated females, expression levels in males are elevated with statistical tendency (p = 0.057). For IL-6 the four animals with increased expression levels encompassed three males and one female. For CIITA, no relevant differences in inflammatory expression between males and females was found.

To conclude, the analysis of GFAP-expressing glia isolated from acutely inflamed intestinal tissue revealed a tendency for this population to upregulate the expression of inflammatory marker. Those include pro-inflammatory cytokines such as IL-1β and IL-6 but also an activator for major histocompatibility complex class II (CIITA), a protein complex responsible for presentation of antigens to activate immune cells.

4.4.3 Colocalization study of GFAP-EGCs and immune cells *in vivo*

The gene expression analysis of GFAP-expressing glia in acutely inflamed intestinal tissue had revealed a tendency for increased expression of genes associated with a crosstalk with immune cells. To approach the question if GFAP-glia indeed interact with lamina propria immune cells under inflammatory conditions, a histological analysis was chosen to assess a potential colocalization of these cell types. In order to gain a good understanding of a large tissue volume, both along the rostro-caudal axis and the serosal-luminal axis, the light sheet fluorescence microscopy technique was employed. This technology allows high-resolution imaging combined with high in-depth penetration of the tissue by a clearing procedure that makes the tissue transparent. The processing procedure involves whole animal perfusion fixation, post-fixation of colon tissue, pre-treatment to permeabilize the tissue and block unspecific binding sites and overnight-incubation with antibodies. Rendering the tissue transparent is done by replacing water with a substance with a refractive index similar to proteins. Hence dehydration with graded ethanol series and submersing the tissue with a clearing substance is necessary, here one part benzyl alcohol and two parts benzyl benzoate (BABB) were employed. Subsequently, stained tissue are illuminated by laser light sheets of different wavelengths. Scanning of the tissue is achieved by moving the sample through the light sheet by a defined increment. Up to 500 images were recorded per channel, changing the excitation wavelength and emission filter plane by plane, resulting in scanned colon segments of up to 2.5 mm length. Figure 4.17 shows representative stainings of colon segments from a DSS-treated animal and an untreated control. The intrinsic autofluorescence of the tissue can be recorded by excitation with a light sheet of 488 nm wavelength and gives information on the tissue architecture (figure 4.17A, G). To visualize GFAP-expressing glia, non-transgenic animals were employed and cells were stained with a specific primary rabbit anti-GFAP antibody, which was then visualized with a secondary Cy$^{\text{TM}}$ 3 anti-rabbit antibody (figure 4.17B,
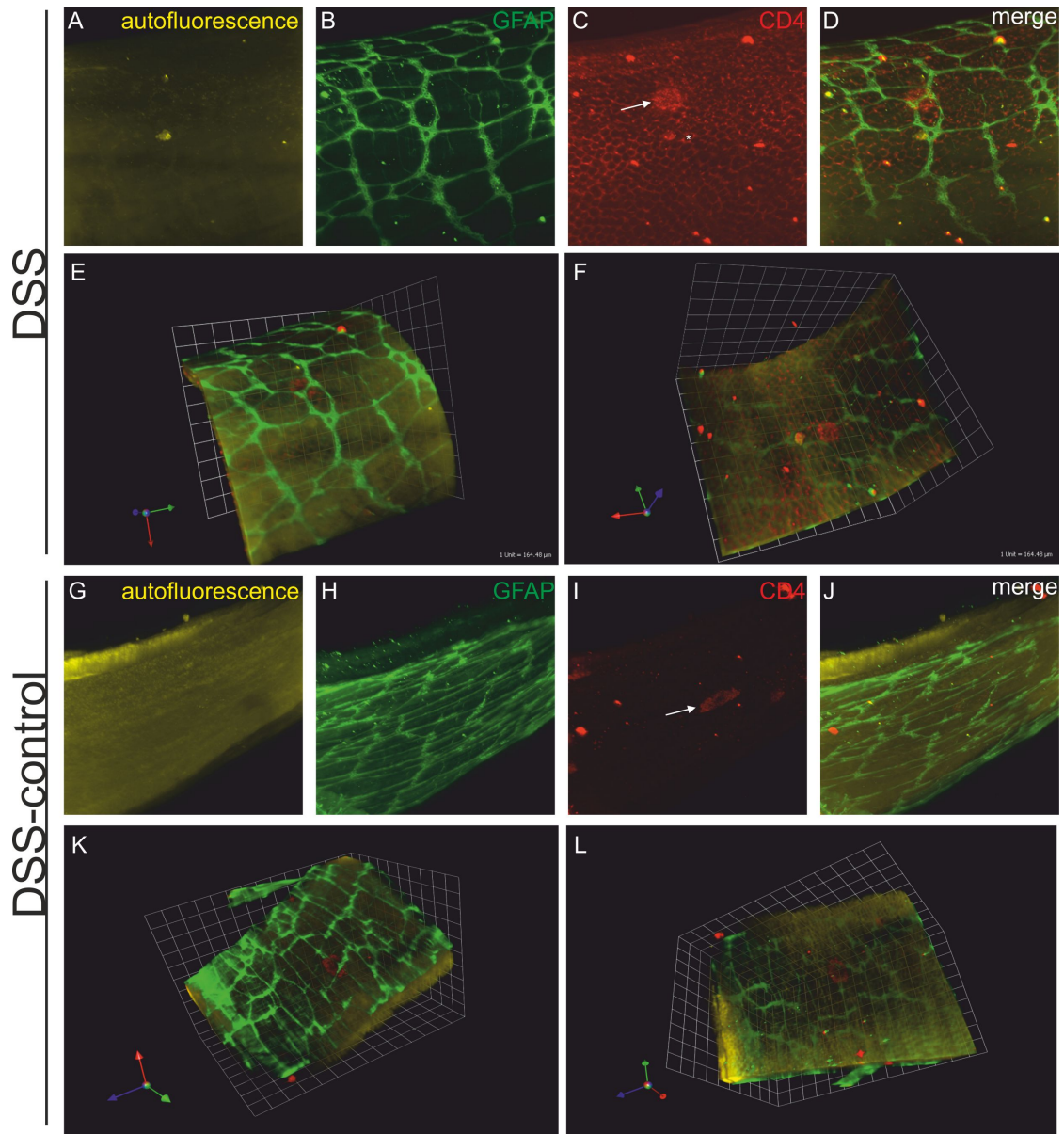
Figure 4.17: Colocalization of GFAP-expressing glia and CD4-positive lymphocytes. Reconstructions of single optical sections obtained by LSFM (x5 objective, 5 μm increment) of colon tissue in 3 color channels. (A-F) Colon tissue sample from a DSS-treated animal and (G-L) from an untreated control. (A, G) 2D reconstruction of optical sections obtained in the green color channel to visualize intrinsic autofluorescence. (B,F) 2D reconstruction of antibody-stainings against GFAP and (C, I) against CD4, arrows indicate immune cell aggregates. (D, J) Color merges of the respective single channels. (E-F) and (K-L) 3D reconstructions of color-merged optical sections reveal the tissue architecture and allow analysis from different perspectives. A grid unit has a length of 165 μm.

H). Transgenic GFP-expressing animals were not used for LSFM, since the fixation denatures GFP and is not well-detectable with the high autofluorescence of the tissue. With this procedure it was possible to visualize the ganglionic architecture of the glial myenteric network, as well as subjacent glial fibers. However, staining intensity in deeper parts of the tissue was not sufficient to visualize finely branched fibers, especially those projecting into the mucosa. When comparing the myenteric glial networks in DSS-treated animals and untreated controls, no evident alterations were observed.

Tissues were simultaneously co-stained with a directly conjugated Alexa Fluor® 647 anti-mouse CD4 antibody (figure 4.17C, I). Here, the tissue from DSS-treated animals showed a dense infiltration with CD4-positive lymphocytes. Distribution of those cells appeared like a fine-meshed network with regular recesses. This appearance is presumably caused by colonic crypts, indicating that these CD4-positive cells are located within the intraepithelial compartment. Additionally, an aggregate of CD4-positive cells was detected, ,likely visualizing an isolated lymphoic follicle (ILF). For the untreated controls no tissue-infiltrating CD4-positive cells, but an ILF-structure was detected.

On overlay of the single-channel picture in 2D (figure 4.17D, J) or in 3D (figure 4.17E-F, K-L) revealed the spatial arrangement of the different cell types within the tissue. Since the myenteric plexus is situated in the muscle layer and lymphocytes are located within the epithelium and lamina propria, no direct colocalization could be visualized.

Taken together, the induction of an acute intestinal inflammation in FVB/N mice was achieved by administration of 3% DSS for 7 days. The resulting phenotype affected the histological appearance of the mucosal and submucosal tissue as well as qualities of feces and colon length. GFAP-expressing glia isolated from this colon tissue showed a tendency to express elevated levels of mRNA coding for pro-inflammatory cytokines and a transactivator for the MHC-II complex. Though this suggests a direct interaction with lamina propria lymphocytes, no spatial colocalization of GFAP-glia with CD4-positive T cells could be visualized.

4.5 Primary 3D intestinal neuro-epithelial models *in vitro*: preliminary data

A thorough understanding of IEB impairments in intestinal pathologies such as in IBD is crucial for the development of therapeutic strategies. Since EGCs and other neural entities are important modulators of IEB homeostasis (see section 1.3), they need to be integrated in next-generation tissue models that allow the mechanistic study of IEB physiology. In preliminary experiments the basis for the establishment of 3D intestinal barrier models for the study of neuro-epithelial interactions was laid (see figure 4.18).
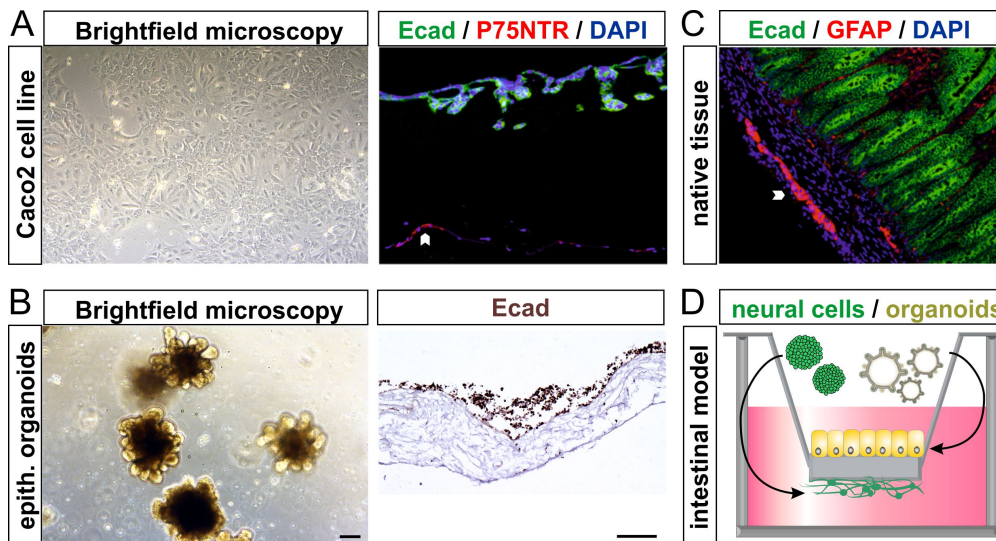

Figure 4.18: Preliminary data on the establishment of a 3D intestinal model for the study of neuro-epithelial interactions. (A) Left: Representative brightfield microscopy image of the epithelial cell line Caco2. Right: IHC of a co-culture of Caco2-cells seeded onto the mucosal side of the SIS-muc with primary unsorted ENS-cells seeded onto the serosal side and stained with antibodies as indicated in the figure. Arrowhead indicates an aggregate of P75NTR$^+$ cells resembling a plexus structure in the native tissue (see arrowhead in (C)). (B) Left: Representative brightfield microscopy image of primary epithelial colonic organoids. Right: IHC of a matrigel-coated SIS seeded with dissociated primary epithelial organoids and stained as indicated. (C) IHC of native intestinal tissue stained as indicated. (D) Proposed co-culture setup for the establishment of 3D intestinal neuro-epithelial models integrating both primary epithelial organoids and primary neural cells grown as neurosphere-like bodies. Scale = 100 μm.

One strategy for physiologically relevant 3D *in vitro* tissue model is to culture primary cells on a matrix that supplies suitable culture conditions and, if possible, mimics the native extracellular matrix (ECM) of the respective organ. Here, two different cell sources of epithelial cells were employed: (i) the human colorectal adenocarcinoma-derived cell line Caco2 and (ii) primary murine colonic epithelial cells expanded as organoids. The first was seeded on the former mucosal side of a decellularized SIS with preserved mucosal layer. As shown in figure 4.18A the cells

adhered well and populated the preserved crypts and villi of the matrix. On the former muscular side primary cells isolated from LMMP-digests were seeded and the containing P75NTR$^+$ cells formed an aggregate reminiscent of plexus structures in the native tissue (figure 4.18C). A future goal for improving this model is to replace the cell line by primary epithelial cells. Seeding of murine colonic epithelial organoid-derived cells onto the SIS could be established, however, the cells did not form a tight monolayer (figure 4.18B, functional data not shown). Further optimization of the seeding and culture protocol is needed to establish functional barrier co-culture models. Such future models will not only encompass a tight barrier of primary epithelial cells but also ENS cells as their modulators (figure 4.18D).

4 Results

5 Discussion

The overall aim of this thesis was to investigate the effects of an intestinal inflammation on the physiology of enteric glial cells on a cellular and molecular level. EGCs were studied in a novel *in vivo* model of sepsis to assess the effects of an acute and severe inflammation (hyperinflammation) that affects all compartments of the intestinal wall. In this study, myenteric glia were found to rapidly respond to inflammation with an increase in gene expression levels of the cytoskeletal component GFAP. Hence, the GFAP-expressing glial population was specifically adressed in *in vivo* and *in vitro* experiments. *In vitro*, primary cell cultures were established using transgenic mice, which express GFP under the human GFAP promotor. From these mice muscle tissue strips were enzymatically digested and the GFAP-expressing glial population was enriched via cell sorting and propagated as spheroid cultures. These gliospheres were exposed to an inflammatory stimulus and resulting changes in gene expression profiles revealed a shift in transcriptomic profiles towards the expression of genes coding for proteins associated with signaling processes linked to immune responses. Additionally this GFP-labeled glial population was studied *in vivo* in a well-established chemically induced disease model of IBD to elucidate its specific contribution to disease manifestation. The GFAP-expressing glial population showed a tendency to upregulate the expression of inflammatory mediators usually expressed by immune cells.

Taken together, these results identify GFAP-expressing EGCs as quickly responsive to systemic and mucosal intestinal inflammation and reveal the induction of a phenotype reminiscent of reactive astrocytes with immunomodulatory capacities.

5.1 ENS alterations in the acute hyperinflammatory model *in vivo*

Alterations within the ENS in response to intestinal inflammation *in vivo* have been investigated extensively [39, 45, 120–124]. Interestingly, the vast majority of these studies have focused on mucosal inflammation such as in CD, UC and the respective experimentally inducible model systems. Mucosal inflammation occurs when the precisely regulated communication between the mucosal immune system and the outside microbiota is disturbed at their contact site, the epithelial barrier. Glial processes in the mucosa have gained attention since they are in intimate association with the epithelial cell layer, form a dense network at the epithelial crypts and release mediators that increase intestinal barrier integrity, potentially beneficial to counteract barrier breakdown [33–37]. In line with this, mucosal glia in CD and UC-patients are described to express significantly altered levels of GFAP compared to healthy controls, which is associated with reactive gliosis [39, 45].

However, the majority of EGCs are located outside the mucosa in the myenteric and submucosal plexus structures. Their activation and contribution to inflammation progression is largely un-

known. Recently, it was shown that plexus-originating glial cells continuously invade the lamina propria to form the mucosal glial network, dependent on signals emanating from the gut microbiota [57]. These findings render ganglionated glial cells highly interesting for the study of inflammation-induced alterations.

Even though a research focus on the IBD-phenotype is justified by its high prevalence of 2.5 - 3 million patients in Europe with rising incidence rates [74], non-IBD inflammatory conditions of the bowel are of clinical importance as well. One such condition is sepsis, a life-threatening complication in critically ill patients commonly seen after impairment of gut motility due to surgical procedures or trauma [125, 126]. Here, EGCs have recently been discussed as potential target cells [122], but knowledge on EGC-contribution to disease progression is scarce.

To add knowledge to EGC physiology under inflammatory conditions, a novel *in vivo* rat model of acute sepsis [98] was applied to study short-term alterations in the ENS after systemic application of LPS. 4 h after LPS-injection (NaCl in the control group) duodenal, ileal and colonic tissue segments were removed and processed for immunohistochemical and transcriptomic analysis. To validate that systemic LPS-injection initiated an intestinal inflammation, H&E stains clearly revealed immune cell infiltrates and significant increases in Sod2 gene expression levels, a biomarker for oxidative stress, were measured. Superoxide dismutase is one of several enzymes cells employ to decompose cytotoxic reactive oxygen species (ROS), which are produced during normal cellular metabolism. During inflammation, ROS-levels can rise dramatically because phagocytic immunocytes (monocytes, macrophages, neutrophils, eosinophils) release excessive amounts of toxic superoxide to destroy tissue-invading microorganisms [127]. The increase in Sod2 mRNA hence reflects the tissue's response to the inflammation-mediated increase in superoxide and resulting oxidative stress.

In a next step we investigated histometric alterations in the inflamed intestinal tissue. A hallmark in persisting intestinal inflammation as in IBD is a thickening of all layers of the gut wall [128]. Other histometric changes in IBD affect the ENS. Both proliferative and degenerative alterations of enteric nerves have been reported in IBD patients, often with a more pronounced phenotype in CD patients. A well-described phenomenon is hypertrophy (i.e. increased size) and hyperplasia (i.e. increased number) of ganglia and nerve bundles in the mucosa, submucosa and myenteric plexus of the ileum and colon [129][130]. Also, neuronal cell death with swollen, empty axons is known to occur in CD and UC [131] with a concurrent increase in glial cell numbers. Based on the abundance of inflammation-induced tissue architecture alterations in IBD-patients, effects of the acute systemic hyperinflammation on ENS morphology were assessed with focus on the myenteric plexus and the muscular tissue layer in which it is embedded. Measurements of the muscle layer thickness and plexus architecture were performed on 10 microscopic pictures per tissue slice from each animal and each intestinal region assessed. These analyses revealed no significant alterations in muscle thickness upon LPS-treatment. In IBD-patients, the gut wall thickening is caused by an excessive deposition of extracellular matrix (ECM), mostly collagen. Mechanistically, the

persisting inflammation leads to an activation of fibroblasts, upon which they express receptors for proinflammatory cytokines and become primary effector cells of the inflammation. In the activated state fibroblasts differentiate into myofibroblasts, which synthesize and deposit ECM proteins that contribute to tissue remodeling and fibrosis [132]. In the acute hyerinflammation model investigated here, several hours are not sufficient to observe activation of fibroblasts and consequently ECM protein synthesis and deposit. It was not possible to significantly prolong the time between stimulation and tissue preparation due to the severe disease progression. After intravenous injection of high LPS concentrations animals showed severe symptoms and multiple organ failure was expected to occur within hours after termination of the experiment.

Quantification of the overall plexus number and the total plexus area showed different non-significant tendencies in the small and in the large intestine. In the small intestinal segments duodenum and ileum both the average plexus number and plexus area were slightly reduced in the LPS-treated animals compared to the sham-treated control. In the large intestine, there was a tendency for increased plexus number with a concurrent decrease of the average plexus area. To calculate the average area per plexus, the total plexus area measured per animal can be divided by the total number of plexus structures. This ratio is not significantly altered in duodenal and ileal samples of LPS-treated animals compared to controls. In colonic samples of LPS-treated animals, however, the ratio of plexus area to plexus number shows a statistical trend of being reduced (0.32-fold±0.02, p $=0.10$), since the total plexus area in LPS-treated animals is lower than in control animals and the total plexus area in LPS-treated animals is higher than in control animals. It follows that the average area of the plexus structures measured is significantly decreased in colonic samples of LPS-treated animals, probably due to a decomposition and fragmentation of plexus structures. To conclude, a hypertrophy of plexus structures was not detected, but the decrease in the average plexus area after LPS-treatment is an indication of a degenerative inflammation-induced process affecting neural cells.

The results on quantification of the overall neuronal population via the Hu- and Uchl1-markers underline these findings. They revealed no significant alterations, however, a tendency for reduced cell numbers assessed by protein quantification was observed in inflamed ileal segments. In persisting tissue inflammation originating from the mucosa as in UC, a loss of enteric neurons is documented [120] as well as in different experimentally induced animal models [133, 134], whereas other studies report no significant alterations in enteric neuronal numbers in IBD patient biopsies [135]. It is conceivable that a loss of enteric neurons occurs due to inflammation-induced changes in the intestinal microenvironment. One such contributor leading to neuronal death is a disturbed purinergic signaling. As described by Gulbransen and colleagues, chronic activation of the purinergic receptor P2X7R on neurons is sufficient to induce neuronal death in colonic myenteric plexus preparations, and this cell loss occurs in the absence of immune cell infiltrates in the myenteric ganglia [133]. Different factors are known to contribute to increased purine levels in the inflamed intestine [136]. It must be noted though that P2X7R activation-dependent neuronal loss has been investigated in chemically induced mouse models of IBD several days

after induction [133]. Hence, the lack of significant reduction of neuronal numbers in the acute hyperinflammation model might be explained by the short time frame between induction of inflammation and analysis.

5.1.1 Glial-specific alterations in the hyperinflammatory model

As in the neuronal quantifications, no significant alterations but a tendency for reduced cell numbers were found for the overall SOX10-positive glial population. On mRNA level, the expression of the glial marker S100b in LPS-treated animals tended to be reduced as well, reaching a highly significant decrease in colonic samples compared to sham-treated controls. This glial marker reduction was surprising, since myenteric glial proliferation in the ileum has been described both in chemically induced acute animal models of inflammation studied via BrdU-incorporation [137] or in UC-patients studied by counting of S100-positive cells [135]. Again, these analyses have been performed either on samples from chronically inflamed tissue as in CD or from samples three days at the earliest after chemical induction of inflammation *in vivo*. Hence, the time frame between onset of the severe systemic hyerinflammation and analysis was probably too short to observe potential glial proliferation. Instead, the tendencies for glial marker decreases are a further indication of the detrimental effect of the systemic hyperinflammation on the maintenance of the ENS architecture.

Interestingly, the inflammation-associated loss of glial marker expression was not observed when analyzing GFAP levels. Instead, Gfap mRNA transcript levels were strongly upregulated in whole gut wall preparations of LPS-treated animals compared to controls in duodenal and colonic segments. In ileal samples, however, LPS-treated animals showed no significant upregulation of Gfap expression compared to controls. To put these differing responses in Gfap expression upon LPS-injection into perspective, the total Gfap mRNA transcript levels normalized to the reference genes were compared among the different intestinal segments. This analysis revealed that LPS-treated animals had lower Gfap mRNA levels in ileal segments than in duodenal or colonic samples, however, sham-treated animals had higher basal Gfap mRNA levels in ileal segments than in duodenal or colonic samples. Hence, the inflammation-induced net change in Gfap transcript levels were lowest in ileal samples. These findings imply that glial cells differ along the intestinal rostro-caudal axis in their Gfap expression patterns. Support for a potentially differing susceptibility of ileal GFAP-expressing EGC come from animal models of glial ablation. Here, immune-mediated ablation of GFAP-EGCs led to a fatal inflammation specifically of the ileum, not the duodenum or proximal colon [41]. It can be reasoned that additional factors besides the LPS-induced tissue inflammation contribute to Gfap expression modulation. One potential factor in the acute systemic hyperinflammation model employed here lies in the surgical procedure. Prior to LPS-injection laparotomy was performed and the GI tract was partially exposed. Such mild manipulation of the intestine has been shown to be sufficient to induce inflammatory

reactions and impaired motility as compared to laparotomy alone[89][94].

In line with this, a preliminary analysis revealed that in untreated (i.e. not sham-operated) rats the level of Gfap expression in the ileum was on average lower than in sham-operated animals. In untreated animals Gfap levels in the ileum were highly similar to duodenal and colonic samples of sham-treated rats, instead. This finding might indicate that sham-treatment alone induces an increase in Gfap expression in the ileum. However, since a different rat strain was employed for the untreated control, this group cannot be compared without doubt to the hyperinflammatory model. To address the effect of the sham-treatment further, animals of the same genetic background and rearing under equal environmental factors (i.e.housing, chow) need to be compared in future experiments.

An unanswered aspect of the Gfap mRNA increase is the cellular source of Gfap expression: Either glial cells that did not express GFAP before (GFAP⁻) became GFAP⁺ or GFAP⁺ EGCs transcribed increased levels of Gfap. Since analysis of the tissue (e.g. by IHC) can only reflect the momentary GFAP-expression status of each cell (GFAP⁻ or GFAP⁺) in the moment of tissue fixation, it is not possible to answer this question in the experimental setup chosen here. Instead, a method of tracing back the GFAP-status of single EGCs to the time point of LPS-injection is necessary, which can then be compared to the GFAP-status in the inflamed tissue. A possibility to address this question is to label GFAP⁺ cells prior to LPS-injection via expression of a reporter protein and to compare the GFAP-status to GFAP-expression in the inflamed tissue analyzed by IHC. A genetic tool to introduce an inducible reporter in a subset of cells (e.g. GFAP⁺ cells) is the site-specific Cre-loxP recombination system. It relies on the bacteriophage-derived protein Cre that catalyzes the recombination between two of its sequence recognition sites (loxP) [138]. Cre-mediated recombination results in the excision of the sequence flanked by the loxP sites [138]. It is usually employed in mice. To generate an inducible reporter system, two mouse strains need to be crossed: (i) A reporter strain with a reporter protein (e.g. a fluorescent protein) preceeded by a loxP-flanked transcriptional termination sequence inserted in an ubiquitously expressed locus (e.g. Rosa26R locus). (ii) A strain expressing an inducible Cre recombinase (e.g. the tamoxifen-inducible recombinase Cre-ER^{T2} [139]) under the transcriptional control of the gene of interest [140]. Such reporter systems under the control of the GFAP-promotor have been established [141–143]. A suitable experimental setup would be to generate double-transgenic mice (GFAP-CreER^{T2}:R26R), in which reporter protein expression by tamoxifen-injection would be induced prior to inducing inflammation. If EGCs in the hyperinflamed tissue would express both the reporter protein and additionally GFAP verified by IHC with a different fluorophore, those double-positive cells must have been GFAP⁺ prior to inflammation. If, however, EGCs would not express the reporter protein but were positive in an IHC-analysis of GFAP, those cells must have been GFAP⁻ prior to inflammation. Such analyses would greatly advance our understanding of activation processes in EGCs.

5.1.1.1 Region-specificity of LPS-responsive EGCs

The heterogeneity of Gfap expression alterations in LPS-responsive glia is not restricted to the rostro-caudal axis of the GI tract but emerges along the serosal-luminal axis as well. Highly significant upregulation of Gfap expression and downregulation of S100b expression were confined to the muscular layer haboring the myenteric plexus and were not found in submucosal or mucosal regions. Myenteric glia have recently gained attention in the context of inflammation-induced impairment of GI motility [122]. Stoffels *et al.* identified IL-1 receptor signaling as essential for surgery induced inflammation and resulting impaired contractility. The group found GFAP-EGC in the myenteric plexus as the predominant IL-1R1-expressing resident intestinal cell type, highlighting the potential of GFAP-EGCs to shape intestinal inflammation. The findings obtained with the hyperinflammation model support this concept of myenteric GFAP-glia as fast-responding, reactive cell type in acute inflammation *in vivo.*

Furthermore, the results presented here challenge the present focus on mucosal GFAP-glia in the context of IBD and highlight the role of myenteric GFAP-EGCs. A potential link between GFAP-positive mucosal glia observed in IBD-patients and the high responsiveness of myenteric EGC to upregulate Gfap upon inflammation come from Kabouridis *et al.* They recently demonstrated that myenteric plexus-originating EGCs continuously invade the lamina propria to form the mucosal network [57]. It is highly interesting to study if the inflammation-responsive Gfap-expressing myenteric glia invade the lamina propria and hence give rise to the GFAP-positive glial network observed in the mucosa of IBD-patients.

5.2 Characterization of GFAP-gliosphere cultures *in vitro*

The studies on the hyperinflammation model had identified myenteric EGCs to quickly respond to an inflammatory environment by upregulating Gfap-mRNA expression and hence made GFAP-EGCs a highly interesting cell population for further studies. Even though multiple studies have described increases in GFAP-expression in glial cells under inflammatory conditions, knowledge on the physiological consequences of Gfap-upregulation is still very scarce.

To specifically study the myenteric GFAP-expressing glial population under inflammatory conditions *in vitro*, the next step of this work included the isolation and expansion of GFAP-EGCs *in vitro* as free-floating murine primary gliospheres. These were generated by flow cytometry-activated sorting of LMMP digests from hGFAP-eGFP mice. Here, an eGFP reporter is expressed under human GFAP promotor control, so that GFAP$^+$ EGCs coexpress eGFP and can hence be purified.

In the intestinal LMMP-preparations investigated here the eGFP label did not completely overlap with GFAP immunostaining. On the one hand this is due to differing cellular localizations of eGFP and GFAP; while the first is a cytoplasmatically expressed diffusible protein, the latter

is an intermediate filament protein. On the other hand immunostainings are more sensitive than recording endogenous eGFP signals in tissue. First, because indirect antibody staining leads to a signal amplification that makes detection of GFAP$^+$ cells more prominent, but also because fixation of the tissue is necessary for subsequent immunohistochemistry, which interferes with GFP fluorescence. Despite these technical limitations, eGFP and GFAP showed good correlation in LMMP-preparations and were used to establish purified cultures of GFAP-EGCs.

The resulting gliospheres showed strong immunostaining for the glial markers S100B and GFAP but not Vimentin after prolonged *in vitro* culture. GFAP and Vimentin are developmentally regulated in reverse manner. Immature glial cells express low levels of GFAP and increased levels of Vimentin, whereas in mature glia GFAP expression is high and Vimentin is weakly expressed [20]. FACS-quantification revealed that 60% of cells within the gliospheres had maintained strong GFP-positivity throughout the culture, which is in line with other works describing the high plasticity of GFAP-expression.[21][46]. Interestingly, gliospheres contained SMA-expressing cells. Given that they were propagated from an initially purified GFP$^+$ population (97% GFP$^+$) it is not expected that the prominent SMA$^+$ proportion grew from a minor fraction of contaminating non-glial muscle cells in the initial culture. It is rather conceivable that dedifferentiation of enteric glia occurred in culture due to a lack of cues from their native microenvironment *in vivo* [19]. Support for this notion comes from studies that document a loss of morphological and molecular characteristics of EGC *ex vivo* [20]. Further, several groups have confirmed that mature EGCs can readily acquire a neurogenic potential *in vitro* but exhibit this neurogenic potential only under very limited conditions *in vivo* [23][24]. Laranjeira *et al.* investigated the potential of Sox10$^+$ EGCs isolated from adult LMMP preparations (Sox10::iCreER^{T2};R26ReYFP, compare section 5.1.1 on reporter strains) to give rise to neurons *in vitro* in detail: The group found that while all Sox10$^+$ cells expressed the mature glial marker GFAP but not the neuronal marker TuJ1 several hours after isolation, approx. 25 % of the culture lost GFAP-expression after several days and expressed neither glial GFAP nor neuronal TuJ1, but expressed Phox2b and Sox2 [24]. The authors interpreted this population as glial-derived enteric neural crest stem cells. Upon modification of culture conditions to induce differentiation, approx. 40 % of the cells expressed pan-neuronal markers (TuJ1, HuC/D) and also subtype markers (nNos, VIP, NPY) were expressed, clearly indicating that mature EGCs aquire a neurogenic potential *in vitro* [24]. Under steady-state conditions, this neurogenic potential was not validated *in vivo*, but after chemical injury via benzalkonium chloride HuC/D-positive neurons were observed that were derived from the Sox10$^+$ population. Noteworthy, the group did not investigate the potential of EGCs to give rise to αSMA$^+$ smooth muscle cells, but another group postulated that a subset of mature EGCs (characterized as CD49b$^+$Lin$^-$, positive for GFAP, S100B, SOX10, p75, and nestin,) gave rise to neurons, glia and αSMA$^+$ cells *in vitro* [23].

These findings clearly support the concept that mature, differentiated EGCs can dedifferentiate *in vitro* into multipotent cells.

5.3 Alterations in enteric gliospheres upon inflammatory stimulation

GFAP-enriched gliospheres were exposed to LPS for 48 h to specifically study the physiological properties of this subpopulation under inflammatory conditions *in vitro*. Previous studies have been conducted to investigate primary EGC cultures stimulated with various inflammatory mediators, however, not in a subpopulation-specific manner. The first study on the effects of inflammatory stimulation on primary EGC cultures *in vitro* was conducted by Anne Rühl, who stimulated primary purified rat EGCs with IL-1β and found that this stimulated pro-inflammatory IL-6 mRNA and protein expression in a dose-dependent manner [66]. Later, von Boyen studied the effect of different pro-inflammatory cytokines and LPS on the expression levels of GFAP and postulated inflammation-induced reactive gliosis in EGC cultures [46]. Further studies have employed LPS in combination with other inflammatory mediators, mostly IFN-γ to stimulate human EGC cultures and tissue biopsies [68][70]. The fact that different pro-inflammatory stimuli have been employed in the different studies complicate comparative conclusions.

A recently published finding on CNS astrocytes gives a potential rationale for the use of different stimuli in different experiments using different species in CNS astrocytes and EGCs: CNS astrocytes respond to LPS and other pro-inflammatory mediators in a highly species-specific manner. While direct LPS-exposure elicits the production of proinflammatory cytokines in murine CNS astrocytes, it has no effect on human CNS astrocytes. The differences in mouse and human CNS astrocytes' responsiveness is caused by differing intracellular signaling mechanims [144].

A further important aspect of previously published studies on EGCs is that they were conducted with the addition of high concentrations of fetal calf serum (FCS), which contains an undefined cocktail of proteins and hence impedes the unambiguous interpretation of the data.

Concludingly, the current knowledge on EGCs under inflammatory stimulation has been obtained using different stimuli and different species for the isolation of EGCs, which have not been cultured under highly defined conditions. Hence, there is a need for well-defined and reproducible studies on EGC physiology in inflammatory conditions, which is addressed with this study. Here, primary murine EGCs were cultured in a defined medium without the addition of FCS and the effects of LPS-stimulation on specifically the GFAP-expressing glial subpopulation were studied on mRNA and on protein level.

5.3.1 Transcriptomic analyis of LPS-stimulated gliospheres

Microarray data analysis revealed a set of 70 genes that were statistically differentially expressed in LPS-treated gliospheres compared to untreated spheres. Before approaching this list of SDEGs and deducing biological meaning, it is important to understand how this list is generated. The raw output data of a microarray analysis is a fluorescence image showing hybridization complexes

of labeled input RNA to specific reporters (see section 5.3.1.1). This raw data is converted to a quantitative information on RNA copy numbers in a series of mathematical operations called the preprocessing, which includes image processing, background adjustment and data normalization [145]. These mathematical operations are performed based on threshold parameters. In a second step the RNA copy numbers in a treated sample are compared to those in an untreated control, and again the thresholds determining significance are based on mathematical models. The end result of such an analysis is a hierarchically ordered list of the genes based on the significance of the differential expression. Depending on how stringent the cut-off values of statistical significance are defined, the resulting list of SDEGs might include the top 70 genes, or it might include the top 300 genes of this list (including those 70 genes from the stringent analysis plus 230 additional genes). Hence, the biological meaning of a microarray dataset does not lie in the fact of whether a single gene meets the criterion of statistical significance. It rather lies in the enrichment of annotations that describe the biological functions of the SDEGs. The longer this list of SDEGs, the more gene products annotated to a biological function must be included for this term to reach significant enrichment.

The list of SDEGs presented here was evaluated based on annotations to three categories given in the GO-database: cellular component, molecular function and biological process. As mentioned in section 4.3 the resulting GO-terms have different hierarchical levels with child terms that are more specialized but largely redundant to the parental terms. In the dataset of LPS-stimulated gliospheres, the terms that are the most significantly enriched annotations to cellular components refer to the extracellular region. An enriched proportion of proteins encoded by those genes that are differentially expressed upon LPS treatment are hence related to processes at the extracellular site of glial cells. This is in line with the analysis of molecular functions that are exerted by those proteins. Here, the enriched terms describe cytokine and chemokine activities. These analyses coherently show that the list of SDEGs encompasses an enriched fraction of proteins that act at extracellular region and convey information to other cells or cell types. The biological processes these gene products are annotated to are most significantly linked to immune response processes. This annotation is not only assigned to a high number of SDEGs but most importantly to those genes with the highest degree of differential expression upon LPS-treatment, as depicted in the voronoi diagram.

Mechanistically, an enriched proportions of SDEG's products are associated to the JNK and p38 MAPK pathway, as revealed by KEGG pathway analysis. These gene products are the receptors FAS and CD14, the intracellular signaling protein GADD45, the kinase MAP3K8 (synonym: TPL2) and the transcription factors NF-κB and RELB. In general, JNKs (Jun N-terminal kinases) and p38 MAPKs (mitogen-activated protein kinases) are both mitogen-activated protein kinases. These kinases are part of signaling cascades that convert extracellular stimuli into cellular responses. The different MAPK are activated by different upstream kinases (MAP-kinase-kinase(-kinase) or MAP2K and MAP3K) and induce different cellular responses (reviewed in [146]). The best-characterized MAPK system is the ERK1/2 pathway that is activated by

growth factors and affects cellular processes such as proliferation and differentiation. JNK and p38 MAPK, however, are activated by cytokines or stress signals and induce inflammatory responses [147].

The signature of immunomodulatory alterations in the transcriptomic profile of glial cells is also observed in reactive astrocytes of the CNS. Interestingly, primary astrocytes and microglia are known to activate MAPK pathways in response to LPS-stimulation as well [148]. JNK and p38 MAPK signaling in activated glia have been shown to mediate the neurotoxic effects induced by glial activation [149] Other proteins are upregulated in activated ENS and CNS glia likewise. The gene product of lipocalin-2 (Lcn2), the gene with the highest fold change increase in this dataset, plays a role in the morphological and functional fate of reactive astrocytes, e.g. by inducing GFAP expression [150]. The gene products of Ccl2 and Ccl5, also known as MCP-1 and RANTES, are described to be produced by β-amyloid peptide-challenged astrocytes and act as microglial and macrophage chemoattractants *in vitro* [151]. Taken together, these data indicate that GFAP-EGCs are reactive to the acute LPS-stimulus *in vitro* and acquire a phenotype reminiscent of reactive CNS astrocytes.

Microarray data should be validated by an independent gene expression profiling method, the current gold standard to do so is to perform qPCR of a selected list of candidate genes. However, in this work a second multiplex transcriptomic profiling approach was employed instead, the nCounter technology. The choice of validation method was based on the fact that microarray and qPCR technologies share sources of error that are circumvented in the nCounter approach. Before discussing the results of this validation, the principles of both the Illumina Expression BeadChip technology and Nanostring's nCounter technology need to be discussed to assess the comparability of data obtained with both.

5.3.1.1 Validation of Illumina Expression BeadChip technology by Nanostring's nCounter technology

Both technologies quantify the expression of multiple genes simultaneously employing the principle of hybridization, the ability of a nucleotide base to bind to its complementary base. The core principle of both technologies is the hybridization of a single-stranded probe with known sequence to its complementary sequence in the nucleic acid mix obtained from the sample of interest and subsequent detection of the double-stranded complex. Even though this principle is common to both, differences exist in input sample processing, probe characteristics and signal detection.

The Illumina BeadChip technology makes use of silica beads onto which probes are synthesized. Each bead carries only one type of probe oligonucleotide, but thousands of copies. Each oligonucleotide consists of two segments: a 50 base probe segment, that is complementary to the target RNA and a shorter address segment, which allows the unambiguous identification of the probe

segment. The beads carrying these oligonucleotides randomly self-assemble onto a matrix with microwells etched into it. Before use, the address segments are decoded and a map is created where the information of the location of each bead and its identity are recorded [152]. Once the identity and position of each bead on the array is known, the total RNA to be applied onto the array needs to be labeled, so that a binding to a bead's oligonucleotide can be detected. For this purpose, the input total RNA of a sample is processed to create copies with incorporated biotin-conjucated nucleotides, which can later be labeled with a streptavidin-conjugated fluorescent dye. This is a multistep-process, in which the input RNA is used as a template for cDNA-synthesis using Oligo(dT) primers with a promotor for the T7 RNA polymerase of the T7 phage. This cDNA serves then as a template for the *in vitro* transcription into cRNA by the T7 RNA polymerase. In this process biotinylated nucleotides are incorporated into the cRNA [153]. Once this labeled RNA has hybridized, the BeadChip can be stained with a fluorescent dye derivatized to steptavidin. The more RNA molecules of one type bind to its specific bead, the higher is staining intensity, which is then scanned. This technology offers a highly parallelized assessment of several thousands of genes with only minimal amounts of input sample required, since RNA is linearly amplified is the process of *in vitro* transcription. However, the extensive RNA processing is a potential source of error, another limitation is the signal detection via laser scanning, which can fail to detect minor alterations in expression levels.

The nCounter technology circumvents both sources of error by waiving RNA processing and counting signal events rather than scanning for cumulative staining intensity. The nCounter approach does not utilize spatially arranged geometric features as it is the case in the bead array, but employs a solution-phase hybridisation [154]. This hybridisation involves the unprocessed target mRNA to hybridize to two different probes at the same time, a reporter probe and a capture probe. Both probes carry a non-overlapping target-specific oligonucleotide sequence that binds to the input RNA. The reporter probe carries a fluorescent 7-digit barcode signal composed of different combinations of four fluorescent dyes. This 7-digit barcode design does not allow as many unique combinations as the 29-base adress segment of the BeadChip probes, and indeed nCounter technology is not suited to perform whole-genome studies. The reporter probe is required to identify the mRNA, whereas the second hybridized probe, the biotinylated capture probe, is used to immobilize the complex for data collection. Once the complexes are immobilized, the optical barcodes are identified and counted one at a time, allowing a very precise resolution of the expression pattern [155].

The advantages of the nCounter technology over qPCR for validation are hence that the input RNA can be processed directly and must not be converted to cDNA. Further, each qPCR analysis must be performed individually per target, whereas nCounter is a multiplex approach, which limits the amount of input material. Also, a qPCR reaction has requirements on the design of the hybridising primers (approx. 20 bases) and the length of the amplicon (approx. 100 bases). Given that the hybridizing base probe segment in the bead array is 50 bases long, it is not possible to amplify the exact same nucleotide segments in both arrays, whereas the hybridising

sequence in nCounter probes can be designed with the identical sequence as the Illumina probe. To add even further value to the validation, not only a different platform was chosen to erase technical bias but also independently prepared RNA lysates were employed to address biological variability.

The nCounter analysis was performed for 60 custom-selected targets, 7 of which were included as reference genes selected for their highly stable expression over multiple comparisons in the microarray dataset. During preprocessing of nCounter data, the 4 most stably expressed of these 7 genes were selected and used as references for the analyses. All 14 genes taht were significantly differentially expressed in the microarray analysis and validated via nCounter resulted in significant differential expression validated by nCounter exept for CD82. Also, when comparing the fold change alteration in expression upon LPS-stimulation detected by the two technologies a highly significant correlation of results was detected ($p < 0.0001$). Microarray data were hence successfully validated.

Aside from the impact of LPS-stimulation on gliospheres, a second aspect was addressed in the analysis, the impact of *in vitro* expansion of primary GFAP-EGCs. To do so, RNA from the $GFAP^+$ population isolated directly after cell sorting without *in vitro* culture was compared to RNA from gliospheres (see section 5.3.3). Here, the scattering of differential expression was greater (a logarithmic fold change ranging from -9 to 9), which was also represented in the subset of genes studied in the validation by nCounter. As for the study on the impact of LPS-stimulation on gliospheres, the correlation of data on the *in vivo/in vitro*-comparison obtained from microarray and nCounter studies correlated highly ($p < 0.002$).

5.3.2 Proteomic analyses of LPS-stimulated gliospheres

In addition to the analysis of altered gene expression the secretion of cytokines from LPS-stimulated GFAP-gliospheres was assessed. In the case of CNS astrocytes, it is well recognized that these cells secrete elevated levels of different cytokines upon LPS-stimulation *in vitro* [156]. Various studies have shown that cytokine secretion by astrocytes is strong 24-28 h after stimulation [157][158]. Further, studies on EGCs have shown that EGC-activation by LPS and subsequent secretion of certain EGC-derived cytokines peaks between 24-48 h [46][66]. Hence, for the analysis of specifically the $GFAP^+$ subpopulation, a time frame of 48 h was chosen to evaluate cytokine secretion by multiplex analysis.

The multiplex bead immunoassay can be thought of as a Sandwich-ELISA conjugated onto beads that allow the parallel measurement and discrimination of different cytokines. The sandwich in a multiplex bead immunoassay consists of four members. At its core is the specific binding of the cytokine that is to be measured to a specific antibody. Each antibody type (capture antibody) is conjugated to a magnetic bead (component 1). Each bead within a specific bead-antibody

complex is internally dyed with a combination of red and infrared fluorophores, giving it unique spectral properties that allow discrimination. After the antigen is added (component 2), the antibody-antigen-complex conjugated to the specific bead is formed. As a third component a second antigen-specific antibody is added that is biotinylated (detection antibody). The fourth component is a streptavidin-conjugated fluorescent protein, which binds to the biotinylated detection antibody and allows quantification of the bead-conjugated immune complex. The signal intensity of the fluorescent protein can then be linked to the bead's spectral profile and hence the identity of the quantified cytokine [159].

Currently, the gold-standard in quantitative protein analysis is the solid-phase, non-multiplexed ELISA. Both the standard ELISA and multiplex bead arrays are premised on the same sandwich immunoassay (i.e. sandwiching the protein of interest between a capture and a detection antibody). Several publications have discussed and generally agreed on the comparability of both techniques [160–162]. However, non-multiplexed ELISA are considered to be more robust, whereas multiplex bead arrays claim to be more sensitive due to the use of a fluorescence reporter system instead of an enzymatic amplification of a colorimetric substrate.

In the analysis of cytokine secretion by LPS-stimulated gliospheres a considerable variance in the independent biological replicates was detected. This variance impeded a statistical significance of the differential secretion upon LPS stimulation. However, several observations can be postulated that apply to all cytokines measured but TNF-α:

(1) Cytokine levels were elevated in supernatants of LPS-stimulated gliospheres compared to untreated controls. This increase in cytokine secretion was statistically significant for the pro-inflammatory mediator IFN-γ and the anti-inflammatory mediator IL-4.

(2) The fluctuations among the biological replicates were greater in the LPS-treated group compared to the untreated control. This finding indicates that the basal cytokine secretion of unstimulated gliosphere cultures is robust and can be measured reproducibly. It supports the claim of accurate quantification by the multiplex array. The diverges among the LPS-treated cultures might be due to heterogeneity in gliosphere cultures. As discussed in sections 5.2 and 5.3.3 the initially purified GFAP$^+$ population changes upon prolonged *in vitro* culture. It is plausible that the proportion of LPS-responsive glia in the population varies in the different cultures. However, on the transcriptomic level the individual replicates of LPS-treated gliospheres showed a strong similarity (see figure 4.11).

Several shortcomings in the experimental design further complicate the interpretation of the proteomic data. First, the analysis gives absolute cytokine quantities and lacks a reliable normalization. Even though the cells for the LPS-stimulated culture and the untreated control of each biological replicate were derived from the same tissue preparation, the initial cell culture was split into two dishes several days prior to the analysis. It is plausible that the shifts observed to occur during *in vitro* culture might have affected the two subcultures differently. Further, comparing the individual biological replicates, the cell numbers employed in the assay was not determined and thus not normalized.

Another technical aspect biases the quantification of cytokines present in high concentrations. The protein quantification in any ELISA relies on the translation of the measured amount of reporter (fluorescence, colorimetric substrate) to a protein concentration. The correlation is given a standard curve, which is generated by plotting the measured reporter intensities of known protein concentrations versus these concentrations. From this standard curve a linear regression is calculated and used to compute exact protein concentrations for any reporter intensity measured in the assay. A prerequisite for this approach is that the measured reporter intensity of an unknown sample lies within the range used to compute the linear regression. All cytokines despite one meet this prerequisite. Only the fluorescence intensity measured to quantify IL-1β concentrations exceeded the highest fluorescence intensity measured to create the standard curve by far. Thus, applying the mathematical model derived from the standard curve (i.e. the equation describing the linear regression) to calculate protein quantities is not legitimate and explains the high fluctuations observed in IL-1β-quantification. The lack of significance of IL-1β-upregulation upon LPS-stimulation is therefore due to a technical limitation of data evaluation.

To conclude, proteomic profiling revealed that numerous pro-and anti-inflammatory signaling molecules are secreted by gliospheres *in vitro* upon LPS-stimulation. This effect is strongest for IL-1β and statistically significant for IFN-γ and IL-4.

5.3.3 Transcriptomic meta-profiling of GFAP-EGCs

The results discussed so far explored the potential of the GFAP-expressing glial population to exert immunomodulatory functions upon stimulation. In a next step this subpopulation was further characterized. One aspect to be addressed was the comparability of the spheroid culture *in vitro* to the native GFAP-expressing glial subpopulation *in vivo*. Immunohistochemical characterization had already indicated a shift in the *in vitro*-cultured population with a decrease of the proportion of GFP-positive cells and an increase of αSMA-expressing cells. To assess this aspect further, whole genome transcriptomic profiles of the gliospheres were compared to data from GFAP-EGCs analyzed directly after cell sorting without *in vitro* culture ("GFAP in *vivo*"). Most interestingly, the transcriptomes of GFAP-EGCs *in vivo* differed from GFAP-gliosphere cultures drastically. The microarray analysis identified 2705 genes to be differentially expressed, of which 1502 were upregulated in the *in vitro* cultured gliospheres and 1203 were downregulated compared to GFAP-EGCs *in vivo*. This distinct transcriptomic shift was also reflected in the subset of genes validated with the nCounter technology. The clustering analysis even revealed that prolonged cell culture altered the transcriptomic profiles to a greater extend than the LPS-stimulation.

To characterize this shift in expression profiles independent GO-queries (see section 4.3) were conducted with the lists of upregulated and of downregulated genes likewise. Most interestingly, those genes that were downregulated in cultured gliospheres *in vitro* compared to GFAP-EGCs

in vivo are annotated to neural functions. Among the enriched terms describing molecular functions are neuropeptide/neurotransmitter binding and receptor activity as well as SNARE binding. SNARE proteins mediate vesicle fusion, for instance the fusion of synaptic vesicles to the presynaptic neuronal membrane, which leads to the release of the vesicles' content into the synaptic cleft. Among the SDEGs annotated to term "SNARE binding" are key SNARE components such Stx1a (syntaxin 1a) and Vamp2 (synaptobrevin). For CNS astrocytes the expression of these SNARE proteins is known *in vivo* [163] and *in vitro* [164] and is thought to be essential for the release of gliotransmitters [165]. The expression of these SNARE proteins in enteric glia or in the GFAP-expressing subpopulation has not been described yet. In line with the annotations to molecular functions, the key biological processes linked to the downregulated genes in this data set include the terms "neuromuscular synaptic transmission", "regulation of smooth muscle contraction" and "hormone secretion".

When assessing the list of upregulated genes in gliospheres cultured *in vitro* compared to GFAP-glia *in vivo* key biological processes that are linked to the SDEGs refer to a negative regulation of cell-matrix adhesion, reflecting the spheroid culture of the cells. Additionally, several processes are listed that refer to tissue morphogenesis, however, including multiple tissue types (e.g. "gland morphogenesis", "ossification", "epithelial tube morphogenesis"). This finding implies that gliospheres derived from GFAP-EGCs dedifferentiate from a glial phenotype and acquire transcriptomic signatures of other tissue types.

An approach to better understand the analogies of GFAP-EGCs to other tissue types is to compare their whole genome transcriptomes in a meta-analysis that groups resembling profiles. This analysis revealed that freshly isolated GFAP-EGCs *in vivo* show a high transcriptomic resemblance to CNS astrocytes and to a much lesser degree to CNS microglia and PNS sciatic nerve cells. A recent analysis not of the GFAP-positive subpopulation, but of the Proteolipid Protein 1 (PLP1)-positive EGC subpopulation identified a close resemblence to PNS Schwann cells and only limited similarity to astrocytes [166]. Since PLP1 and GFAP are co-expressed in only 35-54% of EGCs [166], these findings might point to distinct subpopulations among EGCs. In contrast, GFAP-EGCs cultured as gliospheres *in vitro* resemble sciatic nerve cells most. Interestingly, LPS-exposure to gliospheres induced only a minor shift in transcriptomic profiles, whereas both CNS astrocytes and microglia showed distinct alterations in their transcriptomes upon LPS-exposure. These differing susceptibilities in ENS and CNS glia might be due to a reduced sensitivity of EGCs to LPS because of the physiological exposure to bacterial components in the gut. Another possible explanation is the shift in transcriptomic profiles of gliospheres *in vitro* towards mesenchymal cell entities. GFAP-gliospheres did not cluster with any of the neural cell entities in the global transcriptomic analysis but showed a higher resemblance with different mesenchymal cell types.

5.4 GFAP-Glia in an acute inflammatory bowel disease model *in vivo*

The comparative analysis of GFAP-EGCs *in vivo* and *in vitro* revealed a strong shift in transcriptomic profiles induced by the *in vitro* expansion. Due to this shift the findings on immunomodulatory capacities of GFAP-EGCs *in vitro* cannot be translated to GFAP-EGCs *in vivo* with sufficient confidence. The next step of this work was hence to specifically study the GFAP$^+$ subpopulation in an inflammatory disease model established in hGFAP-eGFP transgenic mice *in vivo*.

DSS and TNBS were employed to chemically induce an acute intestinal inflammation resembling in some aspects the IBD phenotype. DSS acts toxic on epithelial cells and causes a breakdown of the epithelial barrier, the resulting phenotype is considered to resemble UC in humans. TNBS haptenizes colonic proteins and renders them immunogenic to the host immune system. It thereby activates a T_H1-mediated immune response and is thus considered to resemble CD in humans [167]. When comparing the suitability of TNBS and DSS to induce inflammation, the timing of analysis is crucial. In the study presented here, the group of TNBS-treated animals scored higher DAI-values than the DSS-treated group 2-4 days after application of the chemicals. However, 7 days after chemical treatment, DSS-treated animals exhibited higher scoring values on feces consistency and occult blood. This is in line with publications describing the different time courses of TNBS- and DSS-induced colitis [85]. Often, TNBS-induced disease models are evaluated 2-5 days after TNBS-administration, whereas DSS-induced models are evaluated 7-8 days after the start of treatment [85][133][168]. Other factors may have an impact on the experimental time course: In TNBS-models the addition of a presensitization step with transdermal TNBS-application can be necessary. In DSS-models DSS-treatment can be performed repeatedly with intermittent recovery periods. These differences in TNBS- and DSS-mediated disease inductions depend on factors such as the mouse strain employed or the desired phenotype, but impede the comparability of different studies.

With the parameters chosen in the experimental set-up presented here, DSS-treatment was more potent to induce an inflammatory phenotype in FVB/N-mice after 7 days of treatment. The severity of inflammation was most significantly reflected in the histomorphological evaluation. The criteria on which the evaluation was based consider three aspects: (1) the density and depth of immune cell infiltrates, (2) epithelial changes, especially erosions (i.e. loss of surface epithelium) and (3) alterations in the entire mucosa, including ulcerations (i.e. erosions exceeding to the submucosa) [169]. Even though this histomorphological assessment revealed severe alterations in the overall tissue architecture, it was inconclusive of the effects on the glial population.

To specifically study the GFAP-expressing glial population, the colonic tissue was digested, GFAP-eGFP cells were sorted by FACS and analyzed for gene expression of inflammatory mediators by qPCR.
The prototypic response of glial cells to an inflammatory microenvironment is to undergo reactive

gliosis, a process best understood in CNS astrocytes (see section 1.3). The complex molecular changes occurring in CNS astrocytes are orchestrated by various signaling molecules, including cytokines. To give examples, among other cytokines IL-1 and IL-6 has been shown to induce proliferation and to increase GFAP-expression in rodent astrocytes [170–172]. CNS astrocytes secrete those cytokines themselves upon stimulation (e.g. injury) and the cytokines act as intercellular messengers, fueling both the acquisition of the reactive astrocytic phenotype but also the recruitment of microglia.

Modelled after CNS astrocytes, studies on the responsiveness of EGCs to inflammation have focused early on those cytokines (see section 1.5). Among the most relevant and best studied inflammatory mediators secreted by EGCs are the interleukins IL-1β and IL-6. They have been shown to be secreted by EGCs upon stimulation *in vitro* [66, 67]. Noteworthy, the intestinal environment of EGCs differs dramatically from the astrocytes' environment in the brain: The former is not immune-privileged but equipped with the intestinal immune system and is embedded in the muscular tissue, thereby intimately modulating intestinal muscle innervation. So in addition to inducing a reactive gliosis-like phenotype, cytokines released by activated EGCs may modulate additional processes in IBD pathophysiology, and indeed, both IL-1β and IL-6 are known to mediate neuromuscular functions and to recruit inflammatory cells.

Among the main symptoms in IBD are disturbances in intestinal motor functions, including bloating, nausea and vomitting in the stomach and small intestine as well as diarrhea or constipation in the remaining gut [173]. Interestingly, such motor dysfunctions usually occur in the absence of immune cells infiltrates in the deeper neuromuscular layer and even after resolution of mucosal inflammation in IBD remission [174]. Consequently, local sources of mediators have been tracked in the neuromuscular compartment and glial cells have been identified to secrete such mediators, including IL-1β and IL-6. These mediators affect neuromuscular functioning by altering the release of neurotransmitters: IL-1β suppresses the release of acetylcholine [175] and IL-6 can decrease or increase release of noradrenaline in a concentration-dependent manner [176].

In addition to the modulation of neuromuscular functions, interleukins are crucial for the recruitment of immune cells. IL-6 attracts neutrophils in the initial phase of inflammation. IL-6 signaling is then involved in the transition from neutrophil to mononuclear-cell infiltrates (especially macrophages and T-lymphocytes) by triggering the expression of chemokines that attract these cells [177][178]. It further prevents apoptosis of mucosal T cells [179] and influences their differentiation [180]. IL-1β is closely linked to the innate immune response as well. Most interestingly, domains of both IL-1 receptors and toll-like receptors (TLR) are highly homologous, so that IL-1 and TLR ligands can evoke the same fundamental inflammatory processes [181]. IL-1β promotes the activation of neutrophils and leukocytes (dendritic cells, macrophages) [182] and influences T cell activation and survival [183].

To conclude, interleukins impact multiple pathophysiological processes in intestinal inflammation. Understanding which cell types express these signaling molecules is vitally important for

therapeutic strategies. Since the overall EGC population is known to secrete interleukins upon stimulation *in vitro*, the next step of this work was to specifically address their expression of IL-1β and IL-6 by the GFAP-expressing subpopulation in the inflamed gut *in vivo*. Additionally, the expression of MHC-II molecules was assessed. It is well documented that activated glial cells in CD patients express MHC-II heterodimers on their surface to present peptides for recognition by T-cell receptors of CD4$^+$ T helper cells. The presence of MHC-II molecules on glial cells further underlines their involvement in the recruitment and differentiation of infiltrating lymphocytes. Whether MHC-II complexes are expressed specifically by the GFAP-positive population has not been addressed before.

Expression of these inflammation-mediating molecules was assessed on mRNA level by qPCR-analysis of the GFP-positive population from colonic tissue digests. Noteworthy, the yield of GFP-expressing cells was substantially lower in tissue digests from adult colonic tissue compared to early postnatal muscle strips from the small intestine. This might be explained by the thicker and more complex structure of adult tissue that impedes enzymatic breakdown. Indeed, a percentage of less than 1% of GFP-positive cells in the digest's live population indicates either incomplete separation of the tissue into a single cell suspension or a dying of the cells due to the prolonged enzymatic digest. Since the suspension was filtered three times in the course of digestion in order to remove the dissociated cells as early as possible from the potentially damaging enzyme solution, massive cell damage by the digest is unlikely. Nonetheless, the small number of collected GFP$^+$ cells from the tissue digests curtails the significance of further analyses, because they might be based on an unrepresentative fraction of the overall GFAP-expressing population. Expression levels of the interleukins IL-1β, IL-6 and the transcriptional activator of MHC class II molecules (CIITA) were on average elevated in DSS-treated animals compared to untreated controls, for CIITA this effect was statistically significant. For IL-1β expression levels a gender-specific trend was observed: male DSS-treated mice showed higher expression levels than female DSS-treated mice. In line with this, DSS-males scored on average higher DAI values in weight loss, feces consistency and feacal blood, but these effects were not statistically significant. The observations indicate that male FVB/N mice are more susceptible to develop a DSS-induced phenotype, and indeed other studies report a similar trend. Recently, a study investigated the effect of two 5-day cycles of 3% DSS-treatment, each followed by a 7-day phase recovery in FVB/N mice [168]. Ding *et al* describe a more pronounced weight loss and hemoccult positivity in males that was evident during recovery after the first cycle and worsened in the further experimental course. The induced phenotype was severe and required euthanasia of all males prior to completion of the study course. In comparison to these observation, the study presented here yielded less distinct gender-specific differences, which might have become more pronounced in a prolonged study design as the results by Ding *et al* suggest.

Independent of the gender-specific manifestation, the study revealed a trend for an increased mRNA expression of prominent pro-inflammatory factors in glia upon tissue inflammation. It was next addressed if the increased expression of lymphocyte-recruiting interleukins and antigen-

presenting molecules resulted in an increased spatial interaction of GFAP-EGCs with CD4$^+$ T cells. Light sheet fluorescence microscopy was chosen to visualize representative tissue segments instead of single-plane tissue sections employed in conventional microscopy. Even though it was possible to show the architecture of the extensive myenteric ganglia, the technology did not allow to visualize the mucosal GFAP$^+$ glial processes well. These glial processes are localized at the contact interface with lamina propria immune cells and are thus most promising for studies on direct glial-immune interactions. The lack of mucosal glial visualization might be owed to different factors: an overfixation of the tissue, a resulting need for more stringent antigen retrieval or an insufficient permeabilization of deeper tissue structures. Even though the sample preparation and staining protocols were optimized in preliminary experiments, a satisfying visualization of mucosal processes was not achieved.

In conclusion, the results indicate that the GFAP-expressing glial subpopulation exerts similar pro-inflammatory functions *in vivo* as have been accredited to the overall glial population. However, it was yet not possible to validate a functional interaction of GFAP-EGCs with T lymphocytes, a hypothesis that is widely accepted but still has not been sufficiently evidenced by the scientific community.

5.5 Future models for the study of EGCs in intestinal physiology

In vivo approaches such as the hyperinflammatory and the IBD model employed here reflect intestinal physiology in its complexity. However, mechanistic analyses on a cellular and molecular level are difficult. *In vitro* tissue models have enabled mechanisstic studies and have led to the identification of the molecular IEB modulators secreted by EGCs currently known (TGFβ1, 15d-PGJ2, proEGF, GSNO, see section 1.3). However, these early models are highly limited in the extend to which they reflect the *in vivo* situation. They traditionally include epithelial cell lines seeded onto transwell filter inserts co-cultured either with ENS cell lines seeded on the bottom of well plates [36][184][185] or with human submucosal preparations grown on filters [186]. The co-culture model proposed to be established here (see section 4.5) will integrate both primary (subtype-specific) EGCs or other neural entities and primary IECs.

As of now the major bottleneck for the establishment of this model is to achieve a functionally tight IEB. Preliminary analyses on the permeability of fluorescent dyes over the primary epithelial cell layer on the SIS as well as measurements of the transepithelial electrical resistance have indicated that the cell layer is not functionally tight. Further optimization steps (e.g. dynamic culture conditions in a biorector system) are necessary to meet this prerequisite.

Besides the study of neural-epithelial interactions other highly interesting aspects might be adressed in such models, including

(i) the migratory behavior of EGCs. As mentioned before EGCs have been shown to continuously invade the lamina propria to form the mucosal network. By providing the native ECM

environment, such models might be suitable to mechanistically study the migratory potential of this cell entity

(ii) the study of experimentally induced intestinal inflammation. By delivering inflammatory mediators (e.g. locally by impregnated agarose beads [187]) the effects of an inflammatory milieu on neural support of the IEB will be made possible to investigate mechanistically. Appropriate inflammatory mediators might be LPS to simulate contact with bacteria, or defined pro-inflammatory cytokines known to be released in the intestinal inflammatory response, including interleukins (particularly IL-1β, IL-6), interferons (IFN-γ) or tumor necrosis factor α (TNF-α).

Another highly intesting aspect would be to incorporate primary lamina-propria derived immune cells into such models.

5.6 Clinical relevance of the study

This study set out to comprehensively investigate the responses of enteric glia to an acute inflammatory stimulus. The results obtained from different *in vivo* models and *in vitro* studies add up to a consistent concept: EGCs respond to a severe intestinal inflammation with rapid and fulminant upregulation of GFAP expression within a few hours. The degree of upregulation varies along the rostro-caudal and the luminal-serosal axis and was observed to be most pronounced in the myenteric region. Myenteric GFAP-EGCs undergo a shift in gene expression profile upon inflammatory stimulation *in vitro* that predominantly affects expression of genes associated with inflammatory responses (e.g. via MAPK signaling). The GFAP$^+$ subpopulation is hence an active participant in inflammatory pathophysiology. The secretion of inflammatory mediators validated on protein level as well as the increased expression of components of the MHC-II complex by GFAP-EGCs *in vivo* further indicate an active crosstalk of EGCs with the innate and the adaptive lamina propria immune system in acute inflammation.

These findings extend the clinically relevant knowledge on EGC (patho-)physiology in several aspects:

(1) EGCs rapidly respond to tissue inflammation and might be an early modulator of the inflammatory microenvironment.

This renders EGCs attractive candidates for early therapeutic intervention. This work identified a set of genes upregulated in EGCs that are linked to immune-modulating capacities, of special interest are those of the MAPK-signaling pathway. Interestingly, many of these genes are upregulated in injury-activated CNS astrocytes and the respective proteins have been targeted in strategies to counteract adverse effects of CNS neuroinflammation [188]. It will be highly intersting to test these agents in the context of intestinal inflammation as well.

(2) Myenteric glia might be more relevant in intestinal inflammation than mucosal glia.

Previous studies in the IBD-context have strongly focused on glial processes in the mucosa. This was due to (i) the early observation of readily visible increased GFAP-immunopositive mucosal processes in IBD patients [39, 45] and (ii) the discovery of epithelial barrier-stabilizing capacities of EGCs [37]. Even though these findings imply an important modulatory function of EGCs at the site of mucosal inflammation, the vast majority of EGCs is not located in the mucosa but in the myenteric and submucosal plexus structures. Recently, Karoubidis and colleagues demonstrated that the mucosal glial network originates from myenteric glia that continuously invade the lamina propria [57]. It is plausible that the activated glial phenotpye observed in the mucosa of IBD patients results from glia that have been activated in the myenteric plexus and remain in an activated state while populating the lamina propria. This model puts unprecedented focus on the myenteric glial network. Indeed, the findings of this work can be interpreted to support this model: Within hours after acute hyperinflammation an activation of glia in the myenteric compartment but not in the mucosal compartment was observed. Intriguingly, even though the cellular consequences of increased Gfap expression are not fully understood, GFAP is known to be involved in cell motility and migration. Reactive astrocytes in mice deficient of GFAP exhibit profound defects in cell motility, impairing glial scar formation [189][190]. It will be therefore of high importance to understand whether activated GFAP-expressing glia differ in their capacity to invade the lamina propria. Ultimately, the myenteric glial network may be a yet underestimated cellular source for potentially epithelial barrier-stabilizing agents that might be explored therapeutically.

(3) When modeling intestinal (patho-)physiological processes *in vitro*, e.g. in cell culture-based test systems, it is necessary to integrate EGCs as highly modulatory cell type.

To date, commonly used intestinal *in vitro* culture systems rely on epithelial cell lines seeded on transwell filter inserts. A milestone towards physiologically relevant *in vitro* systems was achieved by the intestinal organoid culture system established by Sato and Clevers. It allows the clonal expansion of single crypt-based intestinal stem cells, which give rise to three-dimensional organoids that recapitulate the complete stem cell differentiation hierarchy of the epithelium [191]. Elaborate intestinal models systems are currently developed based on this new cell source *in vitro*. To render such models predictive for the study of barrier properties and uptake processes, not only the epithelial effector cells must be integrated, but also relevant cellular and molecular modulators. In this work an isolation and culture protocol of EGCs is presented under highly defined culture conditions (i.e. without the supplementation of serum) that allows integration of EGCs in intesinal tissue models. Further, a full transcriptomic profiling of this population *in vivo* and *in vitro* is made publicly accessible. These resources have the potential to advance the physiological relevance of intestinal tissue models and consequently to generate more powerful research tools *in vitro*.

5.7 Outlook on future strategies to elucidate the contributions of EGCs to intestinal physiology

As discussed above, 3D co-cultures of EGCs with other intestinal cell entities are a highly promising approach to mechanistically study their interactions. Such studies might enable the identification of clinically applicable, tissue-protective small molecules secreted by EGCs.

A further highly interesting aspect of EGC-physiology to be addressed in future *in vitro* studies is the migratory potential of this cell entity. One approach might be to study how EGCs populate a biodegradable scaffold of appropriate ECM proteins as proposed earlier. An alternative might be to use highly defined and standardized commercially available *in vitro* assays. Currently established in our group are chemotaxis assays, in which cells are seeded in a channel exposed to a chemical gradient of a potentially chemoattractive substance. Cells are then live-imaged over an extended period of time (24-48 h) and cell migration is tracked. A thorough understanding of the molecular cues that direct neural cell migration will be of great benefit for approaches in the field of regenerative medicine. In the context of congenital disorders caused by incorrect intestinal tissue innervation (e.g. HSCR), cell transplantation is an intriguing future therapeutic option. Successful transplantation strategies will require a thorough understanding of how neural cells migrate and repopulate the adult tissue to support and direct this process. Additionally, understanding the mechanisms of tissue innervation will become relevant in the context of engineering tissue-constructs for transplantations. Integrating adequate innervation will be a prerequisite for the functionality of most tissue-engineered constructs. The ENS poses an ideal cell source for such studies, since it allows the isolation of adult neural stem cells by minimally invasive procedures [192].

Such advanced *in vitro* approaches will be complemented by increasingly conclusive *in vivo* models. Transgenic animal models have been engineered that allow the tracing of the clonal progeny of single intestinal stem cells [193]. The genetic reporter construct is termed *confetti*, because it inducibly initiates the expression of individual combinations of fluorescent reporter proteins in single stem cells that are passed on to progeny. Recently, this reporter system has been employed to trace enteric glial progenitor cells [57]. Such systems allow to recapitulate the differentiative and migratory fate of single cells ("fate-mapping") and it will be of great benefit to correlate findings obtained *in vivo* to *in vitro* models.

Lastly, when considering predictive disease models, not only physiologically relevant *in vitro* models are needed but so are advanced *in vivo* models that model the human pathophysiology in its complexity. While the models employed here are well-established, they are highly artificial. One step towards recapitulating the relapsing physiology of chronic IBD conditions is to administer the disease-inducing substances (e.g. DSS) in repetitive cycles with intermediary remissions. All these strategies will contribute to further understanding and therapeutically employing EGC (patho-)physiology.

6 Bibliography

[1] R. F. Schmidt, F. Lang, et al. *Physiologie des Menschen: Mit Pathophysiologie.* 31., über-arbeitete und aktualisierte Aufl. Springer-Lehrbuch. Berlin, Heidelberg: Springer-Verlag, 2011.

[2] H. Gray and W. H. Lewis. *Anatomy of the human body.* 20th ed. New York: Bartleby.com, 2000.

[3] J. B. Furness. "The enteric nervous system and neurogastroenterology". In: *Nature reviews. Gastroenterology & hepatology* 9.5 (2012), pp. 286–294.

[4] N. Barker. "Adult intestinal stem cells: Critical drivers of epithelial homeostasis and regeneration". In: *Nature Reviews Molecular Cell Biology* 15.1 (2013), pp. 19–33.

[5] V. Sasselli, V. Pachnis, et al. "The enteric nervous system". In: *Developmental biology* 366.1 (2012), pp. 64–73.

[6] M. Costa. "Anatomy and physiology of the enteric nervous system". In: *Gut* 47(Suppl 4) (2000), pp. iv15–iv19.

[7] R. Rhoades and D. R. Bell. *Medical Physiology: Principles for Clinical Medicine.* 4th ed. Philadelphia: Wolters Kluwer Health/Lippincott Williams & Wilkins, 2012.

[8] H. M. Said. *Physiology of the Gastrointestinal Tract.* Elsevier Science, 2012.

[9] S. M. Brierley and D. R. Linden. "Neuroplasticity and dysfunction after gastrointestinal inflammation". In: *Nature Reviews Gastroenterology & Hepatology* (2014).

[10] R. M. Berne, M. N. Levy, et al. *Berne & Levy Physiology.* 6th edition. Philadelphia: Elsevier, 2008.

[11] M. Carabotti, A. Scirocco, et al. "The gut-brain axis: interactions between enteric microbiota, central and enteric nervous systems". In: *Annals of gastroenterology : quarterly publication of the Hellenic Society of Gastroenterology* 28.2 (2015), pp. 203–209.

[12] T. A. Heanue and V. Pachnis. "Enteric nervous system development and Hirschsprung's disease: advances in genetic and stem cell studies". In: *Nature reviews. Neuroscience* 8.6 (2007), pp. 466–479.

[13] J. I. Lake and R. O. Heuckeroth. "Enteric nervous system development: migration, differentiation, and disease". In: *American Journal of Physiology - Gastrointestinal and Liver Physiology* 305.1 (2013), G1–G24.

[14] D. Newgreen and H. M. Young. "Enteric nervous system: development and developmental disturbances–part 1". In: *Pediatric and developmental pathology : the official journal of the Society for Pediatric Pathology and the Paediatric Pathology Society* 5.3 (2002), pp. 224–247.

[15] G. Gabella. "Ultrastructure of the nerve plexuses of the mammalian intestine: The enteric glial cells". In: *Neuroscience* 6.3 (1981), pp. 425–436.

[16] S. Hoff, F. Zeller, et al. "Quantitative assessment of glial cells in the human and guinea pig enteric nervous system with an anti-Sox8/9/10 antibody". In: *The Journal of comparative neurology* 509.4 (2008), pp. 356–371.

[17] W. Boesmans, M. A. Martens, et al. "Imaging neuron-glia interactions in the enteric nervous system". In: *Frontiers in Cellular Neuroscience* 7 (2013).

[18]   A. Rühl. "Glial cells in the gut". In: *Neurogastroenterology & Motility* 17.6 (2005), pp. 777–790.

[19]   B. D. Gulbransen. *Enteric glia.* Vol. # 2. Colloquium series on neuroglia in biology and medicine. San Rafael: Morgan & Claypool, 2014.

[20]   K. R. Jessen and R. Mirsky. "Astrocyte-like glia in the peripheral nervous system: an immunohistochemical study of enteric glia". In: *The Journal of neuroscience : the official journal of the Society for Neuroscience* 3.11 (1983), pp. 2206–2218.

[21]   W. Boesmans, R. Lasrado, et al. "Heterogeneity and phenotypic plasticity of glial cells in the mammalian enteric nervous system". In: *Glia* 63.2 (2015), pp. 229–241.

[22]   H. M. Young, A. J. Bergner, et al. "Acquisition of neuronal and glial markers by neural crest-derived cells in the mouse intestine". In: *The Journal of comparative neurology* 456.1 (2003), pp. 1–11.

[23]   N. M. Joseph, S. He, et al. "Enteric glia are multipotent in culture but primarily form glia in the adult rodent gut". In: *Journal of Clinical Investigation* 121.9 (2011), pp. 3398–3411.

[24]   C. Laranjeira, K. Sandgren, et al. "Glial cells in the mouse enteric nervous system can undergo neurogenesis in response to injury". In: *Journal of Clinical Investigation* 121.9 (2011), pp. 3412–3424.

[25]   H. Kettenmann and A. Verkhratsky. "Neuroglia, der lebende Nervenkitt". In: *Fortschritte der Neurologie-Psychiatrie* 79.10 (2011), pp. 588–597.

[26]   A. Costagliola, L. van Nassauw, et al. "Voltage-gated delayed rectifier K v 1-subunits may serve as distinctive markers for enteroglial cells with different phenotypes in the murine ileum". In: *Neuroscience Letters* 461.2 (2009), pp. 80–84.

[27]   E. L. Fletcher, M. J. Clark, et al. "Neuronal and glial localization of GABA transporter immunoreactivity in the myenteric plexus". In: *Cell and tissue research* 308.3 (2002), pp. 339–346.

[28]   N. Braun, J. Sévigny, et al. "Association of the ecto-ATPase NTPDase2 with glial cells of the peripheral nervous system". In: *Glia* 45.2 (2004), pp. 124–132.

[29]   H. Abdo, P. Derkinderen, et al. "Enteric glial cells protect neurons from oxidative stress in part via reduced glutathione". In: *FASEB journal : official publication of the Federation of American Societies for Experimental Biology* 24.4 (2010), pp. 1082–1094.

[30]   T. M. Mathiisen, K. P. Lehre, et al. "The perivascular astroglial sheath provides a complete covering of the brain microvessels: an electron microscopic 3D reconstruction". In: *Glia* 58.9 (2010), pp. 1094–1103.

[31]   G. C. Petzold and V. N. Murthy. "Role of astrocytes in neurovascular coupling". In: *Neuron* 71.5 (2011), pp. 782–797.

[32]   N. J. Abbott, L. Rönnbäck, et al. "Astrocyte-endothelial interactions at the blood-brain barrier". In: *Nature reviews. Neuroscience* 7.1 (2006), pp. 41–53.

[33]   Y. A. Liu, Y. C. Chung, et al. "3-D imaging, illustration, and quantitation of enteric glial network in transparent human colon mucosa". In: *Neurogastroenterology & Motility* 25.5 (2013), e324–38.

[34]   M. Neunlist, P. Aubert, et al. "Enteric glia inhibit intestinal epithelial cell proliferation partly through a TGF-beta1-dependent pathway". In: *AJP: Gastrointestinal and Liver Physiology* 292.1 (2007), G231–41.

[35] K. Bach-Ngohou, M. M. Mahé, et al. "Enteric glia modulate epithelial cell proliferation and differentiation through 15-deoxy-12,14-prostaglandin J2". In: *The Journal of Physiology* 588.Pt 14 (2010), pp. 2533–2544.

[36] L. van Landeghem, J. Chevalier, et al. "Enteric glia promote intestinal mucosal healing via activation of focal adhesion kinase and release of proEGF". In: *AJP: Gastrointestinal and Liver Physiology* 300.6 (2011), G976–G987.

[37] T. C. Savidge, P. Newman, et al. "Enteric Glia Regulate Intestinal Barrier Function and Inflammation Via Release of S-Nitrosoglutathione". In: *Gastroenterology* 132.4 (2007), pp. 1344–1358.

[38] Y. Nasser, E. Fernandez, et al. "Role of enteric glia in intestinal physiology: effects of the gliotoxin fluorocitrate on motor and secretory function". In: *AJP: Gastrointestinal and Liver Physiology* 291.5 (2006), G912–G927.

[39] A. Cornet, T. C. Savidge, et al. "Enterocolitis induced by autoimmune targeting of enteric glial cells: A possible mechanism in Crohn's disease?" In: *Proceedings of the National Academy of Sciences* 98.23 (2001), pp. 13306–13311.

[40] A.-C. Aubé, J. Cabarrocas, et al. "Changes in enteric neurone phenotype and intestinal functions in a transgenic mouse model of enteric glia disruption". In: *Gut* 55.5 (2006), pp. 630–637.

[41] T. G. Bush, T. C. Savidge, et al. "Fulminant Jejuno-Ileitis following Ablation of Enteric Glia in Adult Transgenic Mice". In: *Cell* 93.2 (1998), pp. 189–201.

[42] B. D. Gulbransen and K. A. Sharkey. "Novel functional roles for enteric glia in the gastrointestinal tract". In: *Nature Reviews Gastroenterology & Hepatology* 9.11 (2012), pp. 625–632.

[43] V. Parpura and A. N. Verkhratskii. *Pathological potential of neuroglia: Possible new targets for medical intervention.* New York: Springer, 2014.

[44] M. E. Hamby and M. V. Sofroniew. "Reactive astrocytes as therapeutic targets for CNS disorders". In: *Neurotherapeutics : the journal of the American Society for Experimental NeuroTherapeutics* 7.4 (2010), pp. 494–506.

[45] G. v. Boyen, N. Schulte, et al. "Distribution of enteric glia and GDNF during gut inflammation". In: *BMC Gastroenterology* 11 (2011), p. 3.

[46] G. B. T. v. Boyen, M. Steinkamp, et al. "Proinflammatory cytokines increase glial fibrillary acidic protein expression in enteric glia". In: *Gut* 53.2 (2004), pp. 222–228.

[47] H. Kettenmann and B. R. Ransom. *Neuroglia.* OUP USA, 2013.

[48] G. Bamias, D. Corridoni, et al. "New insights into the dichotomous role of innate cytokines in gut homeostasis and inflammation". In: *Cytokine* 59.3 (2012), pp. 451–459.

[49] P. Brandtzaeg, H. Kiyono, et al. "Terminology: nomenclature of mucosa-associated lymphoid tissue". In: *Mucosal immunology* 1.1 (2008), pp. 31–37.

[50] C. Janeway. *Immunobiology: The immune system in health and disease.* 5th ed. New York: Garland Pub., 2001.

[51] P. Brandtzaeg and R. Pabst. "Let's go mucosal: communication on slippery ground". In: *Trends in immunology* 25.11 (2004), pp. 570–577.

[52] M. F. Neurath, S. Finotto, et al. "The role of Th1/Th2 polarization in mucosal immunity". In: *Nature Medicine* 8.6 (2002), pp. 567–573.

[53]   G. Bouma and W. Strober. "The immunological and genetic basis of inflammatory bowel disease". In: *Nature Reviews Immunology* 3.7 (2003), pp. 521–533.

[54]   F. Heller, P. Florian, et al. "Interleukin-13 Is the Key Effector Th2 Cytokine in Ulcerative Colitis That Affects Epithelial Tight Junctions, Apoptosis, and Cell Restitution". In: *Gastroenterology* 129.2 (2005), pp. 550–564.

[55]   H. Veiga-Fernandes, M. C. Coles, et al. "Tyrosine kinase receptor RET is a key regulator of Peyer's Patch organogenesis". In: *Nature* 446.7135 (2007), pp. 547–551.

[56]   A. Schuchardt, V. D'Agati, et al. "Defects in the kidney and enteric nervous system of mice lacking the tyrosine kinase receptor Ret". In: *Nature* 367.6461 (1994), pp. 380–383.

[57]   P. S. Kabouridis, R. Lasrado, et al. "Microbiota Controls the Homeostasis of Glial Cells in the Gut Lamina Propria". In: *Neuron* (2015).

[58]   R. Franco, R. Pacheco, et al. "The emergence of neurotransmitters as immune modulators". In: *Trends in immunology* 28.9 (2007), pp. 400–407.

[59]   de Jonge, Wouter J. "The Gut's Little Brain in Control of Intestinal Immunity". In: *ISRN gastroenterology* 2013 (2013), p. 630159.

[60]   K. J. Tracey. "The inflammatory reflex". In: *Nature* 420.6917 (2002), pp. 853–859.

[61]   de Jonge, Wouter J, van der Zanden, Esmerij P, et al. "Stimulation of the vagus nerve attenuates macrophage activation by activating the Jak2-STAT3 signaling pathway". In: *Nature immunology* 6.8 (2005), pp. 844–851.

[62]   G. Matteoli and G. E. Boeckxstaens. "The vagal innervation of the gut and immune homeostasis". In: *Gut* 62.8 (2013), pp. 1214–1222.

[63]   G. E. Boeckxstaens and de Jonge, W J. "Neuroimmune mechanisms in postoperative ileus". In: *Gut* 58.9 (2009), pp. 1300–1311.

[64]   K. Geboes, P. Rutgeerts, et al. "Major histocompatibility class II expression on the small intestinal nervous system in Crohn's disease". In: *Gastroenterology* 103.2 (1992), pp. 439–447.

[65]   K. Geboes and S. Collins. "Structural abnormalities of the nervous system in Crohn's disease and ulcerative colitis". In: *Neurogastroenterology and Motility* 10.3 (1998), pp. 189–202.

[66]   A. Rühl, S. Franzke, et al. "Interleukin-6 expression and regulation in rat enteric glial cells". In: *AJP: Gastrointestinal and Liver Physiology* 280.6 (2001), G1163–71.

[67]   M. Murakami, T. Ohta, et al. "Lipopolysaccharides enhance the action of bradykinin in enteric neurons via secretion of interleukin-1b from enteric glial cells". In: *Journal of Neuroscience Research* 87.9 (2009), pp. 2095–2104.

[68]   C. Cirillo, G. Sarnelli, et al. "Proinflammatory stimuli activates human-derived enteroglial cells and induces autocrine nitric oxide production". In: *Neurogastroenterology & Motility* 23.9 (2011), e372–82.

[69]   A. Simi, Y. Edling, et al. "Activation of c-fos by lipopolysaccharide in glial cells via p38 mitogen-activated protein kinase-dependent activation of serum or cyclic AMP/calcium response element". In: *Journal of neurochemistry* 92.4 (2005), pp. 915–924.

[70]   C. Cirillo, G. Sarnelli, et al. "Increased mucosal nitric oxide production in ulcerative colitis is mediated in part by the enteroglial-derived S100B protein". In: *Neurogastroenterology & Motility* 21.11 (2009), 1209–e112.

[71] C. Rumio, D. Besusso, et al. "Activation of smooth muscle and myenteric plexus cells of jejunum via Toll-like receptor 4". In: *Journal of cellular physiology* 208.1 (2006), pp. 47–54.

[72] I. Barajon, G. Serrao, et al. "Toll-like receptors 3, 4, and 7 are expressed in the enteric nervous system and dorsal root ganglia". In: *The journal of histochemistry and cytochemistry : official journal of the Histochemistry Society* 57.11 (2009), pp. 1013–1023.

[73] F. Turco, G. Sarnelli, et al. "Enteroglial-derived S100B protein integrates bacteria-induced Toll-like receptor signalling in human enteric glial cells". In: *Gut* 63.1 (2013), pp. 105–115.

[74] J. Burisch, T. Jess, et al. "The burden of inflammatory bowel disease in Europe". In: *Journal of Crohn's & colitis* 7.4 (2013), pp. 322–337.

[75] R. B. Sartor. "Mechanisms of disease: pathogenesis of Crohn's disease and ulcerative colitis". In: *Nature clinical practice. Gastroenterology & hepatology* 3.7 (2006), pp. 390–407.

[76] G. Bamias, T. T. Pizarro, et al. "Pathway-based approaches to the treatment of inflammatory bowel disease". In: *Translational research : the journal of laboratory and clinical medicine* (2015).

[77] M. F. Neurath. "Cytokines in inflammatory bowel disease". In: *Nature Reviews Immunology* 14.5 (2014), pp. 329–342.

[78] A. Wagnerova and R. Gardlik. "In vivo reprogramming in inflammatory bowel disease". In: *Gene Therapy* 20.12 (2013), pp. 1111–1118.

[79] R. Sartor. "Therapeutic manipulation of the enteric microflora in inflammatory bowel diseases: Antibiotics, probiotics, and prebiotics". In: *Gastroenterology* 126.6 (2004), pp. 1620–1633.

[80] H. Sales-Campos, P. J. Basso, et al. "Classical and recent advances in the treatment of inflammatory bowel diseases". In: *Brazilian journal of medical and biological research* 48.2 (2015), pp. 96–107.

[81] S. J. Brown and L. Mayer. "The immune response in inflammatory bowel disease". In: *The American journal of gastroenterology* 102.9 (2007), pp. 2058–2069.

[82] S. Buhner, C. Buning, et al. "Genetic basis for increased intestinal permeability in families with Crohn's disease: role of CARD15 3020insC mutation?" In: *Gut* 55.3 (2006), pp. 342–347.

[83] A. R. Jurjus, N. N. Khoury, et al. "Animal models of inflammatory bowel disease". In: *Journal of Pharmacological and Toxicological Methods* 50.2 (2004), pp. 81–92.

[84] M. Perše and A. Cerar. "Dextran Sodium Sulphate Colitis Mouse Model: Traps and Tricks". In: *Journal of Biomedicine and Biotechnology* 2012.1 (2012), pp. 1–13.

[85] S. Wirtz, C. Neufert, et al. "Chemically induced mouse models of intestinal inflammation". In: *Nature Protocols* 2.3 (2007), pp. 541–546.

[86] R. P. Dellinger, M. M. Levy, et al. "Surviving sepsis campaign: international guidelines for management of severe sepsis and septic shock: 2012". In: *Critical care medicine* 41.2 (2013), pp. 580–637.

[87] E. A. Deitch. "Gut-origin sepsis: evolution of a concept". In: *The surgeon : journal of the Royal Colleges of Surgeons of Edinburgh and Ireland* 10.6 (2012), pp. 350–356.

[88] R. Mittal and C. M. Coopersmith. "Redefining the gut as the motor of critical illness". In: *Trends in molecular medicine* 20.4 (2014), pp. 214–223.

[89] B. Y. d. Winter. "Interplay between inflammation, immune system and neuronal pathways: Effect on gastrointestinal motility". In: *World Journal of Gastroenterology* 16.44 (2010), p. 5523.

[90] M. K. Eskandari, J. C. Kalff, et al. "LPS-induced muscularis macrophage nitric oxide suppresses rat jejunal circular muscle activity". In: *The American journal of physiology* 277.2 Pt 1 (1999), G478–86.

[91] S. Torihashi, H. Ozaki, et al. "Resident macrophages activated by lipopolysaccharide suppress muscle tension and initiate inflammatory response in the gastrointestinal muscle layer". In: *Histochemistry and Cell Biology* 113.2 (2000), pp. 73–80.

[92] S. Calatayud, E. García-Zaragozá, et al. "Downregulation of nNOS and synthesis of PGs associated with endotoxin-induced delay in gastric emptying". In: *American journal of physiology. Gastrointestinal and liver physiology* 283.6 (2002), G1360–7.

[93] de Jonge, Wouter J, van den Wijngaard, René M, et al. "Postoperative ileus is maintained by intestinal immune infiltrates that activate inhibitory neural pathways in mice". In: *Gastroenterology* 125.4 (2003), pp. 1137–1147.

[94] F. The, C. Cailotto, et al. "Central activation of the cholinergic anti-inflammatory pathway reduces surgical inflammation in experimental post-operative ileus". In: *British journal of pharmacology* 163.5 (2011), pp. 1007–1016.

[95] C. Nolte, M. Matyash, et al. "GFAP promoter-controlled EGFP-expressing transgenic mice: a tool to visualize astrocytes and astrogliosis in living brain tissue". In: *Glia* 33.1 (2001), pp. 72–86.

[96] Y. Sambuy, I. d. Angelis, et al. "The Caco-2 cell line as a model of the intestinal barrier: influence of cell and culture-related factors on Caco-2 cell functional characteristics". In: *Cell biology and toxicology* 21.1 (2005), pp. 1–26.

[97] P. Artursson and J. Karlsson. "Correlation between oral drug absorption in humans and apparent drug permeability coefficients in human intestinal epithelial (Caco-2) cells". In: *Biochemical and biophysical research communications* 175.3 (1991), pp. 880–885.

[98] M. A. Schick, C. Wunder, et al. "Phosphodiesterase-4 inhibition as a therapeutic approach to treat capillary leakage in systemic inflammation". In: *The Journal of Physiology* 590.11 (2012), pp. 2693–2708.

[99] J. Wollborn, C. Wunder, et al. "Phosphodiesterase-4 inhibition with rolipram attenuates hepatocellular injury in hyperinflammation in vivo and in vitro without influencing inflammation and HO-1 expression". In: *Journal of pharmacology & pharmacotherapeutics* 6.1 (2015), pp. 13–23.

[100] C. Hegewald, R. Alt, et al. "Reduced oxygen stress promotes propagation of murine postnatal enteric neural progenitors in vitro". In: *Neurogastroenterology & Motility* 23.10 (2011), e412–e424.

[101] C. Moll, J. Reboredo, et al. "Tissue engineering of a human 3D in vitro tumor test system". In: *Journal of visualized experiments : JoVE* 78 (2013).

[102] C. Brede, M. Friedrich, et al. "Mapping immune processes in intact tissues at cellular resolution". In: *Journal of Clinical Investigation* 122.12 (2012), pp. 4439–4446.

[103] P. A. Santi. "Light Sheet Fluorescence Microscopy: A Review". In: *Journal of Histochemistry & Cytochemistry* 59.2 (2011), pp. 129–138.

[104] R Development Core Team. *R: A Language and Environment for Statistical Computing.* Ed. by the R Foundation for Statistical Computing. Vienna, 2013.

[105] R. Edgar, M. Domrachev, et al. "Gene Expression Omnibus: NCBI gene expression and hybridization array data repository". In: *Nucleic acids research* 30.1 (2002), pp. 207–210.

[106] D. W. Huang, B. T. Sherman, et al. "Systematic and integrative analysis of large gene lists using DAVID bioinformatics resources". In: *Nature Protocols* 4.1 (2009), pp. 44–57.

[107] M. Ashburner, C. A. Ball, et al. "Gene ontology: tool for the unification of biology. The Gene Ontology Consortium". In: *Nature genetics* 25.1 (2000), pp. 25–29.

[108] "Gene Ontology Consortium: going forward". In: *Nucleic acids research* 43.Database issue (2015), pp. D1049–56.

[109] J. Bernhardt, S. Funke, et al. "Visualizing Gene Expression Data via Voronoi Treemaps". In: *2009 Sixth International Symposium on Voronoi Diagrams (ISVD)*, pp. 233–241.

[110] R. Turner. *deldir: Delaunay Triangulation and Dirichlet (Voronoi) Tessellation*. 2015.

[111] A. Heider and R. Alt. "virtualArray: a R/bioconductor package to merge raw data from different microarray platforms". In: *BMC bioinformatics* 14 (2013), p. 75.

[112] A. I. Saeed, N. K. Bhagabati, et al. "TM4 microarray software suite". In: *Methods in enzymology* 411 (2006), pp. 134–193.

[113] M. V. Han and C. M. Zmasek. "phyloXML: XML for evolutionary biology and comparative genomics". In: *BMC bioinformatics* 10 (2009), p. 356.

[114] M. B. Eisen, P. T. Spellman, et al. "Cluster analysis and display of genome-wide expression patterns". In: *Proceedings of the National Academy of Sciences of the United States of America* 95.25 (1998), pp. 14863–14868.

[115] G. K. Geiss, R. E. Bumgarner, et al. "Direct multiplexed measurement of gene expression with color-coded probe pairs". In: *Nature biotechnology* 26.3 (2008), pp. 317–325.

[116] NanoString Technologies. *nCounter Brochure*. 22.03.2016.

[117] S. Flemming, N. Schlegel, et al. "Phosphodiesterase 4 inhibition dose dependently stabilizes microvascular barrier functions and microcirculation in a rodent model of polymicrobial sepsis". In: *Shock* 41.6 (2014), pp. 537–545.

[118] M. A. Schick, T. J. Isbary, et al. "The impact of crystalloid and colloid infusion on the kidney in rodent sepsis". In: *Intensive care medicine* 36.3 (2010), pp. 541–548.

[119] C. Rosenbaum, M. A. Schick, et al. "Activation of Myenteric Glia during Acute Inflammation In Vitro and In Vivo". In: *PLoS ONE* 11.3 (2016), e0151335.

[120] N. Bernardini, C. Segnani, et al. "Immunohistochemical analysis of myenteric ganglia and interstitial cells of Cajal in ulcerative colitis". In: *Journal of Cellular and Molecular Medicine* 16.2 (2012), pp. 318–327.

[121] M. Steinkamp, I. Geerling, et al. "Glial-derived neurotrophic factor regulates apoptosis in colonic epithelial cells". In: *Gastroenterology* 124.7 (2003), pp. 1748–1757.

[122] B. Stoffels, K. J. Hupa, et al. "Postoperative ileus involves interleukin-1 receptor signaling in enteric glia". In: *Gastroenterology* 146.1 (2014), 176–87.e1.

[123] J. H. Winston, Q. Li, et al. "Paradoxical regulation of ChAT and nNOS expression in animal models of Crohn's colitis and ulcerative colitis". In: *AJP: Gastrointestinal and Liver Physiology* 305.4 (2013), G295–G302.

[124] G. Esposito, E. Capoccia, et al. "Palmitoylethanolamide improves colon inflammation through an enteric glia/toll like receptor 4-dependent PPAR- activation". In: *Gut* (2013).

[125] A. M. Binkowska, G. Michalak, et al. "Current views on the mechanisms of immune responses to trauma and infection". In: *Central-European journal of immunology* 40.2 (2015), pp. 206–216.

[126] K.-M. Kaukonen, M. Bailey, et al. "Systemic inflammatory response syndrome criteria in defining severe sepsis". In: *The New England journal of medicine* 372.17 (2015), pp. 1629–1638.

[127] E. M. Conner, S. J. Brand, et al. "Role of reactive metabolites of oxygen and nitrogen in inflammatory bowel disease: Toxins, mediators, and modulators of gene expression". In: *Inflammatory Bowel Diseases* 2.2 (1996), pp. 133–147.

[128] J. P. Burke, J. J. Mulsow, et al. "Fibrogenesis in Crohn's disease". In: *The American journal of gastroenterology* 102.2 (2007), pp. 439–448.

[129] S. E. Lakhan and A. Kirchgessner. "Neuroinflammation in inflammatory bowel disease". In: *Journal of Neuroinflammation* 7.1 (2010), p. 37.

[130] G. Barbara, V. Stanghellini, et al. "What is the effect of inflammation on intestinal function?" In: *Inflammatory Bowel Diseases* 14 Suppl 2 (2008), S140–4.

[131] V. Vasina, G. Barbara, et al. "Enteric neuroplasticity evoked by inflammation". In: *Autonomic neuroscience : basic & clinical* 126-127 (2006), pp. 264–272.

[132] F. Rieder and C. Fiocchi. "Intestinal fibrosis in inflammatory bowel disease - Current knowledge and future perspectives". In: *Journal of Crohn's & colitis* 2.4 (2008), pp. 279–290.

[133] B. D. Gulbransen, M. Bashashati, et al. "Activation of neuronal P2X7 receptor–pannexin-1 mediates death of enteric neurons during colitis". In: *Nature Medicine* 18.4 (2012), pp. 600–604.

[134] R. d. Giorgio, S. Guerrini, et al. "Inflammatory neuropathies of the enteric nervous system". In: *Gastroenterology* 126.7 (2004), pp. 1872–1883.

[135] V. Villanacci, G. Bassotti, et al. "Enteric nervous system abnormalities in inflammatory bowel diseases". In: *Neurogastroenterology & Motility* 20.9 (2008), pp. 1009–1016.

[136] J. A. Roberts, M. K. Lukewich, et al. "The roles of purinergic signaling during gastrointestinal inflammation". In: *Current Opinion in Pharmacology* 12.6 (2012), pp. 659–666.

[137] J. S. Bradley, E. J. Parr, et al. "Effects of inflammation on cell proliferation in the myenteric plexus of the guinea-pig ileum". In: *Cell and tissue research* 289.3 (1997), pp. 455–461.

[138] D. L. Hamilton and K. Abremski. "Site-specific recombination by the bacteriophage P1 lox-Cre system. Cre-mediated synapsis of two lox sites". In: *Journal of molecular biology* 178.2 (1984), pp. 481–486.

[139] R. Feil, J. Wagner, et al. "Regulation of Cre recombinase activity by mutated estrogen receptor ligand-binding domains". In: *Biochemical and biophysical research communications* 237.3 (1997), pp. 752–757.

[140] S. Srinivas, T. Watanabe, et al. "Cre reporter strains produced by targeted insertion of EYFP and ECFP into the ROSA26 locus". In: *BMC Developmental Biology* 1 (2001), p. 4.

[141] J. Silbereis, E. Cheng, et al. "Precursors with Glial Fibrillary Acidic Protein Promoter Activity Transiently Generate GABA Interneurons in the Postnatal Cerebellum". In: *Stem Cells* 27.5 (2009), pp. 1152–1163.

[142] L. M. L. Chow, J. Zhang, et al. "Inducible Cre recombinase activity in mouse mature astrocytes and adult neural precursor cells". In: *Transgenic Research* 17.5 (2008), pp. 919–928.

[143] P. G. Hirrlinger, A. Scheller, et al. "Temporal control of gene recombination in astrocytes by transgenic expression of the tamoxifen-inducible DNA recombinase variant CreERT2". In: *Glia* 54.1 (2006), pp. 11–20.

[144] L. Tarassishin, H.-S. Suh, et al. "LPS and IL-1 differentially activate mouse and human astrocytes: role of CD14". In: *Glia* 62.6 (2014), pp. 999–1013.

[145] Z. Wu. "A review of statistical methods for preprocessing oligonucleotide microarrays". In: *Statistical methods in medical research* 18.6 (2009), pp. 533–541.

[146] W. ZHANG and H. T. LIU. "MAPK signal pathways in the regulation of cell proliferation in mammalian cells". In: *Cell research* 12.1 (2002), pp. 9–18.

[147] A. S. Dhillon, S. Hagan, et al. "MAP kinase signalling pathways in cancer". In: *Oncogene* 26.22 (2007), pp. 3279–3290.

[148] N. R. Bhat, P. Zhang, et al. "Extracellular signal-regulated kinase and p38 subgroups of mitogen-activated protein kinases regulate inducible nitric oxide synthase and tumor necrosis factor-alpha gene expression in endotoxin-stimulated primary glial cultures". In: *The Journal of neuroscience : the official journal of the Society for Neuroscience* 18.5 (1998), pp. 1633–1641.

[149] Z. Xie, C. J. Smith, et al. "Activated glia induce neuron death via MAP kinase signaling pathways involving JNK and p38". In: *Glia* 45.2 (2004), pp. 170–179.

[150] S. Lee, J.-Y. Park, et al. "Lipocalin-2 is an autocrine mediator of reactive astrocytosis". In: *The Journal of neuroscience : the official journal of the Society for Neuroscience* 29.1 (2009), pp. 234–249.

[151] M. Johnstone, A. J. Gearing, et al. "A central role for astrocytes in the inflammatory response to b-amyloid; chemokines, cytokines and reactive oxygen species are produced". In: *Journal of Neuroimmunology* 93.1-2 (1999), pp. 182–193.

[152] M. B. Miller and Y.-W. Tang. "Basic concepts of microarrays and potential applications in clinical microbiology". In: *Clinical microbiology reviews* 22.4 (2009), pp. 611–633.

[153] Life Technologies Corporation 02.2011. "Illumina TotalPrep RNA Amplification Kit Protocol: (PN IL1791M Rev E)". In: ().

[154] P. Fortina and S. Surrey. "Digital mRNA profiling". In: *Nature biotechnology* 26.3 (2008), pp. 293–294.

[155] N. Technologies. *nCounter Elements™ Workflow | NanoString Technologies*.

[156] A. P. Lieberman, P. M. Pitha, et al. "Production of tumor necrosis factor and other cytokines by astrocytes stimulated with lipopolysaccharide or a neurotropic virus". In: *Proceedings of the National Academy of Sciences of the United States of America* 86.16 (1989), pp. 6348–6352.

[157] E. Cuadrado, M. H. Jansen, et al. "Chronic exposure of astrocytes to interferon-a reveals molecular changes related to Aicardi-Goutieres syndrome". In: *Brain : a journal of neurology* 136.Pt 1 (2013), pp. 245–258.

[158] S. Bhowmick, R. Duseja, et al. "Induction of IP-10 (CXCL10) in astrocytes following Japanese encephalitis". In: *Neuroscience Letters* 414.1 (2007), pp. 45–50.

[159] Invitrogen Corporation. "Mouse Cytokine 20-Plex Panel". In: ().

[160] W. d. Jager and G. T. Rijkers. "Solid-phase and bead-based cytokine immunoassay: a comparison". In: *Methods* 38.4 (2006), pp. 294–303.

[161] M. F. Elshal and J. P. McCoy. "Multiplex bead array assays: performance evaluation and comparison of sensitivity to ELISA". In: *Methods* 38.4 (2006), pp. 317–323.

[162] S. X. Leng, J. E. McElhaney, et al. "ELISA and multiplex technologies for cytokine measurement in inflammation and aging research". In: *The journals of gerontology. Series A, Biological sciences and medical sciences* 63.8 (2008), pp. 879–884.

[163] V. Schubert, D. Bouvier, et al. "SNARE protein expression in synaptic terminals and astrocytes in the adult hippocampus: a comparative analysis". In: *Glia* 59.10 (2011), pp. 1472–1488.

[164] V. Maienschein, M. Marxen, et al. "A plethora of presynaptic proteins associated with ATP-storing organelles in cultured astrocytes". In: *Glia* 26.3 (1999), pp. 233–244.

[165] N. B. Hamilton and D. Attwell. "Do astrocytes really exocytose neurotransmitters?" In: *Nature reviews. Neuroscience* 11.4 (2010), pp. 227–238.

[166] M. Rao, B. D. Nelms, et al. "Enteric glia express proteolipid protein 1 and are a transcriptionally unique population of glia in the mammalian nervous system". In: *Glia* (2015).

[167] P. K. Randhawa, K. Singh, et al. "A Review on Chemical-Induced Inflammatory Bowel Disease Models in Rodents". In: *The Korean Journal of Physiology & Pharmacology* 18.4 (2014), p. 279.

[168] S. Ding, K. L. W. Walton, et al. "Mucosal Healing and Fibrosis after Acute or Chronic Inflammation in Wild Type FVB-N Mice and C57BL6 Procollagen alpha1(I)-Promoter-GFP Reporter Mice". In: *PLoS ONE* 7.8 (2012), e42568.

[169] U. Erben, C. Loddenkemper, et al. "A guide to histomorphological evaluation of intestinal inflammation in mouse models". In: *International journal of clinical and experimental pathology* 7.8 (2014), pp. 4557–4576.

[170] D. Giulian, J. Woodward, et al. "Interleukin-1 injected into mammalian brain stimulates astrogliosis and neovascularization". In: *The Journal of neuroscience : the official journal of the Society for Neuroscience* 8.7 (1988), pp. 2485–2490.

[171] D. Giulian and L. B. Lachman. "Interleukin-1 stimulation of astroglial proliferation after brain injury". In: *Science* 228.4698 (1985), pp. 497–499.

[172] K. W. Selmaj, M. Farooq, et al. "Proliferation of astrocytes in vitro in response to cytokines. A primary role for tumor necrosis factor". In: *Journal of immunology* 144.1 (1990), pp. 129–135.

[173] S. M. Collins. "The immunomodulation of enteric neuromuscular function: implications for motility and inflammatory disorders". In: *Gastroenterology* 111.6 (1996), pp. 1683–1699.

[174] B. Isgar, M. Harman, et al. "Symptoms of irritable bowel syndrome in ulcerative colitis in remission". In: *Gut* 24.3 (1983), pp. 190–192.

[175] G. van Assche and S. M. Collins. "Leukemia inhibitory factor mediates cytokine-induced suppression of myenteric neurotransmitter release from rat intestine". In: *Gastroenterology* 111.3 (1996), pp. 674–681.

[176] A. Rühl, S. Hurst, et al. "Synergism between interleukins 1 beta and 6 on noradrenergic nerves in rat myenteric plexus". In: *Gastroenterology* 107.4 (1994), pp. 993–1001.

[177] S. M. Hurst, T. S. Wilkinson, et al. "IL-6 and Its Soluble Receptor Orchestrate a Temporal Switch in the Pattern of Leukocyte Recruitment Seen during Acute Inflammation". In: *Immunity* 14.6 (2001), pp. 705–714.

[178] R. M. McLoughlin, B. J. Jenkins, et al. "IL-6 trans-signaling via STAT3 directs T cell infiltration in acute inflammation". In: *Proceedings of the National Academy of Sciences of the United States of America* 102.27 (2005), pp. 9589–9594.

[179] R. Atreya, J. Mudter, et al. "Blockade of interleukin 6 trans signaling suppresses T-cell resistance against apoptosis in chronic intestinal inflammation: Evidence in Crohn disease and experimental colitis in vivo". In: *Nature Medicine* 16.11 (2010), p. 1341.

[180] S. Diehl and M. Rincon. "The two faces of IL-6 on Th1/Th2 differentiation". In: *Molecular immunology* 39.9 (2002), pp. 531–536.

[181] C. A. Dinarello. "Immunological and Inflammatory Functions of the Interleukin-1 Family". In: *Annual Review of Immunology* 27.1 (2009), pp. 519–550.

[182] M. Coccia, O. J. Harrison, et al. "IL-1beta mediates chronic intestinal inflammation by promoting the accumulation of IL-17A secreting innate lymphoid cells and CD4 + Th17 cells". In: *The Journal of Experimental Medicine* 209.9 (2012), pp. 1595–1609.

[183] S. Z. Ben-Sasson, J. Hu-Li, et al. "IL-1 acts directly on CD4 T cells to enhance their antigen-driven expansion and differentiation". In: *Proceedings of the National Academy of Sciences* 106.17 (2009), pp. 7119–7124.

[184] R. Moriez, H. Abdo, et al. "Neuroplasticity and neuroprotection in enteric neurons: role of epithelial cells". In: *Biochemical and biophysical research communications* 382.3 (2009), pp. 577–582.

[185] G. A. Cheadle, T. W. Costantini, et al. "Enteric Glia Cells Attenuate Cytomix-Induced Intestinal Epithelial Barrier Breakdown". In: *PLoS ONE* 8.7 (2013), e69042.

[186] M. Neunlist, F. Toumi, et al. "Human ENS regulates the intestinal epithelial barrier permeability and a tight junction-associated protein ZO-1 via VIPergic pathways". In: *American journal of physiology. Gastrointestinal and liver physiology* 285.5 (2003), G1028–36.

[187] H. M. Young, C. J. Hearn, et al. "GDNF is a chemoattractant for enteric neural cells". In: *Developmental biology* 229.2 (2001), pp. 503–516.

[188] A. M. Colangelo, L. Alberghina, et al. "Astrogliosis as a therapeutic target for neurodegenerative diseases". In: *Astrocytes in the Injured Brain: Is Gliosis Adaptive or Maladaptive?* 565 (2014), pp. 59–64.

[189] E. A. Lepekhin, C. Eliasson, et al. "Intermediate filaments regulate astrocyte motility". In: *Journal of neurochemistry* 79.3 (2001), pp. 617–625.

[190] M. Pekny, C. B. Johansson, et al. "Abnormal reaction to central nervous system injury in mice lacking glial fibrillary acidic protein and vimentin". In: *The Journal of cell biology* 145.3 (1999), pp. 503–514.

[191] T. Sato and H. Clevers. "Growing self-organizing mini-guts from a single intestinal stem cell: mechanism and applications". In: *Science (New York, N.Y.)* 340.6137 (2013), pp. 1190–1194.

[192] M. Metzger, C. Caldwell, et al. "Enteric nervous system stem cells derived from human gut mucosa for the treatment of aganglionic gut disorders". In: *Gastroenterology* 136.7 (2009),

[193] H. J. Snippert, van der Flier, Laurens G, et al. "Intestinal crypt homeostasis results from neutral competition between symmetrically dividing Lgr5 stem cells". In: *Cell* 143.1 (2010), pp. 134–144.

Curriculum vitae

Personal details

Corinna Rosenbaum

███████████
███████████
██████████████
█████████████████████████

Professional Experience

04/2016 - present   **Scientific researcher**
Department of Tissue Engineering and Regenerative Medicine
University hospital Würzburg

05/2012 - present   **Doctoral researcher**
in the group Intestinal Tissue Engineering
Department of Tissue Engineering and Regenerative Medicine
University hospital Würzburg

10/2011 - 04/2012   **Scientific Employee**
Fraunhofer Project Group "Regenerative Therapies for Oncology and
Musculoskeletal Diseases" Würzburg

Student assistant positions
10/2010 - 09/2011   Department of Tissue Engineering and Regenerative Medicine
05/2009 - 04/2010   Institute of Psychiatry, University of Würzburg

Education

05/2012 - present   **PhD thesis**
Department of Tissue Engineering and Regenerative Medicine
University hospital Würzburg
supervised by Prof. Heike Walles

10/2005 - 09/2011   **Diplom (German) in Biology**
Julius-Maximilian-University Würzburg
specifications: neurobiology, microbiology, biochemistry

2005   **Abitur & International Baccalaureate**

1996 - 2005   **German Gymnasium**
Friedrich-Ebert-Gymnasium Bonn
in 2002 stay abroad at Nayland College, Nelson, New Zealand

. . . .

Place, Date   Signature

A2

List of Publications

Data presented in the thesis are partially published in the peer-reviewed article:
Rosenbaum C, Schick MA, Wollborn J, Heider A, Scholz C-J, Cecil A, et al. (2016) *Activation of Myenteric Glia during Acute Inflammation In Vitro and In Vivo*. PLoS ONE 11(3).

Further peer-reviewed publications:
Hetz S., Acikgoez A., **Moll C.**, Jahnke H.G., Robitzki A.A., Metzger R., Metzger M., (2014) *Age related analysis of enteric ganglia of human colon using laser microdissection*. Front. Neuroscience, 15(6).
Moll, C., Reboredo, J., Schwarz, T., Appelt, A., Schürlein, S., Walles, H., Nietzer, S., (2013) *Tissue engineering of a human 3D in vitro tumor test system*. J Vis Exp.

Additional publications:
Moll, C., *Entwicklung eines in vitro Tumortestsystems für Nervenscheidentumore*, annual report of the Fraunhofer Institute for Interfacial Engineering and Biotechnology (IGB) Stuttgart, 2012.

Oral conference presentations:
Moll, C., et al., *The role of enteric glial cells under acute inflammatory conditions of the murine bowel*, 22. annual meeting of the German Society for Neurogastroenterology and Motility, 2015, Freising, Germany.
Moll, C., et al., *Enteric glial cells actively contribute to an inflammatory microenvironment in the bowel in vivo and in vitro*, 21. annual meeting of the German Society for Neurogastroenterology and Motility, 2014, Freising, Germany.
Moll, C., et al., *Analysis of enteric glial cells in an LPS-induced in vivo sepsis model of the rat*, 20. annual meeting of the German Society for Neurogastroenterology and Motility, 2013, Freising, Germany.

Poster presentations at national and international conferences:
Rosenbaum, C., et al., *Role of enteric glial cells during acute inflammation in vitro and in vivo*, Development of the enteric nervous system. 2015, Rotterdam, Netherlands.
Rosenbaum, C., et al., *Integration of primary enteric glial cells in intestinal tissue models in vitro*, WITE. 2015, Würzburger Initiative Tissue Engineering e.V. Würzburg, Germany.
Moll, C., et al., *The role of enteric glial cells in inflammatory diseases of the bowel*, The First Federation of Neurogastroenterology and Motility Meeting (FNM). 2014, The Chinese Society of Gastrointestinal Motility, Guangzhou, China.
Moll, C., et al., *Analysis of enteric glial cells in an LPS-induced in vivo sepsis model of the rat*, World Conference on Regenerative Medicine. 2013, Fraunhofer IZI, Leipzig.
Moll, C., et al., *Molecular and cellular effects of lipopolysaccharide (LPS) treatment on enteric*

glial cells in vitro and in vivo, 7th GSLS PhD Symposium 2012, Graduate School of Life Sciences Würzburg.

Moll, C., et al., *Development of a human 3D in vitro tumor test system for nerve sheath tumors*, 3rd International Conference "Strategies in Tissue Engineering". 2012, Würzburger Initiative TISSUE ENGINEERING e.V. Würzburg, Germany.

Moll, C., et al., *3D in vitro tumor test systems of nerve sheath tumors*, 3rd TERMIS World Congress "Tissue Engineering and Regenerative Medicine". 2012, Tissue Engineering & Regenerative Medicine International Society: Vienna, Austria.

Affidavit

I hereby confirm that my thesis entitled "The role of enteric glial cells under inflammatory conditions of the intestine" is the result of my own work. I did not receive any help or support from commercial consultants. All sources and / or materials applied are listed and specified in the thesis.

Furthermore, I confirm that this thesis has not yet been submitted as part of another examination process neither in identical nor in similar form.

....
Place, Date   Signature

Eidesstattliche Erklärung

Hiermit erkläre ich an Eides statt, die Dissertation "Die Rolle von enterischen Gliazellen unter entzündlichen Bedingungen im Darm" eigenständig, d.h. insbesondere selbständig und ohne Hilfe eines kommerziellen Promotionsberaters, angefertigt und keine anderen als die von mir angegebenen Quellen und Hilfsmittel verwendet zu haben.

Ich erkläre außerdem, dass die Dissertation weder in gleicher noch in ähnlicher Form bereits in einem anderen Prüfungsverfahren vorgelegen hat.

....
Ort, Datum   Unterschrift

Danksagung

Meinen besonderen Dank möchte ich Prof. Dr. Heike Walles dafür aussprechen, dass ich meine Promotion unter ihrer Betreuung am Lehrstuhl für Tissue Engineering und Regenerative Medizin anfertigen durfte. Ich danke ihr für die uneingeschränkte Unterstützung auch über die Projektgrenzen hinweg. Durch ihre stets engagierte, offene und vertrauensvolle Anleitung ist sie mir zum Vorbild geworden.

Bei PD Dr. Beate Niesler und Prof. Dr. Erhard Wischmeyer bedanke ich mich herzlich dafür, dass sie mich stets engagiert als weitere Gutachter dieser Arbeit betreut haben.

Besonders bedanken möchte ich mich bei Dr. Marco Metzger. Von ihm durfte ich mein Promotionsthema übernehmen, bei dem er mir jederzeit uneingeschränkt helfend und motivierend zur Seite stand. Seine Begeisterung für die Wissenschaft, seine qualifizierte Expertise und sein stets hoher persönlicher Einsatz haben meine Promotion enorm bereichert. Dafür möchte ich mich von Herzen bedanken.

Ebenfalls gilt mein herzlicher Dank dem gesamten Team des Lehrstuhls für Tissue Engineering und Regenerative Medizin in Würzburg. Ich danke Euch für die große Hilfsbereitschaft, die stets offene, kollegiale Arbeitsatmosphäre und auch die vielen schönen Erlebnisse außerhalb des Labors. Jenny Reboredo, Sabine Wilhelm, Matthias Schweinlin, Christian Lotz, Sebastian Schürlein, Sylvia Murawicki - damit seien nur ein paar Namen genannt.
Insbesondere bedanken möchte ich mich auch bei Lina Kötzner, die sich als Tierpflegerin vorbildlich um die Mäuse kümmerte.

Viele Kooperationspartner in- und außerhalb der Universität Würzburg haben zum Gelingen dieser Arbeit beigetragen, auch bei Ihnen möchte ich mich herzlich bedanken. Besonderer Dank gilt hier Dr. Martin Schick und Dr. Jakob Wollborn von der Anästhesie der Universitätsklinik für die Gelegenheit, das von ihnen etablierte Hyperinflammations-Rattenmodell für meine Arbeit zu nutzen sowie den stets sehr engagierten Austausch über die Ergebnisse. Bei Dr. Christian Brede aus der Arbeitsgruppe Beilhack bedanke ich mich für die große Unterstützung bei der Lichtblattmikroskopie. Auch den Bioinformatikern Claus-Jürgen Scholz, Alexander Cecil und Andreas Heider danke ich für die engagierte Hilfe bei der Auswertung der Microarray-Daten.

Von Herzen danken möchte ich meiner Familie, die mich vorbehaltlos unterstützt und stets ermutigt hat. Ich danke Euch für den Halt während der letzten Jahre.
Meinen größten Dank möchte ich meinem Mann Tobias aussprechen. Ich bin dir von Herzen dankbar für deine liebevolle Unterstützung, die mir immer wieder Kraft gegeben hat. Danke für all die schönen Erlebnisse, die mein Leben so bereichern, für deinen Glauben an mich und deine Freude auf unsere gemeinsame Zukunft.